ISSN 2663-9084 (Print)
ISSN 2663-9092 (Online)

Ukrainian Neurosurgical Journal

Vol. 31, N4, 2025

Is a scholarly Open Access journal
Founded in April 1995. Quarterly.
State Registration Certificate KV No 23771-13611PR dated 14 February 2019

The journal is on the List of Scientific Professional Editions of Ukraine, where results of thesis research for earning academic degrees of doctor and candidate of sciences and PhD may be published (Order of the Ministry of Education and Science of Ukraine No. 1721 dated 10 December 2024)
The journal is included in the Scopus scientometric database.

Journal publishes peer-reviewed works.

Founders
Romodanov Neurosurgery Institute
Ukrainian Association of Neurosurgeons
National Academy of Medical Sciences of Ukraine

Publisher
Romodanov Neurosurgery Institute

Contact
32 Platona Mayborody st., Kyiv, 04050, Ukraine
tel. +380 44 483-91-98
fax +380 44 489-35-61
E-mail: unj.office@gmail.com
http://theunj.org

The journal went to press 05 December 2025
Format 60 × 841/8. Offset Paper No.1
Order No. 25-32

Circulation 300 copies

Polygraphic services
FOP Golosuy IE
Certificate AA No. 9221702
86 Kyrylivska st., Kyiv, 04080, Ukraine
Tel. +380 44 239-19-85

The master layout of the journal was approved and recommended for publication and distribution via the Internet at the joint meeting of the Editorial Board of the Ukrainian Neurosurgical Journal and the Academic Council of Romodanov Neurosurgery Institute (Meeting Minutes N. 18 dated 24 October 2025)

On the cover
Figures from the article by Dharmikkumar Velani, Varshesh Shah, Krushi Soladhra, Renish Padshala, Nazar Imam, Jaimin Modh, Arvind Verma "Comprehensive assessment of surgical, clinical, and radiological outcomes in craniovertebral junction anomalies with basilar invagination and atlantoaxial dislocation: An initial experience of 5 cases", p. 45-57

Content

Review article

Original article

Case report

Review article

Ukrainian Neurosurgical Journal. 2025;31(4):3-10
doi: 10.25305/unj.331349

Changes in the neuro-glial-vascular interface in metabolic intoxications in children (based on acetonemic syndrome and hyperammonemia)

Yaroslav D. Bondarenko [1], Oksana I. Kauk [2], Svitlana O. Stetsenko [3], Svitlana V.Rykhlik [4]

[1] Third Faculty of Medicine, Kharkiv National Medical University, Kharkiv, Ukraine
[2] Department of Neurology, Kharkiv National Medical University, Kharkiv, Ukraine
[3] Department of Biological Chemistry, Kharkiv National Medical University, Kharkiv, Ukraine
[4] Department of Histology, Cytology and Embryology, Kharkiv National Medical University, Kharkiv, Ukraine

Received: 31 May 2025
Accepted: 27 June 2025

Address for correspondence: *Yaroslav D. Bondarenko, Third Faculty of Medicine, Kharkiv National Medical University, 4 Nauky avenue, Kharkiv, 61022, Ukraine, e-mail: ydbondarenko.3m21@knmu.edu.ua*

Objective: To investigate morphofunctional changes of the neuro-glial-vascular interface in children with metabolic intoxications, particularly in acetonemic syndrome and hyperammonemia.

Materials and methods: A systematic literature review with elements of narrative analysis was conducted following PRISMA guidelines. Literature search was performed in PubMed/MEDLINE, Web of Science Core Collection, Scopus, and Cochrane Library for the period 1990-2024. Included studies involved children from birth to 18 years and investigated neurotoxic effects of acetonemic syndrome and hyperammonemia. Study quality was assessed using Newcastle-Ottawa Scale, AMSTAR-2, and SYRCLE tools.

Results: Key morphofunctional disorders of the neuro-glial-vascular interface were identified: cytotoxic astrocytic swelling due to glutamine accumulation during ammonia detoxification; blood-brain barrier disruption with decreased expression of tight junction proteins (claudin-5, occludin, ZO-1); impaired energy metabolism due to glycolysis inhibition and mitochondrial dysfunction; excitotoxicity resulting from glutamate-glutamine cycle disruption; microglial activation with increased expression of CD68, Iba1, MHC II, and pro-inflammatory cytokine secretion.

Conclusions: Morphofunctional changes of the neuro-glial-vascular interface with acetonemic syndrome and hyperammonemia are characterized by complex disruptions of blood-brain barrier (BBB) structure and function, energy metabolism, neurotransmitter balance, and neuroinflammatory processes. A personalized approach to diagnosis and treatment using biomarkers of BBB damage and neuroinflammation is necessary.

Keywords: *neuro-glial-vascular interface; acetonemic syndrome; hyperammonemia; blood-brain barrier; astrocytes; excitotoxicity; neuroinflammation; children*

Relevance

Metabolic intoxications in children, particularly acetonemic syndrome [3] and hyperammonemia [1, 2, 10], represent a serious clinical problem in pediatrics. "Prolonged hyperammonemia causes irreversible damage to the central nervous system leading to cortical atrophy, ventricular system enlargement, and inhibition of myelination processes, which can subsequently result in cognitive impairments, seizures, and cerebral palsy" [1, 2]. In turn, "acetoacetate and beta-hydroxybutyrate stimulate the activity of the Na-K-Cl cotransporter in endothelial cells of brain microvessels, making them more susceptible to damage" [58].

One of the most vulnerable targets in such conditions is the neuro-glial-vascular interface—a complex morphofunctional system that provides metabolic, barrier, and signaling interactions between neurons, glial cells (primarily astrocytes), and the brain's capillary network [4, 7]. Under normal conditions, this interface regulates the permeability of the blood-brain barrier (BBB), ensures substance exchange between blood and nervous tissue, maintains ionic balance, participates in the detoxification of neurotransmitters (particularly glutamate) and neutralizes ammonia through the synthesis of glutamine in astrocytes [4, 5, 6].

Morphologically, the neuro-glial-vascular interface consists of endothelial cells and their associated pericytes, astrocytes, neurons, and microglia [7]. Under physiological conditions, astrocytes are in close interaction with the endothelium, regulating metabolism and protecting neurons from toxic influences [4, 7]. Their ability to bind excess ammonia and maintain the acid-base homeostasis of brain tissue is of particular importance [9].

In acetonemic syndrome, due to the accumulation of ketone bodies, and in hyperammonemia—because of the excessive concentration of ammonia in the blood and tissues— the function of this interface is disrupted [9, 10]. Toxic metabolites penetrate the BBB [12], causing astrocyte swelling [13, 23, 24], sodium-potassium pump dysfunction [14], impaired glucose transport [15], activation of microglia, and increased production of pro-inflammatory cytokines (IL-1β, TNF-α) [16]. This is accompanied by neurotransmitter imbalance [17], loss

of BBB integrity [18], decreased neuronal activity, and eventually the development of encephalopathy, seizures, impaired consciousness, and delays in cognitive and psychomotor development.

Particularly concerning is the fact that, the neuro-glial system is morphofunctionally immature in childhood, and the BBB has increased permeability, which enhances the brain tissue's sensitivity to metabolic toxins [19]. Moreover, the compensatory capacity of a child's body is still limited, and signs of intoxication may develop rapidly, even with short-term exposure [20].

Despite the high clinical significance of these conditions, the morphofunctional changes of the neuro-glial-vascular interface in various forms of metabolic intoxication in children remain poorly understood [21]. The lack of clear understanding regarding the nature and dynamics of these changes prevents early detection of CNS damage, complicates prognosis, and hampers the development of personalized therapeutic approaches [22]. Therefore, targeted research into structural and functional changes of the neuro-glial-vascular interface in children with acetonemic syndrome and hyperammonemia becomes especially relevant, as it may improve diagnosis, prevent severe outcomes, and optimize the management of patients with metabolic crises.

Research objective

To analyze scientific approaches and review current literature on the morphofunctional changes of the neuroglial-vascular interface in children with metabolic intoxications (based on acetonemic syndrome and hyperammonemia) in order to identify the mechanisms of central nervous system damage, improve early diagnosis of neurotoxic complications, and substantiate approaches to personalized therapy**.**

Materials and methods

A systematic literature review with elements of narrative analysis was conducted to investigate the morphofunctional changes in the neuro-glial-vascular interface in children with metabolic intoxications, particularly in cases of acetonemic syndrome and hyperammonemia. The study followed the PRISMA (Preferred Reporting Items for Systematic Reviews and Meta-Analyses) guidelines for systematic reviews. Literature sources were searched in the following electronic databases: PubMed/MEDLINE, Web of Science Core Collection, Scopus, and Cochrane Library for the period 1990–2024, with additional searches performed via Google Scholar. English-language keywords and term combinations were used in the search, including "acetonemic syndrome," "hyperammonemia," "blood-brain barrier," "astrocyte swelling," "excitotoxicity," "neuroinflammation," and relevant MeSH terms.

The review included publications that met the following inclusion criteria: original studies, systematic reviews, and meta-analyses published in English; studies involving children from birth to 18 years of age; papers investigating the neurotoxic effects of acetonemic syndrome and/or hyperammonemia; and research on morphofunctional changes of the BBB in metabolic disorders. Experimental studies on animal models relevant to pediatric practice were also included. Exclusion criteria were as follows: conference abstracts without full texts, case reports with fewer than three patients, studies exclusively involving adult populations, publications unrelated to the neurotoxic effects of the studied syndromes, and duplicate publications.

The selection of sources was carried out in two stages: an initial screening based on titles and abstracts using the inclusion/exclusion criteria, followed by full-text review of the selected articles. Each study was independently assessed by two reviewers, with discrepancies resolved through discussion until consensus was reached. Additional relevant studies were identified through manual searches of reference lists from selected articles.

To assess the quality of the included studies, the following tools were used: the Newcastle-Ottawa Scale (NOS) for cohort and case-control studies, AMSTAR-2 for systematic reviews, and SYRCLE's Risk of Bias tool for animal studies. Evaluation criteria included methodological quality, appropriateness of study design to objectives, adequacy of statistical analysis, presence of control groups, and sample representativeness.

From each included publication, the following data were extracted: study characteristics (authors, year, country, design), population details (age, sex, sample size), research methods and diagnostic criteria, main findings and conclusions, and study limitations. A qualitative (narrative) synthesis of the data was conducted, with thematic grouping into the following categories: morphological changes of the neuro-glial-vascular interface, pathophysiological mechanisms of BBB disruption, disturbances in energy metabolism, neurotransmitter imbalances and excitotoxicity, inflammatory processes and microglial activation, clinical manifestations and diagnostic approaches, and therapeutic strategies.

Due to the heterogeneity of the included studies, a quantitative meta-analysis was deemed inappropriate.

Results

Changes in the structure of the neuro-glial-vascular interface in acetonemic syndrome and hyperammonemia are of key importance in the development of neurological symptoms and the progression of encephalopathy [1–10, 13, 15].

Morphofunctional disorganization of the neuro-glial-vascular interface. This interface, composed of neurons, astrocytes, endothelial cells of capillaries, pericytes, microglia, and the basal membrane, performs essential functions in metabolic exchange between blood and nervous tissue, regulation of BBB permeability, and maintenance of brain homeostasis [1–10, 13, 15]. In metabolic disorders characteristic of these syndromes, the BBB undergoes significant morphofunctional disorganization [20]. One of the earliest and consistent histological manifestations found in scientific studies is pronounced astrocyte swelling [1–10, 13, 15]. Biochemically, this phenomenon is caused by an excess of ammonia in the blood, which freely passes through

This article contains some figures that are displayed in color online but in black and white in the print edition

the BBB and enters brain tissue [1, 2, 5, 6, 9, 23, 24]. In the brain, ammonia is detoxified in astrocytes through the activity of the enzyme glutamine synthetase, which catalyzes the reaction of glutamine formation from glutamate and ammonia [1, 2, 5, 6, 9, 23, 24]. It has been proven that glutamine synthesized in large amounts can accumulate in astrocytes, creating osmotic pressure that leads to water influx into the cell and the development of intracellular (cytotoxic) edema [13]. Morphologically, this process is accompanied by an increase in astrocyte volume, destruction of their processes, deformation of contacts with capillaries, which impairs the metabolic support of neurons [23, 24].

Impairment of BBB function. Alongside the aforementioned changes, there is also a disruption in the functional state of the BBB [1–10, 13, 15]. With an excess of ketone bodies (in particular, β-hydroxybutyrate and acetoacetate) and ammonia, damage to endothelial cells of capillaries is observed. It has been established that this pathological process may be caused by oxidative stress, reduced activity of cellular respiration enzymes, and the disintegration of intercellular tight junctions [25, 26, 28, 29–34].

Oxidative stress occurs when the increase in energy output produced by aerobic metabolism leads to elevated formation of potentially harmful reactive oxygen species (ROS). During incomplete O_2 oxidation, ROS such as superoxide anion radical, hydrogen peroxide, and hydroxyl radical are formed. These highly reactive compounds are capable of damaging cellular proteins, lipids, and DNA. When the ROS burden in a cell exceeds its own antioxidant capacity, a state of oxidative stress arises. In the context of metabolic disorders, elevated concentrations of ketone bodies and ammonia potentiate oxidative stress, leading to endothelial dysfunction, impaired microcirculation, and intensified inflammatory responses. This creates a vicious cycle of damage, where metabolic disorders intensify oxidative stress, and oxidative stress in turn deepens metabolic disturbances, causing progressive tissue damage [34]. At the molecular level, this process manifests as decreased expression of claudin-5, occludin, and ZO-1 proteins, leading to increased BBB permeability [31]. Histochemically, it is accompanied by extravasation of plasma proteins (albumin, immunoglobulins), which can be detected in brain tissues, as well as swelling of the perivascular space, signs of hyperemia, and leukocyte diapedesis [35]. As a result, vasogenic edema develops, leading to compression of capillaries, impaired cerebral perfusion, and worsening ischemic injury to nervous tissue [35].

Astrocytic disturbances and effects on water-electrolyte balance. Special attention is warranted for the disruption of astrocytic contacts with capillaries. Normally, astrocyte end-feet form a glio-vascular mantle that covers almost the entire surface of brain capillaries and regulates the transport of water, ions, and energy substrates, particularly through the aquaporin AQP4 [36]. It has been shown that in acetonemia and hyperammonemia, these structures become disorganized, which is either accompanied by a decrease in AQP4 expression (disrupting osmoregulation) or by compensatory upregulation (which, conversely, enhances astrocyte swelling). Both mechanisms lead to pathological accumulation of fluid in brain tissue and disruption of metabolic exchange between neurons and capillaries, as reflected in the study by Rama Rao K. V. et al. [37]. To determine the potential role of aquaporins in astrocyte swelling, the authors measured AQP4 protein expression in cultured astrocytes exposed to 5 mM NH_4Cl. It was found that AQP4 levels significantly increased 10 hours after ammonia treatment and showed progressive growth up to 48 hours, preceding the onset of astrocyte swelling. The researchers concluded that AQP4 may be involved in astrocyte edema associated with hyperammonemic conditions [37].

Energy metabolism in neurons and astrocytes in acetonemia and hyperammonemia. The primary energy source for brain cells, particularly neurons and astrocytes—which require constant energy supply for maintaining electrical excitability, synaptic transmission, and osmoregulation—is glucose [38]. Its transport to brain tissue is facilitated by transporters—mainly GLUT1 in capillary endothelium and astrocytes [39], and GLUT3 in neurons [39]. Under acetonemia, there is competition for BBB transport between glucose and ketone bodies (especially β-hydroxybutyrate), which may reduce glucose entry into the brain [40].

Simultaneously, due to excess ammonia accumulating in brain tissue, the activity of the key glycolytic enzyme phosphofructokinase decreases, which further worsens ATP production. In astrocytes, energy flow is redirected toward ammonia detoxification (via the glutamine synthetase reaction), which diverts resources from supplying neurons with lactate—a key product of astrocytic metabolism necessary for neuronal function [41]. This mechanism is known as the astrocyte-neuron lactate shuttle (ANLS), which provides neurons with energy through their metabolic connection to astrocytes [41]. Normally, neuronal activity leads to glutamate release, which stimulates glycolysis in astrocytes and lactate production. Lactate is transported to neurons via monocarboxylate transporters and used as a readily available energy source. When this pathway is disrupted, particularly by the toxic effects of ammonia, lactate production and delivery to neurons decrease [41]. As a result, neurons do not receive enough energy substrate and experience energy starvation, impairing their function and viability.

A decrease in intracellular ATP levels leads to dysfunction of the Na^+/K^+-ATPase (sodium-potassium pump), which maintains the electrochemical gradient between the neuron's inner and outer membranes [42]. This pump actively removes three Na^+ ions from the cell and brings in two K^+ ions, which is necessary for restoring the resting potential after a nerve impulse. When this mechanism is inhibited, excessive accumulation of sodium in neurons and extracellular potassium is observed, which causes depolarization of the cell membrane, excessive excitability or impulse transmission blockade, and the opening of ion channels that allow uncontrolled calcium influx [42–44]. Excess intracellular Ca^{2+} activates enzyme cascades, particularly phospholipases, proteinases, and endonucleases, ultimately leading to membrane damage, DNA fragmentation, and the initiation of apoptosis or necrosis of neurons [42–44].

Neurotransmitter imbalance and its role in the development of encephalopathy. Neurotransmitter imbalance is a key pathophysiological mechanism in the development of central nervous system damage in acetonemic syndrome and hyperammonemia [2]. One of the key factors in the impairment of neuronal function in many neurological pathologies is the excessive accumulation of glutamate [2]. Glutamate activates ionotropic postsynaptic receptors—N-methyl-D-aspartate (NMDA) and AMPA/kainate receptors—causing depolarization of the neuronal membrane through the influx of Na^+ ions and the initiation of an action potential. Normally, after performing its signaling function, glutamate should be rapidly removed from the synaptic cleft [2]. If this does not occur, two pathological effects arise: excessive stimulation of receptors, which complicates the recognition of new signals and may cause cellular edema; and glutamate that escapes the synapse can activate extra synaptic NMDA receptors, causing Ca^{2+} influx and the initiation of cell death cascades [2].

Astrocytes in turn play a critical role in preventing excitotoxicity. They provide rapid glutamate clearance from the extracellular environment due to high expression of specific transporters—GLT-1 (EAAT2) and GLAST (EAAT1). These belong to the excitatory amino acid transporter family (EAAT1–5), are electrogenic and sodium-dependent, and are capable of transporting glutamate against its concentration gradient through co-transport with Na^+, H^+, and K^+ [2]. Astrocytes compensate for associated changes in membrane potential and pH through ion channel systems (particularly KIR4.1) and exchangers, as well as through the ability to dissipate ionic changes throughout the astrocytic network via connexin-dependent gap junctions [2].

Once captured, glutamate can enter several metabolic pathways within astrocytes. One of them is its conversion to α-ketoglutarate via the action of glutamate dehydrogenase or transaminase, followed by entry into the Krebs cycle [2]. Another key pathway is the transformation of glutamate into the non-toxic glutamine via the enzyme glutamine synthetase. Glutamine is transported back into the extracellular space using the Na^+-dependent transporter SNAT3 and enters neurons, where phosphate-activated glutaminase converts it back to glutamate [2]. Thus, the glutamate-glutamine cycle occurs, which is considered a key mechanism for maintaining the balance of excitatory transmission and neuronal metabolism.

Impairment of the function or expression of glutamate transporters, especially EAAT1 and EAAT2, leads to elevated extracellular glutamate levels, promoting the development of excitotoxicity, neuroinflammation, and oxidative stress [2, 34].

In this case, the excessive amount of glutamate not only fails to be cleared from the synaptic cleft but can also be released into the extracellular space, activating ionotropic (NMDA, AMPA, kainate) and metabotropic receptors on the surface of neurons [2, 45, 46]. Activation of NMDA receptors is particularly dangerous, leading to massive Ca^{2+} influx into the cell and initiating the so-called "excitotoxicity" cascade [2, 45, 46]. This process is accompanied by the activation of calcium-dependent enzymes (NO synthase, phospholipases, caspases), contributing to oxidative stress, disruption of cell membrane structure, and mitochondrial dysfunction. As noted by Todd and Hardingham, "If glutamate escapes the synaptic region, it can activate extrasynaptic NMDA receptors: excessive Ca^{2+} influx through these extrasynaptic NMDA receptors induces signaling cascades that initiate cell death programs" [46].

Inflammatory process and microglial activation. "In the 'resting' state, microglia vigorously infiltrate the local microenvironment, extending and retracting motile processes equipped with a vast number of surface receptors. Detection of any specific or nonspecific stimuli related to infection or tissue damage stimulates microglia to perform an appropriate response" [47]. In response to infectious or damaging signals, microglia transition to a reactive state, changing both morphology and functional activity [47]. Activated microglia phenotypes are traditionally divided into M1 (pro-inflammatory, neurotoxic) and M2 (anti-inflammatory, neuroprotective), although modern transcriptomic and proteomic studies show that such classification is conditional, as in vivo microglia display a wide spectrum of mixed functional states [47]. M1-like microglia produce pro-inflammatory cytokines (IL-1β, TNF-α, IL-6), chemokines, eicosanoids, and reactive oxygen/nitrogen species; this, in turn, leads to further damage to neurons and astrocytes [47]. M2-like microglia, on the contrary, promote inflammation resolution and tissue repair by producing anti-inflammatory mediators and enzymes, including arginase [47]. Histochemically, activated microglia are characterized by elevated expression of specific markers such as CD68, Iba1, and major histocompatibility complex class II (MHC II), which is used as an indicator of the cell's immunological activity [48]. The release of pro-inflammatory cytokines, particularly IL-1β, TNF-α, and IL-6, in this context exacerbates damage to surrounding neurons and astrocytes, creating a pathological cycle of inflammation [47, 48].

Clinical manifestations of acetonemic syndrome and hyperammonemia. The clinical consequences of acetonemic syndrome and hyperammonemia are closely associated with the neurotoxic effects of metabolic disturbances affecting the functioning of the central nervous system in children [49]. Common manifestations include seizure syndrome, transient or prolonged consciousness disturbances (ranging from stupor to coma), coordination disorders, irritability or conversely lethargy, as well as cognitive impairments—such as delays in speech, language and psychomotor development [49].

Pathophysiologically, these symptoms are caused by the action of elevated concentrations of ketone bodies and ammonia on brain tissue [50–51]. The presence of ketone bodies exacerbates this effect by lowering pH in brain tissues and impairing the function of neuroglial structures. This contributes to impaired synaptic transmission, reduced activity of the GABAergic (inhibitory) system, and, consequently, the development of seizure syndrome [50–51]. The obtained data are shown schematically in ***Fig. 1***.

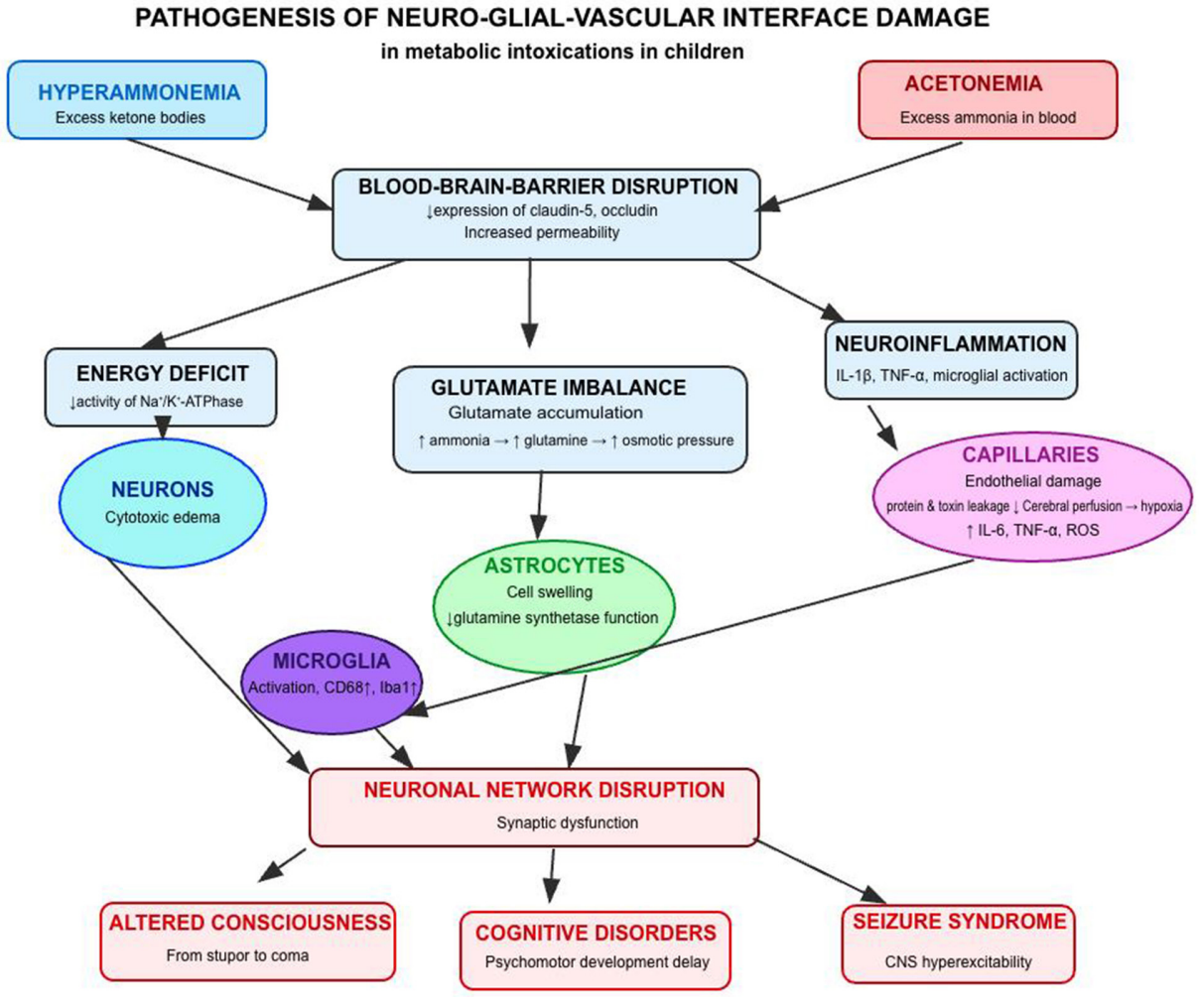

Fig. 1. Pathogenesis of neuro-glial-vascular interface damage in metabolic intoxications in children

Morphofunctional changes in the central nervous system. At the morphofunctional level, histologically, swelling of astrocytes, perivascular infiltrates, neuronal destruction, and activated microglia can be observed. Lesions predominantly affect subcortical structures, cerebral cortex, hippocampus, and cerebellum — areas most sensitive to hypoxia and metabolic imbalance [52-55].

Therapeutic aspects of managing pediatric patients with disturbances of the neuro-glial-vascular interface in metabolic intoxications, particularly in acetonemic syndrome and hyperammonemia, should be multi-step and include comprehensive treatment aimed at eliminating toxic metabolites, restoring water-electrolyte balance, as well as stabilizing structural and functional disorders caused by the effects of toxins on the neuro-glial-vascular interface.

In cases of severe hypoglycemia, intravenous administration of glucose is indicated to restore its normal level in the blood [56]. One of the most important aspects of treatment is the correction of elevated ammonia levels in hyperammonemia and ketone bodies in acetonemic syndrome.

For hyperammonemia, pharmacological agents such as L-arginine or sodium benzoate are used to help reduce ammonia levels, which have a toxic effect on the nervous system. Treatment begins with an initial dose and continues as maintenance therapy depending on the patient's age and weight. L-arginine can be prescribed at a dose of 250–400 mg/kg (maximum 12 g) for children up to 20 kg, and for children over 20 kg — 250 mg/kg up to 12 g per day [56].

Sodium benzoate and sodium phenylacetate are used to improve detoxification. For children up to 20 kg, the dosage is 250 mg/kg; for children over 20 kg, the dosage is 5.5 g/m² per day, not exceeding 12 g/day [56].

Other drugs used to correct disturbances related to hyperammonemia include carnitine, which promotes the removal of toxic metabolic products. It is administered at an initial dose of 50 mg/kg followed by a maintenance dose of 100 mg/kg per day divided into 4 doses [56]. Coenzyme therapy, including biotin and hydroxocobalamin, is also applied to help normalize metabolic processes in the body [56]. To reduce levels of toxic metabolites, particularly ammonia, osmotic laxatives (polyethylene glycol) and antibacterial drugs such as rifaximin are recommended [56].

Successful management of patients with acetonemic syndrome and hyperammonemia requires continuous monitoring of ammonia levels, ketone bodies, electrolytes, and other biochemical parameters [56].

Treatment must be individualized, with dosage adjustments and selection of therapeutic measures depending on the dynamics of the patient's clinical condition. Comorbidities, as well as the age and other individual characteristics of children, should also be taken into account. Since the diseases may be accompanied not only by physical but also psychological changes, it is important to provide psychological support for both patients and their families. This is especially relevant for children who may be frightened by frequent hospitalizations, pain, and the need for prolonged treatment.

Moreover, attention should be paid to preventing relapses through dietary and lifestyle correction, especially in children with a burdened hereditary background or predisposition to metabolic disorders.

Conclusions

Morphofunctional changes of the neuro-glial-vascular interface in acetonemic syndrome and hyperammonemia in children are associated with disruptions of the BBB structure, manifested by decreased expression of tight junction proteins such as claudin-5, occludin, and ZO-1. This is accompanied by cytotoxic astrocyte swelling, disorganization of astrocytic endfeet, and disturbed aquaporin expression. The main mechanisms of central nervous system injury are energy imbalance due to impaired glycolysis and mitochondrial dysfunction, disruption of sodium-potassium pumps leading to depolarization of cell membranes, as well as dysregulation of neurotransmitter balance, particularly excessive glutamate accumulation causing excitotoxicity. An important aspect is microglial activation with increased expression of CD68, Iba1, MHC II, and secretion of proinflammatory cytokines.

For the early diagnosis of neurotoxic complications, comprehensive monitoring of biomarkers such as S100β, NSE, GFAP for BBB damage, as well as IL-1β, TNF-α for neuroinflammation and indicators of neuronal dysfunction in serum and cerebrospinal fluid is necessary. Personalized therapy should consider different mechanisms of injury, including the use of membrane stabilizers for BBB damage, energotropic drugs to correct energy metabolism disturbances, and modulators of glutamatergic transmission for treating excitotoxicity. A multidisciplinary approach—aimed at early detection and correction of cognitive and behavioral disorders, as well as individualized neurorehabilitation programs considering age-related neuroplasticity features — is essential.

To improve diagnosis and treatment, educational programs for pediatricians and family doctors should be developed to facilitate in early diagnosis of neuro-glial-vascular interface disorders. Additionally, studies of potential neuroprotective agents that can stabilize astrocyte-endothelial interactions should be conducted, as well as preventive strategies developed for children with hereditary predisposition to metabolic disorders. Establishing a national patient registry would enable the study of long-term outcomes and evaluation of the effectiveness of various therapeutic approaches, improving the diagnosis and management of pediatric metabolic intoxications.

Disclosure

Conflict of interest

The authors declare no conflict of interest.

Funding

The research had no sponsor support.

References

1. Cagnon L, Braissant O. Hyperammonemia-induced toxicity for the developing central nervous system. Brain Res Rev. 2007 Nov;56(1):183-97. doi: 10.1016/j.brainresrev.2007.06.026
2. Rojas CR, Chapman J, Regier D. Hyperammonemia in the Pediatric Emergency Department. Pediatr Emerg Care. 2024 Feb 1;40(2):156-161. doi: 10.1097/PEC.0000000000003121
3. Khilchevska VS. Clinical and anamnestic features of acetonemic syndrome in children with patholigy of the digestive system. Journal of Education, Health and Sport. 2018 Aug 14;8(8):701-5. https://apcz.umk.pl/JEHS/article/view/5812
4. Banerjee S, Bhat MA. Neuron-glial interactions in blood-brain barrier formation. Annu Rev Neurosci. 2007;30:235-58. doi: 10.1146/annurev.neuro.30.051606.094345
5. Butterworth RF. Glutamate transporter and receptor function in disorders of ammonia metabolism. Ment Retard Dev Disabil Res Rev. 2001;7(4):276-9. doi: 10.1002/mrdd.1038
6. Hawkins RA, Viña JR. How Glutamate Is Managed by the Blood-Brain Barrier. Biology (Basel). 2016 Oct 8;5(4):37. doi: 10.3390/biology5040037
7. Lochhead JJ, Williams EI, Reddell ES, Dorn E, Ronaldson PT, Davis TP. High Resolution Multiplex Confocal Imaging of the Neurovascular Unit in Health and Experimental Ischemic Stroke. Cells. 2023 Feb 17;12(4):645. doi: 10.3390/cells12040645
8. Smith BC, Tinkey RA, Shaw BC, Williams JL. Targetability of the neurovascular unit in inflammatory diseases of the central nervous system. Immunol Rev. 2022 Oct;311(1):39-49. doi: 10.1111/imr.13121
9. Cooper AJ. Role of glutamine in cerebral nitrogen metabolism and ammonia neurotoxicity. Ment Retard Dev Disabil Res Rev. 2001;7(4):280-6. doi: 10.1002/mrdd.1039
10. Parekh PJ, Balart LA. Ammonia and Its Role in the Pathogenesis of Hepatic Encephalopathy. Clin Liver Dis. 2015 Aug;19(3):529-37. doi: 10.1016/j.cld.2015.05.002
11. Hasselbalch SG, Knudsen GM, Jakobsen J, Hageman LP, Holm S, Paulson OB. Blood-brain barrier permeability of glucose and ketone bodies during short-term starvation in humans. Am J Physiol. 1995 Jun;268(6 Pt 1):E1161-6. doi: 10.1152/ajpendo.1995.268.6.E1161
12. Zhang J, Zhang M, Sun B, Li Y, Xu P, Liu C, Liu L, Liu X. Hyperammonemia enhances the function and expression of P-glycoprotein and Mrp2 at the blood-brain barrier through NF-κB. J Neurochem. 2014 Dec;131(6):791-802. doi: 10.1111/jnc.12944
13. Jayakumar AR, Norenberg MD. The Na-K-Cl Co-transporter in astrocyte swelling. Metab Brain Dis. 2010 Mar;25(1):31-8. doi: 10.1007/s11011-010-9180-3
14. Rangroo Thrane V, Thrane AS, Wang F, Cotrina ML, Smith NA, Chen M, Xu Q, Kang N, Fujita T, Nagelhus EA, Nedergaard M. Ammonia triggers neuronal disinhibition and seizures by impairing astrocyte potassium buffering. Nat Med. 2013 Dec;19(12):1643-8. doi: 10.1038/nm.3400
15. Patching SG. Glucose Transporters at the Blood-Brain Barrier: Function, Regulation and Gateways for Drug Delivery. Mol Neurobiol. 2017 Mar;54(2):1046-1077. doi: 10.1007/s12035-015-9672-6
16. Smith JA, Das A, Ray SK, Banik NL. Role of pro-inflammatory cytokines released from microglia in neurodegenerative diseases. Brain Res Bull. 2012 Jan 4;87(1):10-20. doi: 10.1016/j.brainresbull.2011.10.004
17. Tang C, Jin Y, Wang H. The biological alterations of synapse/synapse formation in sepsis-associated encephalopathy. Front Synaptic Neurosci. 2022 Dec 2;14:1054605. doi: 10.3389/fnsyn.2022.1054605
18. Doney E, Cadoret A, Dion-Albert L, Lebel M, Menard C. Inflammation-driven brain and gut barrier dysfunction in

stress and mood disorders. Eur J Neurosci. 2022 May;55(9-10):2851-2894. doi: 10.1111/ejn.15239
19. Keep RF, Ennis SR, Beer ME, Betz AL. Developmental changes in blood-brain barrier potassium permeability in the rat: relation to brain growth. J Physiol. 1995 Oct 15;488 (Pt 2)(Pt 2):439-48. doi: 10.1113/jphysiol.1995.sp020978
20. Baker PR 2nd. Recognizing and Managing a Metabolic Crisis. Pediatr Clin North Am. 2023 Oct;70(5):979-993. doi: 10.1016/j.pcl.2023.05.009
21. Wu BA, Chand KK, Bell A, Miller SL, Colditz PB, Malhotra A, Wixey JA. Effects of fetal growth restriction on the perinatal neurovascular unit and possible treatment targets. Pediatr Res. 2024 Jan;95(1):59-69. doi: 10.1038/s41390-023-02805-w
22. Sugiyama Y, Murayama K. Acute Encephalopathy Caused by Inherited Metabolic Diseases. J Clin Med. 2023 May 31;12(11):3797. doi: 10.3390/jcm12113797
23. McConnell HL, Li Z, Woltjer RL, Mishra A. Astrocyte dysfunction and neurovascular impairment in neurological disorders: Correlation or causation? Neurochem Int. 2019 Sep;128:70-84. doi: 10.1016/j.neuint.2019.04.005
24. Patabendige A, Singh A, Jenkins S, Sen J, Chen R. Astrocyte Activation in Neurovascular Damage and Repair Following Ischaemic Stroke. Int J Mol Sci. 2021 Apr 20;22(8):4280. doi: 10.3390/ijms22084280
25. Gowrikumar S, Tarudji A, McDonald BZ, Balusa SS, Kievit FM, Dhawan P. Claudin-1 impairs blood-brain barrier by downregulating endothelial junctional proteins in traumatic brain injury. Tissue Barriers. 2025 Feb 28:2470482. doi: 10.1080/21688370.2025.2470482
26. Liu G, Wang Q, Tian L, Wang M, Duo D, Duan Y, Lin Y, Han J, Jia Q, Zhu J, Li X. Blood-Brain Barrier Permeability is Affected by Changes in Tight Junction Protein Expression at High-Altitude Hypoxic Conditions-this may have Implications for Brain Drug Transport. AAPS J. 2024 Aug 6;26(5):90. doi: 10.1208/s12248-024-00957-z
27. Zou P, Yang F, Ding Y, Zhang D, Liu Y, Zhang J, Wu D, Wang Y. Lipopolysaccharide downregulates the expression of ZO-1 protein through the Akt pathway. BMC Infect Dis. 2022 Oct 5;22(1):774. doi: 10.1186/s12879-022-07752-1
28. Hong F, Mu X, Ze Y, Li W, Zhou Y, Ji J. Damage to the Blood Brain Barrier Structure and Function from Nano Titanium Dioxide Exposure Involves the Destruction of Key Tight Junction Proteins in the Mouse Brain. J Biomed Nanotechnol. 2021 Jun 1;17(6):1068-1078. doi: 10.1166/jbn.2021.3083
29. Jiao H, Wang Z, Liu Y, Wang P, Xue Y. Specific role of tight junction proteins claudin-5, occludin, and ZO-1 of the blood-brain barrier in a focal cerebral ischemic insult. J Mol Neurosci. 2011 Jun;44(2):130-9. doi: 10.1007/s12031-011-9496-4
30. Alluri H, Peddaboina CS, Tharakan B. Determination of Tight Junction Integrity in Brain Endothelial Cells Based on Tight Junction Protein Expression. Methods Mol Biol. 2024;2711:235-240. doi: 10.1007/978-1-0716-3429-5_19
31. Wen J, Qian S, Yang Q, Deng L, Mo Y, Yu Y. Overexpression of netrin-1 increases the expression of tight junction-associated proteins, claudin-5, occludin, and ZO-1, following traumatic brain injury in rats. Exp Ther Med. 2014 Sep;8(3):881-886. doi: 10.3892/etm.2014.1818
32. Yi X, Xu C, Huang P, Zhang L, Qing T, Li J, Wang C, Zeng T, Lu J, Han Z. 1-Trifluoromethoxyphenyl-3-(1-Propionylpiperidin-4-yl) Urea Protects the Blood-Brain Barrier Against Ischemic Injury by Upregulating Tight Junction Protein Expression, Mitigating Apoptosis and Inflammation *InVivo* and *In Vitro* Model. Front Pharmacol. 2020 Aug 7;11:1197. doi: 10.3389/fphar.2020.01197
33. Meroni E, Papini N, Criscuoli F, Casiraghi MC, Massaccesi L, Basilico N, Erba D. Metabolic Responses in Endothelial Cells Following Exposure to Ketone Bodies. Nutrients. 2018 Feb 22;10(2):250. doi: 10.3390/nu10020250
34. Tebay LE, Robertson H, Durant ST, Vitale SR, Penning TM, Dinkova-Kostova AT, Hayes JD. Mechanisms of activation of the transcription factor Nrf2 by redox stressors, nutrient cues, and energy status and the pathways through which it attenuates degenerative disease. Free Radic Biol Med. 2015 Nov;88(Pt B):108-146. doi: 10.1016/j.freeradbiomed.2015.06.021
35. Solár P, Zamani A, Lakatosová K, Joukal M. The blood-brain barrier and the neurovascular unit in subarachnoid hemorrhage: molecular events and potential treatments. Fluids Barriers CNS. 2022 Apr 11;19(1):29. doi: 10.1186/s12987-022-00312-4
36. Haj-Yasein NN, Vindedal GF, Eilert-Olsen M, Gundersen GA, Skare Ø, Laake P, Klungland A, Thorén AE, Burkhardt JM, Ottersen OP, Nagelhus EA. Glial-conditional deletion of aquaporin-4 (Aqp4) reduces blood-brain water uptake and confers barrier function on perivascular astrocyte endfeet. Proc Natl Acad Sci U S A. 2011 Oct 25;108(43):17815-20. doi: 10.1073/pnas.1110655108
37. Rama Rao KV, Chen M, Simard JM, Norenberg MD. Increased aquaporin-4 expression in ammonia-treated cultured astrocytes. Neuroreport. 2003 Dec 19;14(18):2379-82. doi: 10.1097/00001756-200312190-00018
38. Beard E, Lengacher S, Dias S, Magistretti PJ, Finsterwald C. Astrocytes as Key Regulators of Brain Energy Metabolism: New Therapeutic Perspectives. Front Physiol. 2022 Jan 11;12:825816. doi: 10.3389/fphys.2021.825816. Erratum in: Front Physiol. 2022 Feb 25;13:867827. doi: 10.3389/fphys.2022.867827
39. Leino RL, Gerhart DZ, van Bueren AM, McCall AL, Drewes LR. Ultrastructural localization of GLUT 1 and GLUT 3 glucose transporters in rat brain. J Neurosci Res. 1997 Sep 1;49(5):617-26. doi: 10.1002/(SICI)1097-4547(19970901)49:5<617::AID-JNR12>3.0.CO;2-S
40. Xu W, Borges K. Case for supporting astrocyte energetics in glucose transporter 1 deficiency syndrome. Epilepsia. 2024 Aug;65(8):2213-2226. doi: 10.1111/epi.18013
41. Kim Y, Dube SE, Park CB. Brain energy homeostasis: the evolution of the astrocyte-neuron lactate shuttle hypothesis. Korean J Physiol Pharmacol. 2025 Jan 1;29(1):1-8. doi: 10.4196/kjpp.24.388
42. Ritter L, Kleemann D, Hickmann FH, Amaral AU, Sitta Â, Wajner M, Ribeiro CA. Disturbance of energy and redox homeostasis and reduction of Na+,K+-ATPase activity provoked by in vivo intracerebral administration of ethylmalonic acid to young rats. Biochim Biophys Acta. 2015 May;1852(5):759-67. doi: 10.1016/j.bbadis.2015.01.003
43. Tian J, Xie ZJ. The Na-K-ATPase and calcium-signaling microdomains. Physiology (Bethesda). 2008 Aug;23:205-11. doi: 10.1152/physiol.00008.2008
44. Yuan Z, Cai T, Tian J, Ivanov AV, Giovannucci DR, Xie Z. Na/K-ATPase tethers phospholipase C and IP3 receptor into a calcium-regulatory complex. Mol Biol Cell. 2005 Sep;16(9):4034-45. doi: 10.1091/mbc.e05-04-0295
45. Churn SB, Limbrick D, Sombati S, DeLorenzo RJ. Excitotoxic activation of the NMDA receptor results in inhibition of calcium/calmodulin kinase II activity in cultured hippocampal neurons. J Neurosci. 1995 Apr;15(4):3200-14. doi: 10.1523/JNEUROSCI.15-04-03200.1995
46. Todd AC, Hardingham GE. The Regulation of Astrocytic Glutamate Transporters in Health and Neurodegenerative Diseases. Int J Mol Sci. 2020 Dec 17;21(24):9607. doi: 10.3390/ijms21249607
47. Czapski GA, Strosznajder JB. Glutamate and GABA in Microglia-Neuron Cross-Talk in Alzheimer's Disease. Int J Mol Sci. 2021 Oct 28;22(21):11677. doi: 10.3390/ijms222111677
48. Hendrickx DAE, van Eden CG, Schuurman KG, Hamann J, Huitinga I. Staining of HLA-DR, Iba1 and CD68 in human microglia reveals partially overlapping expression depending on cellular morphology and pathology. J Neuroimmunol. 2017 Aug 15;309:12-22. doi: 10.1016/j.jneuroim.2017.04.007
49. Gropman AL, Summar M, Leonard JV. Neurological implications of urea cycle disorders. J Inherit Metab Dis. 2007 Nov;30(6):865-79. doi: 10.1007/s10545-007-0709-5
50. McNally MA, Hartman AL. Ketone bodies in epilepsy. J Neurochem. 2012 Apr;121(1):28-35. doi: 10.1111/j.1471-4159.2012.07670.x
51. Norenberg MD, Rao KV, Jayakumar AR. Mechanisms of ammonia-induced astrocyte swelling. Metab Brain Dis. 2005 Dec;20(4):303-18. doi: 10.1007/s11011-005-7911-7
52. Jayakumar AR, Tong XY, Ruiz-Cordero R, Bregy A, Bethea JR, Bramlett HM, Norenberg MD. Activation of NF-κB mediates astrocyte swelling and brain edema in traumatic

brain injury. J Neurotrauma. 2014 Jul 15;31(14):1249-57. doi: 10.1089/neu.2013.3169
53. Sapkota A, Halder SK, Milner R. Blood-brain barrier disruption and microglial activation during hypoxia and post-hypoxic recovery in aged mice. Brain Commun. 2024 Dec 17;7(1):fcae456. doi: 10.1093/braincomms/fcae456
54. Cui C, Jiang X, Wang Y, Li C, Lin Z, Wei Y, Ni Q. Cerebral Hypoxia-Induced Molecular Alterations and Their Impact on the Physiology of Neurons and Dendritic Spines: A Comprehensive Review. Cell Mol Neurobiol. 2024 Aug 6;44(1):58. doi: 10.1007/s10571-024-01491-4
55. Bhalala US, Koehler RC, Kannan S. Neuroinflammation and neuroimmune dysregulation after acute hypoxic-ischemic injury of developing brain. Front Pediatr. 2015 Jan 14;2:144. doi: 10.3389/fped.2014.00144
56. Bélanger-Quintana A, Arrieta Blanco F, Barrio-Carreras D, Bergua Martínez A, Cañedo Villarroya E, García-Silva MT, Lama More R, Martín-Hernández E, López AM, Morales-Conejo M, Pedrón-Giner C, Quijada-Fraile P, Stanescu S, Casanova MM. Recommendations for the Diagnosis and Therapeutic Management of Hyperammonaemia in Paediatric and Adult Patients. Nutrients. 2022 Jul 2;14(13):2755. doi: 10.3390/nu14132755
57. S3-Leitlinie Diagnostik und Therapie von Harnstoffzyklusstörungen [S3 guideline on diagnosis and therapy of urea cycle disorders]. Arbeitsgemeinschaft der Wissenschaftlichen Medizinischen Fachgesellschaften (AWMF); 2020. https://register.awmf.org/de/leitlinien/detail/027-006
58. Azova S, Rapaport R, Wolfsdorf J. Brain injury in children with diabetic ketoacidosis: Review of the literature and a proposed pathophysiologic pathway for the development of cerebral edema. Pediatr Diabetes. 2021 Mar;22(2):148-160. doi: 10.1111/pedi.13152

Review article

Ukrainian Neurosurgical Journal. 2025;31(4):11-19
doi: 10.25305/unj.333217

Platelet-rich plasma in discogenic pain: therapeutic potential of multifactorial action

Mykhailo V. Khyzhnyak [1], Iryna G. Vasilyeva [2], Yuriy G. Gafiychuk [3]

[1] Department of Miniinvasive and Laser Spinal Neurosurgery, Romodanov Neurosurgery Institute, Kyiv, Ukraine
[2] Department of Neurobiochemistry, Romodanov Neurosurgery Institute, Kyiv, Ukraine
[3] Neurosurgery Department, Military Medical Clinical Center of the Southern Region, Odesa, Ukraine

Received: 20 June 2025
Accepted: 17 July 2025

Address for correspondence:
Iryna G. Vasilyeva, Department of Neurobiochemistry, Romodanov Neurosurgery Institute, 32 Platona Maiborody st., Kyiv, 04050, Ukraine, e-mail: vigvasileva@gmail.com

Intervertebral disc degeneration (IVDD) is one of the leading causes of chronic low back pain and disability. The key pathogenetic mechanism of IVDD is chronic inflammation, which leads to extracellular matrix catabolism and the death of disc cells. It has been established that these changes are based on the activation of pro-inflammatory signaling cascades, particularly NF-κB, MAPK, and JAK/STAT pathways, as well as the induction of caspase-dependent apoptosis.

Objective: To summarize the current understanding of the molecular signaling pathways involved in degenerative processes within the intervertebral disc, and to elucidate the mechanisms of action of platelet-rich plasma (PRP) components capable of modulating these pathways.

Materials and methods: A comprehensive analysis of contemporary experimental and clinical studies was performed to evaluate the effects of the main growth factors present in PRP (TGF-β, PDGF, IGF-1, FGF, CTGF, EGF, HGF) on signaling pathways in intervertebral disc cells associated with catabolism, apoptosis, and inflammation.

Results: PRP-derived factors exert their effects predominantly through activation of the Smad, PI3K/AKT, MAPK, and JAK/STAT pathways while attenuating NF-κB activity, leading to decreased levels of pro-inflammatory cytokines (IL-1β, TNF-α) and metalloproteinases (MMPs, ADAMTS). These effects are accompanied by enhanced expression of type II collagen and aggrecan, stabilization of the extracellular matrix, restoration of tissue homeostasis and increased cell proliferation.

Conclusions: PRP therapy demonstrates considerable potential as a pathogenetically oriented regenerative strategy for the treatment of IVDD. Its efficacy arises from a multimodal influence on inflammatory, catabolic, and apoptotic pathways. Further clinical research is warranted to standardize treatment protocols and confirm the long-term therapeutic effectiveness of PRP.

Keywords: *intervertebral disc; degeneration; platelet-rich plasma; growth factors; NF-κB; signaling pathways; regeneration.*

Introduction

Intervertebral disc degeneration (IVDD) is a major cause of chronic low back pain and one of the most common reasons for disability worldwide (affecting more than 600 million people), leading to significant social and economic burdens. Discogenic pain arises as a result of inflammation within the intervertebral disc (IVD), which activates nociceptive receptors and triggers pain signal transmission to the central nervous system. Inflammation of the IVD is accompanied by the accumulation of pro-inflammatory cytokines such as TNF-α (tumor necrosis factor-α), IL-1β (interleukin 1β), IL-6 (interleukin-6), prostaglandins (PGE2, PGI2), bradykinin, and matrix metalloproteinases (MMPs). The main nociceptors involved in discogenic pain include transient receptor potential vanilloid 1 (TRPV1), which are activated by inflammation, heat, and acidic pH; ASIC3 (acid-sensing ion channel 3), which responds to pH reduction during degeneration; and P2X3 (ATP receptor), which is activated under mechanical stress [1]. Prolonged exposure to pain mediators leads to nociceptor sensitization and a lowered activation threshold, resulting in pain even from minimal stimuli. The transmission of pain signals to the thalamus occurs via the spinothalamic tract, forming both sensory (localization and intensity) and emotional aspects of pain perception (through the limbic system, contributing to the affective-emotional component of pain perception). When pain becomes chronic, the spinal cord and brain adapt to constant stimulation, characterized by increased expression of NMDA-receptors (enhancing pain signaling) and decreased activity of inhibitory neurons, such as gamma-aminobutyric acid (GABA) and glycine [2]. Thus, discogenic pain represents a complex mechanism encompassing both peripheral (inflammatory and nociceptor activation) and central pain signal transmission processes.

Initially, pro-inflammatory cytokines are produced predominantly by resident disc cells. Nucleus pulposus (NP) cells, annulus fibrosus (AF) cells, and senescent cells produce pro-inflammatory cytokines in response to mechanical or oxidative stress and other external stressors [3]. These cytokines spread through the disc tissue via exocytosis, membrane vesicles, and diffusion. The intervertebral disc is normally poorly innervated and vascularized; however, during degeneration, neovascularization and the ingrowth of nociceptive nerve endings into the annulus fibrosus and vertebral endplates occur [4]. In healthy discs, immune cells are absent, but neovascularization allows immune cell infiltration. Infiltrated M1-type macrophages activate TNF-α, IL-1β, and IL-6 receptors. TNF-α, in turn, activates NF-κB (Nuclear Factor kappa-light-chain-enhancer of activated B cells), which promotes the expression of pro-inflammatory cytokine genes. Consequently, the inflammatory process within the IVD can become self-amplifying and capable of persisting even after resolution of the initial trigger has resolved. NF-κB activation is accompanied by the progression of catabolic processes, with increased synthesis of metalloproteinases and aggrecanases (ADAMTS) that degrade key extracellular matrix components such as aggrecan and collagen type II. As a result of catabolic pathway activation in IVD cells, anabolic signaling pathways (TGF-β and PI3K/Akt — phosphoinositide 3-kinase/RAC-alpha serine/threonine-protein kinase), which are responsible for maintaining collagen and proteoglycan synthesis, lose their capacity to sustain matrix homeostasis [3].

A wide range of conservative methods aimed at reducing discogenic pain has been tested for its therapy. Currently, as an alternative to symptomatic procedures, new therapeutic options are being explored that target the inhibition of signaling pathways involved in degenerative processes and the activation of anabolic mechanisms. Therapeutic strategies aimed at modulating these pathways have the potential to slow down or halt the degenerative process. Autologous platelet-rich plasma (PRP) is considered a promising approach for regenerative treatment.

Growth factors released from platelets are believed to play an essential role in reducing inflammation and can also induce cellular proliferation and matrix remodeling. The most relevant growth factors present in PRP include transforming growth factor-β (TGF-β), platelet-derived growth factor (PDGF), fibroblast growth factor (FGF), insulin-like growth factor-1 (IGF-1), connective tissue growth factor (CTGF), epidermal growth factor (EGF), and hepatocyte growth factor (HGF). It is known that IVD cells express receptors for EGF, IGF, HGF, CTGF, PDGF, FGF, and TGF. These receptors play a key role in maintaining disc homeostasis, regulating cell proliferation and differentiation, and responding to tissue injury. The expression and activation of these receptors are critical for preserving the structure and function of the IVD, as well as its capacity for recovery following damage [5, 6].

Randomized controlled trials investigating the effects of PRP on IVD cells following direct injection into the nucleus pulposus have demonstrated pain reduction, improved functionality, and long-lasting therapeutic outcomes. A relevant current objective is to further investigate the mechanisms underlying catabolic activation in IVD cells, as well as the molecular pathways through which PRP components may inhibit degenerative processes in the disc [7].

Objective: To summarize current knowledge on the molecular signaling pathways involved in degenerative processes of the intervertebral disc, as well as the mechanisms of action of platelet-rich plasma components capable of modulating these processes.

Signaling pathways involved in degenerative processes of the intervertebral disc

NF-κB signaling pathway – a catabolic activator in intervertebral disc degeneration

The NF-κB signaling pathway in IVD tissues plays a crucial role in regulating inflammatory processes and cellular responses to stress stimuli. Activation of NF-κB in NP and AF cells is associated with enhanced inflammation, extracellular matrix degradation, apoptosis induction, and the progression of IVDD [8]. The main activators of NF-κB include cytokines TNF-α and IL-1β, mechanical and oxidative stress, hypoxia, microbial lipopolysaccharides (LPS), and viral infection [9–12].

Signal transduction from ligands to receptors via adaptor proteins activates the IKK complex (IKKα, IKKβ, IKKγ), followed by deactivation of the inhibitor IκB, which normally retains NF-κB in an inactive state within the cytoplasm. As a result of IκB phosphorylation and degradation, NF-κB is released. The liberated NF-κB p65/p50 dimer translocates to the nucleus, where it regulates the transcription of proinflammatory (TNF-α, IL-1β, IL-6) and catabolic (MMP-3, MMP-9, MMP-13, ADAMTS-4, ADAMTS-5) genes [9]. Activation of NF-κB also enhances the expression of inflammatory mediators such as iNOS (inducible nitric oxide synthase) and COX-2 (cyclooxygenase-2), whose activity products—namely nitric oxide (NO) and prostaglandins—inhibit aggrecan expression in the NP. Furthermore, NF-κB contributes to the destructive processes in the IVD by activating hypoxia-inducible factor HIF-2α. The target genes of activated HIF-2α include MMP-13 and ADAMTS-4, which regulate the metabolism of type II collagen and aggrecan (***Fig. 1***) [13, 14].

The major pathways mediating the proinflammatory response in IVD cells under various stimuli are illustrated in ***Fig. 1***. Bacterial pathogens activate Toll-like receptors (TLR2/4) or intracellular NOD receptors, initiating a signaling cascade via MyD88, IRAK, and TRAF6 to IKK, which subsequently activates the transcription factor NF-κB. Cytokines IL-1β and TNF-α induce NF-κB activation through the IL-1R (MyD88-dependent) and TNFR1 (TRADD/RIPK1-mediated) pathways. Viral components are recognized by TLR3/7/9, triggering NF-κB activation and an interferon-mediated response.

Mechanical loading is sensed by TRPV4 channels and integrins, which activate FAK, MAPK, and PI3K/Akt pathways that potentiate NF-κB activation. Oxidative stress, characterized by excessive accumulation of reactive oxygen species (ROS), activates the MAPK p38/JNK/ERK signaling cascade, leading to the activation of the transcription factor AP-1 and subsequent upregulation of IL-6, IL-8, COX-2, iNOS, and MMPs.

This article contains some figures that are displayed in color online but in black and white in the print edition

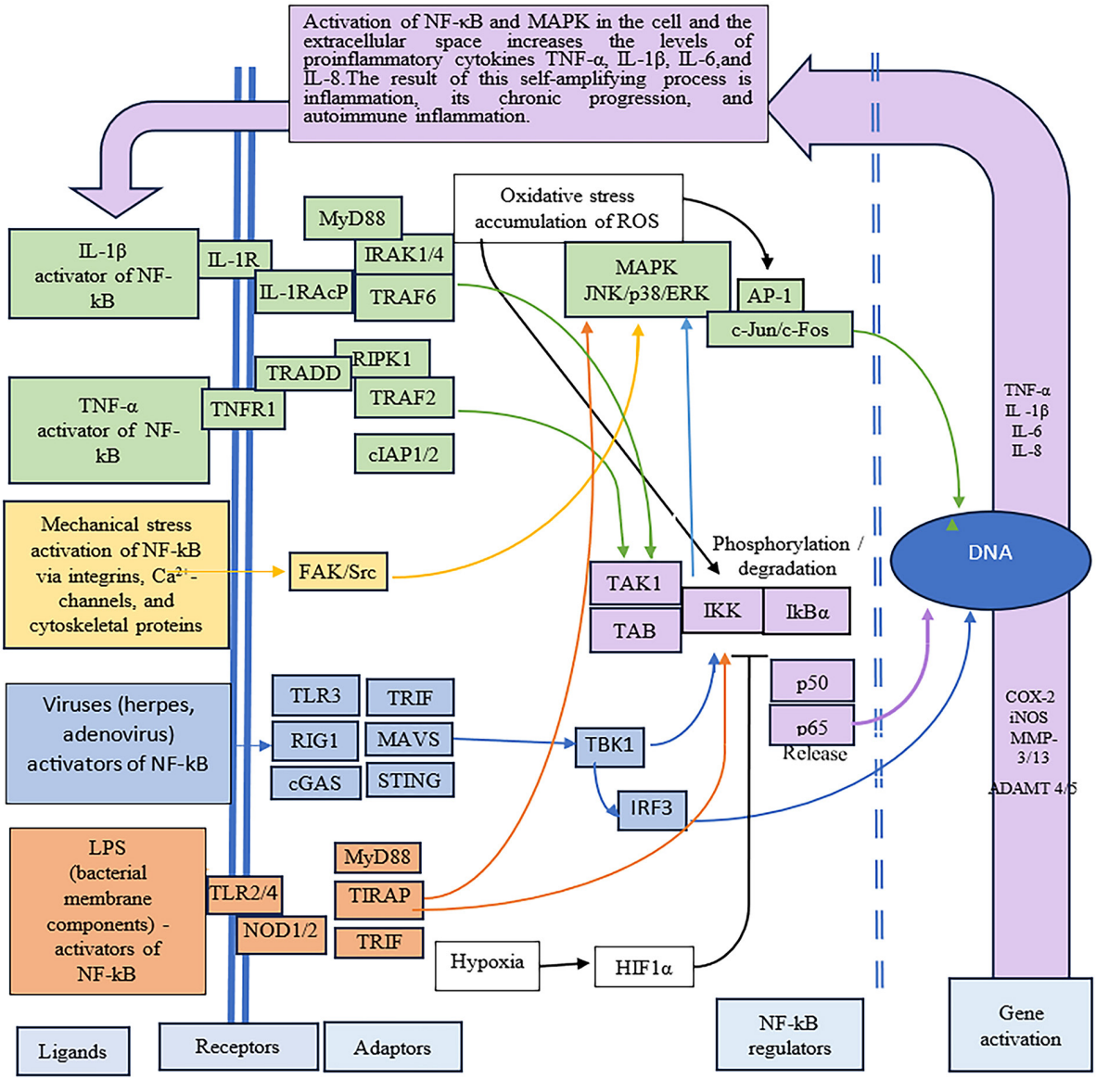

Fig. 1. Major signaling pathways of NF-κB activation in intervertebral disc cells under the influence of proinflammatory cytokines (TNF-α, IL-1β), bacterial components (LPS), mechanical stress, hypoxia, and oxidative damage (based on KEGG PATHWAY Database for NF-κB signaling pathway (map04064), MAPK signaling pathway (map04010), Toll-like receptor signaling pathway (map04620), HIF-1 signaling pathway (map04066), TNF signaling pathway (map04668) [67]) (explanation provided in the text)

ROS promote phosphorylation of IKK and degradation of IκBα, resulting in NF-κB translocation to the nucleus and stimulation of proinflammatory gene expression. Through NLRP3 involvement, ROS activate caspase-1, driving the maturation of IL-1β and IL-18 and amplifying sterile inflammation.

Hypoxia—reduced oxygen availability in IVD tissues—activates hypoxia-inducible factors (HIFs), while HIF-1α stabilizes NF-κB, enhancing the transcription of proinflammatory genes.

All these pathways converge at the level of the IKK complex and NF-κB, leading to increased expression of IL-1β, IL-6, TNF-α, MMPs, and ADAMTS, which in turn drive chronic inflammation, matrix degradation, and progression of degenerative changes within the intervertebral disc.

IL-1β is one of the key proinflammatory cytokines and plays a crucial role in IVD degeneration. It binds to the IL-1R1 receptor on the surface of NP and AF cells. This complex activates the adaptor protein MyD88, initiating downstream signaling cascades (see ***Fig. 1***). The subsequent effects are mediated through several interconnected mechanisms and pathways (NF-κB, MAPK, JAK/STAT), which collectively promote inflammation, matrix degradation, and cellular dysfunction [12].

TNF-α is another major inflammatory cytokine that activates the NF-κB pathway through TNF receptors. The signal is further transduced via TRADD to the TNFR-associated signaling complex and TRAFs [15].

LPS—components of the outer membrane of Gram-negative bacteria—are potent inducers of the

inflammatory response in IVD cells. They activate the NF-κB signaling pathway through interaction with Toll-like receptors, particularly TLR4, via the adaptor protein MyD88, which is shared by both TLR and IL-1R pathways [16].

Viral infection has been recognized as another factor capable of NF-κB activation. Viral signaling involves induction of immune and inflammatory responses. Viruses trigger the NF-κB pathway through various pathogen recognition receptors and associated molecules (TLRs, RIG-I, MDA5). Cellular receptors recognize viral ligands, including dsRNA, ssRNA, viral DNA, capsid proteins, and surface glycoproteins. Signals from activated receptors are transmitted via adaptor molecules such as MyD88, TRIF, and MAVS, leading to NF-κB activation and enhanced transcription of proinflammatory genes. NF-κB activation in response to viral exposure may sustain chronic inflammation in the IVD, which, upon reaching a critical threshold, can induce apoptosis of disc cells [17–19].

Oxidative stress plays a pivotal role in degenerative processes within the IVD, primarily through mechanisms mediated by reactive oxygen species (ROS) [20]. In IVD cells, mitochondria represent the main source of ROS. Elevated ROS levels induce mitochondrial dysfunction and DNA damage, resulting in apoptosis of NP and AF cells. ROS further promote inflammation, extracellular matrix (ECM) degradation, and apoptosis through the MAPK (particularly p38 and JNK) and NF-κB signaling pathways [21–23].

Hypoxia, characterized by reduced oxygen availability in IVD tissues (especially within the NP), stimulates the expression of HIF-1α and HIF-2α. The transcriptional activity of HIF-1α/2α induces proinflammatory activation via upregulation of COX-2, iNOS, and the cytokine IL-1β. Moreover, HIF-1α stabilizes NF-κB, enhancing the transcription of proinflammatory and catabolic genes. Under chronic or dysregulated hypoxic conditions, persistent HIF activation leads to cellular dysfunction and sustained inflammation in the IVD, ultimately contributing to the progression of degenerative changes [24].

Mechanical loading acts as an activator of the inflammatory process via NF-κB signaling. It is well established that intervertebral disc (IVD) cells convert mechanical stress into biological signals integrated into cellular responses through the regulation of gene transcription. Abnormal mechanical loading enhances catabolic activity in nucleus pulposus (NP) cells through the NF-κB signaling pathway. A key role in this process is played by Piezo1, a mechanosensitive transmembrane cation channel (encoded by the FAM38A gene), which facilitates nonselective permeation of Ca^{2+}, Mg^{2+}, and Mn^{2+} ions, activates the NF-κB signaling cascade, increases IL-1β expression in annulus fibrosus (AF) cells, promotes the formation of a proinflammatory microenvironment within AF tissue, and accelerates IVD degeneration [25].

Differences in NF-κB signaling between nucleus pulposus chondrocytes and annulus fibrosus fibroblasts. A characteristic feature of NF-κB activation in NP cells is their greater sensitivity to oxidative stress and inflammatory stimuli. In NP cells, NF-κB is activated by proinflammatory cytokines (IL-1β, TNF-α), hypoxia, oxidative and osmotic stress, and dehydration. This activation enhances the expression of MMPs and ADAMTS, leading to degradation of aggrecan and type II collagen. The upregulation of inflammatory processes also increases the expression of proinflammatory cytokines IL-6 and IL-8, as well as COX-2, which stimulates prostaglandin synthesis. Under conditions of prolonged inflammation, NF-κB activation may induce apoptosis of NP cells [26, 27].

In contrast, the primary stimulus of NF-κB signaling in AF fibroblasts is mechanical stress (stretching and shear loading). NF-κB activation in AF cells leads to increased production of type I collagen—the main structural component of the AF. AF fibroblasts are also sensitive to proinflammatory cytokines such as IL-1β and TNF-α. In these cells, extracellular matrix (ECM) degradation is less pronounced compared to NP cells. AF fibroblasts exhibit a higher degree of adaptation to mechanical stress through ECM remodeling, primarily by synthesizing type I collagen. In AF cells, NF-κB plays a protective role by promoting fibrotic remodeling; however, under conditions of chronic activation, it may contribute to fibrotic sclerosis [26].

The MAPK signaling pathway — an activator of degenerative processes in the intervertebral disc

The mitogen-activated protein kinase (MAPK) signaling pathway plays an important role in IVD degeneration. MAPK signaling comprises the ERK (extracellular signal-regulated kinase), JNK (c-Jun N-terminal kinase) and p38 subpathways. The MAPK/p38 and MAPK/JNK subpathways are principally involved in the activation of inflammatory responses and induction of metalloproteinase synthesis. [28] Inflammatory activation mediated by MAPK signaling is triggered via TNFR, IL-1R, Toll-like receptors, integrins and viral recognition receptors. [29–33] Extracellular stimuli are relayed through MAPK cascades to activate the MAPK transcription factor AP-1 (c-Fos/c-Jun), which in turn drives transcription of catabolic enzymes such as MMP-3, MMP-13, ADAMTS-4 and ADAMTS-5 that are responsible for ECM degradation. The inflammatory response is further amplified through increased transcription of proinflammatory cytokines including IL-1β and TNF-α [34, 35]. MAPK signaling, particularly the p38 MAPK axis, potentiates proinflammatory processes and apoptosis in part by modulatory cross-talk with the catabolic NF-κB pathway (see ***Fig. 1***). [36, 37]

PRP-derived factors — activators of anabolism and inhibitors of catabolic processes in the intervertebral disc

Growth factors contained in PRP act in a synergistic manner by engaging multiple intracellular signaling pathways that regulate inflammation, cell death, and extracellular matrix metabolism. These factors contribute to the reduction of proinflammatory cytokine production, suppression of metalloproteinase activity, attenuation of apoptosis in NP cells, and stimulation of the synthesis of key matrix components such as type II collagen and aggrecan. This multifactorial influence not only slows the progression of degenerative changes but also promotes endogenous repair processes within the disc tissue. Collectively, these effects position PRP as a promising bioactive therapeutic strategy, particularly at early stages of IVDD, when residual elements of cellular and matrix homeostasis can still be modulated to reverse the pathological process (***Fig. 2***).

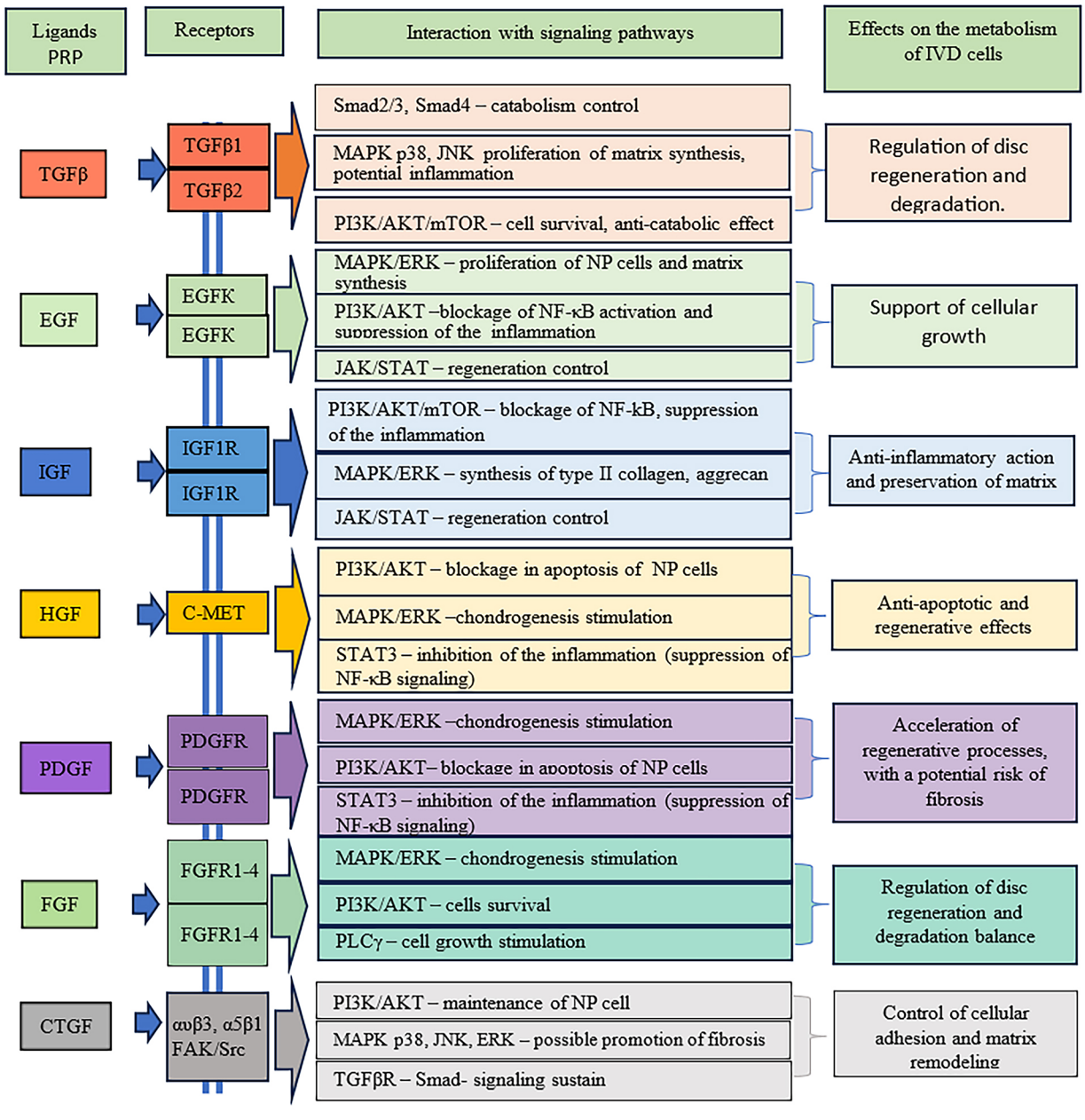

Fig. 2. The main signaling pathways activated by PRP-derived factors: TGF-β/Smad, MAPK/ERK, PI3K/AKT/mTOR, JAK/STAT, Wnt/β-catenin, and HIF-1 (according to the KEGG PATHWAY Database [67])

Figure 2 illustrates the molecular interactions between PRP ligands (TGF-β, EGF, IGF-1, HGF, PDGF, FGF, CTGF) and their corresponding receptors (TGFβR, EGFR, IGF1R, c-MET, PDGFR, FGFR, αVβ3), which lead to the activation of intracellular signaling cascades such as Smad, MAPK/ERK, PI3K/AKT/mTOR, JAK/STAT, and PLCγ. The activation of these pathways is accompanied by the suppression of the pro-inflammatory factor NF-κB, inhibition of apoptosis, stimulation of chondrogenesis, cell proliferation, and synthesis of extracellular matrix components (type II collagen, aggrecan). These effects indicate the complex homeostatic influence of PRP on intervertebral disc tissue and substantiate its use as a pathogenetically oriented regenerative therapy for IVDD.

TGF-β – a key growth factor in PRP

1. TGF-β is a crucial regulator that suppresses inflammatory processes and maintains the structure of the IVD, counteracting degenerative changes. The concentration of TGF-β in PRP varies depending on the preparation method and the individual characteristics of the donor. On average, TGF-β levels range from 10–50 ng/mL in activated PRP fractions, although some samples may show significantly higher or lower concentrations [38, 39].

The primary effects of TGF-β are mediated through the Smad signaling pathway. The interaction of TGF-β with the TGFBR receptor triggers the phosphorylation of Smad2 and Smad3, which subsequently form a complex with Smad4. The Smad2/3/4 complex

indirectly suppresses NF-κB transcriptional activity the transcriptional activity of NF-κB — through induction of IκB expression and/or modulation of shared transcriptional cofactors (p300/CBP) — thereby reducing its ability to activate the expression of pro-inflammatory cytokine genes such as IL-1β, IL-6, and TNF-α, and consequently decreasing inflammation and degeneration within the IVD. The complex is then translocated into the cell nucleus, where it activates the expression of genes responsible for suppressing inflammation and supporting the structure of the extracellular matrix of the disc [40].

2. TGF-β activates the PI3K/AKT pathway. The PI3K/AKT pathway operates independently of Smad signaling but is often activated in parallel through TGFBR1 and ShcA/p85 [41]. Following TGF-β receptor activation, the adaptor proteins ShcA or p85 stimulate PI3K and initiate a downstream cascade leading to AKT activation. The downstream effects of AKT activation in the context of IVD degeneration include enhanced cell survival and anti-apoptotic activity via the inhibition of pro-apoptotic factors (such as BAD) and activation of anti-apoptotic proteins (Bcl-2). An important aspect of metabolic regulation is that AKT modulates glucose uptake and metabolism, thereby promoting the synthesis of extracellular matrix (ECM) components, including collagen and aggrecan [42].

3. TGF-β also activates the MAPK/ERK signaling pathway (mitogen-activated protein kinases), which can interact with NF-κB and modulate its transcriptional activity, thus influencing inflammatory responses. Under certain conditions, the MAPK/ERK pathway may exert a protective or even anti-inflammatory role by reducing the expression of pro-inflammatory genes (see ***Fig. 2***) [41].

4. Through the Rho/ROCK signaling pathway, TGF-β regulates cytoskeletal structural rearrangements and supports the maintenance of the extracellular matrix. This stabilizes disc tissue, reduces structural damage, and indirectly attenuates the inflammatory response [42].

The TGF-β, NF-κB, MAPK, PI3K/AKT, and Rho/ROCK signaling pathways interact to form a complex regulatory network that enables TGF-β to control inflammatory processes, cell apoptosis, and the structural integrity of the IVD. The TGF-β pathway is crucial for maintaining ECM homeostasis and facilitating anabolic processes within the disc [43].

PDGF exerts its effects through the activation of several intracellular signaling pathways. The primary action of PDGF in IVDD is mediated by its binding to PDGFR-α and PDGFR-β receptors, which belong to the receptor tyrosine kinase family. Ligand binding induces dimerization and autophosphorylation of tyrosine residues within the intracellular domain of the receptor, enabling the recruitment of signaling proteins and initiating multiple downstream signaling cascades. In particular, the MAPK/ERK pathway triggers mitogen-mediated cell proliferation, while the PI3K/AKT pathway promotes cell survival and inhibits apoptosis. STAT3 is activated via JAK- or Src-dependent pathways and regulates the expression of genes associated with inflammation, angiogenesis, and tissue remodeling. As a result, there is stimulation of IVD cells proliferation and enhanced synthesis of ECM components, including type I/II collagen and aggrecan [40].

The concentration of PDGF in PRP ranges from 10 to 50 ng/mL, depending on the individual characteristics of the sample and preparation conditions; however, in samples with extremely high platelet counts, PDGF levels may exceed 100 ng/mL [43].

PDGF signaling via PRP, when monitored at optimal concentrations, can promote reparative processes and prevent degenerative changes within IVD tissue [44, 45].

FGF interacts with specific receptors (FGFR1–FGFR4), and the activation of this signaling pathway stimulates the proliferation of nucleus pulposus and fibrocartilage cells. The major pathways activated by FGF include MAPK/ERK, PI3K/AKT, and JAK/STAT [46]. The key transcription factor regulating the expression of chondrocyte-specific genes, such as type II collagen and aggrecan, is Sox9 [47]. By stimulating tissue inhibitors of metalloproteinases (TIMP), FGF decreases their activity, thereby suppressing ECM degradation [48]. Furthermore, FGF downregulates the expression of proinflammatory cytokines (e.g., IL-1β and TNF-α), which play a critical role in disc degeneration, and inhibits the NF-κB signaling pathway. Through suppression of inflammatory signaling, FGF promotes angiogenesis, improving the delivery of nutrients and regenerative factors. It has been demonstrated that PRP preparations containing a high concentration of FGF can be administered via intradiscal injections to stimulate tissue regeneration. This approach reduces pain associated with degenerative changes and slows the progression of degeneration. However, the use of FGF requires precise dosing and monitoring, as its concentration in PRP may vary depending on the preparation method and platelet count, ranging from 20 to 200 pg/mL [49].

IGF-1, a key component of PRP, plays an essential role in tissue repair and regeneration, particularly in degenerative processes of the IVD. Its binding to the IGF-1 receptor (IGF-1R) activates the latter, initiating intracellular signaling cascades that are crucial for cell growth, survival, and recovery. IGF-1 primarily transmits signals through the PI3K/AKT pathway, which promotes cell survival by inhibiting apoptosis and stimulating matrix synthesis, including the production of proteoglycans and type II collagen. This pathway also provides protection against oxidative stress and cellular senescence. The concentration of IGF-1 in PRP may vary depending on the preparation technique and platelet yield (ranging from 70 to 250 ng/mL). When PRP is used therapeutically, it is essential to determine the IGF-1 content in the preparation to ensure reproducibility and treatment efficacy [50, 51].

CTGF (connective tissue growth factor) is a bioactive protein that plays a significant role in tissue repair and regeneration, especially in degenerative conditions of the IVD [52]. It binds to TGF-β receptors, enhancing the activation of Smad2/3, thereby inhibiting IKK and IκB-α. As a result, NF-κB remains in the cytoplasm and does not activate pro-inflammatory genes such as TNF-α and IL-1β [53]. CTGF also activates the MAPK/ERK signaling pathway, promoting cell proliferation and survival, as well as PI3K and Akt, which enhance cell viability by suppressing apoptosis in disc cells. Indirectly, CTGF modulates the NF-κB pathway and activates the Wnt (Wingless-related Integration Site) signaling pathway, which regulates cellular proliferation, differentiation, and

matrix homeostasis in the IVD. Through its interaction with vascular endothelial growth factor (VEGF), CTGF also modulates angiogenesis. By activating these pathways, CTGF contributes to inflammation regulation, tissue regeneration, and the maintenance of disc homeostasis, while preventing cell death—making it a pivotal factor in the therapeutic effects of PRP [54–56]. The concentration of CTGF in PRP may vary substantially depending on the preparation method and donor platelet count (20–300 ng/mL) [56].

EGF plays a crucial role in tissue repair and regeneration, particularly in IVDD. It binds to the epidermal growth factor receptor (EGFR), a transmembrane receptor that undergoes dimerization, autophosphorylation, and initiation of intracellular signaling cascades. Studies have shown that EGF activates the MAPK/ERK signaling pathway, leading to the formation of the AP-1 complex, which regulates the expression of genes responsible for cell proliferation and the synthesis of extracellular matrix components [57]. Activation of the PI3K/AKT and JAK/STAT pathways supports anti-apoptotic processes, collagen and proteoglycan synthesis, thereby promoting the restoration of IVDD structure. Despite the controversial nature of EGF activity in the context of IVD (due to the avascular nature of the disc), it contributes to angiogenesis, which may improve nutrient delivery to the disc, and modulates inflammatory responses by suppressing the synthesis of pro-inflammatory cytokines IL-1β and TNF-α. Within PRP, EGF helps create a microenvironment favorable for disc repair and reduction of degenerative processes. It acts synergistically with other growth factors present in PRP (TGF-β, PDGF, and IGF-1) [57].

The concentration of EGF in PRP depends on the preparation method and individual sample characteristics, typically ranging from ~100 to 300 pg/mL in non-activated PRP [59].

HGF binds to the tyrosine kinase receptor MET, expressed on the surface of target NP and AF cells. Activation of the MET receptor triggers downstream signaling pathways essential for cell recovery and survival. The key activated signaling cascades include PI3K/AKT, which promotes cell survival and reduces apoptosis; RAS/MAPK, which stimulates cell proliferation and enhances tissue repair; and the STAT pathway, which regulates anti-inflammatory responses and supports the expression of genes involved in tissue regeneration. The Wnt pathway contributes to cell differentiation and matrix synthesis [60]. Protection of disc tissue by HGF occurs through suppression of TNF-α and IL-1β cytokine activity. Moreover, HGF promotes the synthesis of ECM components, including collagen and proteoglycans. Controlled modulation of matrix metalloproteinase (MMP) activity and inhibition of their tissue inhibitors allows for ECM remodeling. HGF also induces angiogenesis in surrounding tissues, enhancing nutrient and oxygen delivery to the IVD and thereby potentially improving its regenerative capacity. Its antifibrotic effect is based on the ability to inhibit TGF-β activity [61, 62].

The concentration of HGF in PRP may vary depending on the preparation protocol and other factors. Studies have demonstrated HGF levels of approximately 377.7–386.3 pg/mL in PRP samples, which reflects variations in platelet activation protocols and growth factor release [63].

Clinical research data on PRP application indicate its therapeutic potential. A systematic review and meta-analysis covering 10 studies involving intradiscal PRP injections in patients with vertebrogenic and discogenic pain [64] demonstrated positive effects on pain reduction and spinal function improvement. Similar beneficial outcomes have been reported in other studies, including the work of S. Kawabata et al. [65], emphasizing the importance of a critical approach to data interpretation and caution in drawing clinical conclusions [66].

Conclusions

Platelet-rich plasma is a multifunctional biological agent capable of modulating degenerative processes in IVDD. IVD cells express receptors for key growth factors present in PRP (TGF-β, PDGF, IGF-1, FGF, CTGF, EGF, HGF). The interaction of these ligands with their corresponding receptors (TGFβR, PDGFR, IGF1R, FGFR, EGFR, c-Met) activates several intracellular signaling cascades (Smad, PI3K/AKT, MAPK, JAK/STAT, etc.), which collectively inhibit the catabolic factor NF-κB and trigger anabolic processes. This leads to enhanced synthesis of extracellular matrix components (collagen, aggrecan), increased cell survival, and reduced inflammation within disc tissues. Specifically, TGF-β via the Smad cascade suppresses the expression of pro-inflammatory cytokines and promotes matrix synthesis; PDGF and IGF-1 activate the PI3K/AKT and MAPK pathways to enhance proliferation and protect cells from apoptosis. FGF and EGF engage the ERK/MAPK and JAK/STAT pathways, stimulating disc cell regeneration, while HGF complements the actions of other factors by reducing inflammation and fibrosis and supporting matrix synthesis through activation of the MET receptor and AKT/MAPK pathways.

Thus, at the current stage of scientific understanding, PRP is considered a pathogenetically justified therapeutic approach for influencing discogenic pain associated with degenerative changes of the IVD. However, PRP should not be regarded as a universal treatment modality for treating all forms of degeneration. To substantiate the long-term efficacy and safety of this method, large-scale randomized controlled trials are required, considering the clinical forms of pathology, inclusion criteria, PRP dosing, injection techniques, and standardized efficacy outcomes.

Disclosure

Conflict of interest

The authors declare no conflict of interest.

Ethical Standards

This article is a literature review; therefore, ethical approval was not required.

Funding

The study received no external funding or sponsorship.

References

1. Zàaba NF, Ogaili RH, Ahmad F, Mohd Isa IL. Neuroinflammation and nociception in intervertebral disc degeneration: a review of precision medicine perspective. Spine J. 2025 Jan 13:S1529-9430(25)00008-7. doi: 10.1016/j.spinee.2024.12.033

2. Mohd Isa IL, Teoh SL, Mohd Nor NH, Mokhtar SA. Discogenic Low Back Pain: Anatomy, Pathophysiology and Treatments of Intervertebral Disc Degeneration. Int J Mol Sci. 2022 Dec 22;24(1):208. doi: 10.3390/ijms24010208
3. Zhang GZ, Deng YJ, Xie QQ, et al. Sirtuins and intervertebral disc degeneration: Roles in inflammation, oxidative stress, and mitochondrial function. Clin Chim Acta. 2020;508:33–42. doi: 10.1016/j.cca.2020.04.038
4. Peng BG. Fundamentals of intervertebral disc degeneration and related discogenic pain. World J Orthop. 2025 Jan 18;16(1):102119. doi: 10.5312/wjo.v16.i1.102119
5. Pratsinis H, Kletsas D. PDGF, bFGF and IGF-I stimulate the proliferation of intervertebral disc cells in vitro via the activation of the ERK and Akt signaling pathways. Eur Spine J. 2007 Nov;16(11):1858-66. doi: 10.1007/s00586-007-0408-9
6. Tolonen J, Grönblad M, Vanharanta H, et al. Growth factor expression in degenerated intervertebral disc tissue. Eur Spine J. 2006 May;15(5):588-96. doi: 10.1007/s00586-005-0930-6
7. Sono T, Shima K, Shimizu T, et al. Regenerative therapies for lumbar degenerative disc diseases: a literature review. Front Bioeng Biotechnol. 2024 Aug 26;12:1417600. doi: 10.3389/fbioe.2024.1417600
8. Liang H, Luo R, Li G, et al. The Proteolysis of ECM in Intervertebral Disc Degeneration. Int J Mol Sci. 2022 Feb 2;23(3):1715. doi: 10.3390/ijms23031715
9. Zhang GZ, Liu MQ, Chen HW, et al. NF-κB signalling pathways in nucleus pulposus cell function and intervertebral disc degeneration. Cell Prolif. 2021 Jul;54(7):e13057. doi: 10.1111/cpr.13057
10. Wang Y, Cheng H, Wang T, et al. Oxidative stress in intervertebral disc degeneration: Molecular mechanisms, pathogenesis and treatment. Cell Prolif. 2023 Sep;56(9):e13448. doi: 10.1111/cpr.13448
11. Wu J, Chen Y, Liao Z, et al. Self-amplifying loop of NF-κB and periostin initiated by PIEZO1 accelerates mechano-induced senescence of nucleus pulposus cells. Mol Ther. 2022 Oct 5;30(10):3241-3256. doi: 10.1016/j.ymthe.2022.05.021
12. Li H, Pan H, Xiao C, et al. IL-1β-mediated inflammatory responses in intervertebral disc degeneration: Mechanisms and therapeutic potential. Heliyon. 2023 Sep 7;9(9):e19951. doi: 10.1016/j.heliyon.2023.e19951
13. Huang Y, Wang Y, Wu C, Tian W. Elevated expression of hypoxia-inducible factor-2alpha regulated catabolic factors during intervertebral disc degeneration. Life Sci. 2019 Sep 1;232:116565. doi: 10.1016/j.lfs.2019.116565
14. Li Y, Chen L, Gao Y, et al. Oxidative Stress and Intervertebral Disc Degeneration: Pathophysiology, Signaling Pathway, and Therapy. Oxid Med Cell Longev. 2022 Oct 10;2022:1984742. doi: 10.1155/2022/1984742
15. Tao C, Lin S, Shi Y, et al. Inactivation of Tnf-α/Tnfr signaling attenuates progression of intervertebral disc degeneration in mice. JOR Spine. 2024 Oct 8;7(4):e70006. doi: 10.1002/jsp2.70006
16. Li W, Tu J, Zheng J, et al. Gut Microbiome and Metabolome Changes in Chronic Low Back Pain Patients With Vertebral Bone Marrow Lesions. JOR Spine. 2025 Jan 27;8(1):e70042. doi: 10.1002/jsp2.70042
17. Zhao J, He S, Minassian A, et al. Recent advances on viral manipulation of NF-κB signaling pathway. Curr Opin Virol. 2015 Dec;15:103-11. doi: 10.1016/j.coviro.2015.08.013
18. Walker BF, Armson AJ, O'Dea MA, et al. Are viruses associated with disc herniation? A clinical case series. BMC Musculoskelet Disord. 2020 Jan 14;21(1):27. doi: 10.1186/s12891-020-3052-8
19. Granville Smith I, Danckert NP, Freidin MB, et al. Evidence for infection in intervertebral disc degeneration: a systematic review. Eur Spine J. 2022 Feb;31(2):414-430. doi: 10.1007/s00586-021-07062-1
20. Mai Y, Wu S, Zhang P, et al. The anti-oxidation related bioactive materials for intervertebral disc degeneration regeneration and repair. Bioact Mater. 2024 Nov 9;45:19-40. doi: 10.1016/j.bioactmat.2024.10.012
21. Wang Y, Hu Y, Wang H, et al. Deficiency of MIF accentuates overloaded compression-induced nucleus pulposus cell oxidative damage via depressing mitophagy. Oxid Med Cell Longev. 2021 Jul 1;2021:6192498. doi: 10.1155/2021/6192498
22. Wang J, Jiang Y, Zhu C, et al. Mitochondria-engine with self-regulation to restore degenerated intervertebral disc cells via bioenergetic robust hydrogel design. Bioact Mater. 2024 May 31;40:1-18. doi: 10.1016/j.bioactmat.2024.05.044
23. Elmounedi N, Bahloul W, Kharrat A, et al. Ozone therapy (O2-O3) alleviates the progression of early intervertebral disc degeneration via the inhibition of oxidative stress and the interception of the PI3K/Akt/NF-κB signaling pathway. Int Immunopharmacol. 2024 Mar 10;129:111596. doi: 10.1016/j.intimp.2024.111596
24. Imtiyaz HZ, Simon MC. Hypoxia-inducible factors as essential regulators of inflammation. Curr Top Microbiol Immunol. 2010;345:105-20. doi: 10.1007/82_2010_74
25. Peng F, Sun M, Jing X, et al. Piezo1 promotes intervertebral disc degeneration through the Ca2+/F-actin/Yap signaling axis. Mol Med. 2025;31:90. doi: 10.1186/s10020-025-01147-z
26. Krzyzanowska AK, Frawley RJ, Damle S, et al. Activation of nuclear factor-kappa B by TNF promotes nucleus pulposus mineralization through inhibition of ANKH and ENPP1. Sci Rep. 2021;11:8271. doi: 10.1038/s41598-021-87665-2
27. Zheng SK, Zhao XK, Wu H, et al. Oxidative stress-induced EGR1 upregulation promotes NR4A3-mediated nucleus pulposus cells apoptosis in intervertebral disc degeneration. Aging (Albany NY). 2024 Jun 28;16(12):10216-10238. doi: 10.18632/aging.205920
28. Liu G, Gao L, Wang Y, et al. The JNK signaling pathway in intervertebral disc degeneration. Front Cell Dev Biol. 2024 Sep 19;12:1423665. doi: 10.3389/fcell.2024.1423665
29. Tian Z, Gao H, Xia W, Lou Z. S1PR3 suppresses the inflammatory response and extracellular matrix degradation in human nucleus pulposus cells. Exp Ther Med. 2024 Apr 25;27(6):265. doi: 10.3892/etm.2024.12553
30. Lin J, Gu J, Fan D, Li W. Herbal formula modified Bu-Shen-Huo-Xue decoction attenuates intervertebral disc degeneration via regulating inflammation and oxidative stress. Evid Based Complement Alternat Med. 2022 Feb 2;2022:4284893. doi: 10.1155/2022/4284893
31. Zhou Z, Wang Y, Liu H, et al. PBN protects NP cells from AAPH-induced degenerative changes by inhibiting the ERK1/2 pathway. Connect Tissue Res. 2021 Jul;62(4):359-368. doi: 10.1080/03008207.2020.1743697
32. Cambria E, Heusser S, Scheuren AC, et al. TRPV4 mediates cell damage induced by hyperphysiological compression and regulates COX2/PGE2 in intervertebral discs. JOR Spine. 2021 May 6;4(3):e1149. doi: 10.1002/jsp2.1149
33. Zhu F, Duan W, Zhong C, et al. The protective effects of dezocine on interleukin-1β-induced inflammation, oxidative stress and apoptosis of human nucleus pulposus cells and the possible mechanisms. Bioengineered. 2022 Jan;13(1):1399-1410. doi: 10.1080/21655979.2021.2017700
34. Peng Y, Lin H, Tian S, et al. Glucagon-like peptide-1 receptor activation maintains extracellular matrix integrity by inhibiting the activity of mitogen-activated protein kinases and activator protein-1. Free Radic Biol Med. 2021 Dec;177:247-259. doi: 10.1016/j.freeradbiomed.2021.10.034
35. Pei S, Ying J, Zhang Y, et al. RhTSG-6 inhibits IL-1β-induced extracellular matrix degradation and apoptosis by suppressing the p38, and JNK pathways in nucleus pulposus cells. Folia Histochem Cytobiol. 2020;58(3):227-234. doi: 10.5603/FHC.a2020.0019
36. Huang Y, Peng Y, Sun J, et al. Nicotinamide phosphoribosyl transferase controls NLRP3 inflammasome activity through MAPK and NF-κB signaling in nucleus pulposus cells, as suppressed by melatonin. Inflammation. 2020 Jun;43(3):796-809. doi: 10.1007/s10753-019-01166-z
37. Cui H, Du X, Liu C, et al. Visfatin promotes intervertebral disc degeneration by inducing IL-6 expression through the ERK/JNK/p38 signalling pathways. Adipocyte. 2021 Dec;10(1):201-215. doi: 10.1080/21623945.2021.1910155
38. Staszkiewicz R, Gładysz D, Sobański D, et al. Assessment of the concentration of transforming growth factor beta 1-3 in degenerated intervertebral discs of the lumbosacral region of the spine. Curr Issues Mol Biol. 2024 Nov 11;46(11):12813-12829. doi: 10.3390/cimb46110763
39. Taylor W, Erwin WM. Intervertebral disc degeneration and

regeneration: new molecular mechanisms and therapeutics: obstacles and potential breakthrough technologies. Cells. 2024 Dec 19;13(24):2103. doi: 10.3390/cells13242103
40. Wang H, Zhu J, Xia Y, et al. Application of platelet-rich plasma in spinal surgery. Front Endocrinol (Lausanne). 2023 Mar 15;14:1138255. doi: 10.3389/fendo.2023.1138255
41. Deng Z, Fan T, Xiao C, et al. TGF-β signaling in health, disease, and therapeutics. Signal Transduct Target Ther. 2024 Mar 22;9(1):61. doi: 10.1038/s41392-024-01764-w
42. Giarratana AO, Prendergast CM, Salvatore MM, et al. TGF-β signaling: critical nexus of fibrogenesis and cancer. J Transl Med. 2024 Jun 26;22(1):594. doi: 10.1186/s12967-024-05411-4
43. Tseranidou S, Segarra-Queralt M, Chemorion FK, et al. Nucleus pulposus cell network modelling in the intervertebral disc. NPJ Syst Biol Appl. 2025 Jan 31;11(1):13. doi: 10.1038/s41540-024-00479-6
44. Shnayder NA, Ashkhotov AV, Trefilova VV, et al. Molecular basic of pharmacotherapy of cytokine imbalance as a component of intervertebral disc degeneration treatment. Int J Mol Sci. 2023 Apr 22;24(9):7692. doi: 10.3390/ijms24097692
45. Andia I, Atilano L, Maffulli N. Moving toward targeting the right phenotype with the right platelet-rich plasma (PRP) formulation for knee osteoarthritis. Ther Adv Musculoskelet Dis. 2021 Mar 29;13:1759720X211004336. doi: 10.1177/1759720X211004336
46. Rayrikar AY, Wagh GA, Santra MK, et al. Ccn2a-FGFR1-SHH signaling is necessary for intervertebral disc homeostasis and regeneration in adult zebrafish. Development. 2023 Jan 1;150(1):dev201036. doi: 10.1242/dev.201036
47. Uebelhoer M, Lambert C, Grisart J, et al. Interleukins, growth factors, and transcription factors are key targets for gene therapy in osteoarthritis: a scoping review. Front Med (Lausanne). 2023 Apr 3;10:1148623. doi: 10.3389/fmed.2023.1148623
48. Lu S, Lin C. Lentivirus mediated transfer of gene encoding fibroblast growth factor 18 inhibits intervertebral disc degeneration. Exp Ther Med. 2021;22:856. doi: 10.3892/etm.2021.10288
49. Kikuchi N, Yoshioka T, Arai N, et al. A retrospective analysis of clinical outcome and predictive factors for responders with knee osteoarthritis to a single injection of leukocyte-poor platelet-rich plasma. J Clin Med. 2021 Oct 31;10(21):5121. doi: 10.3390/jcm10215121
50. Amable PR, Carias RB, Teixeira MV, et al. Platelet-rich plasma preparation for regenerative medicine: optimization and quantification of cytokines and growth factors. Stem Cell Res Ther. 2013 Jun 7;4(3):67. doi: 10.1186/scrt218
51. Beitia M, Delgado D, Mercader J, et al. Action of platelet-rich plasma on in vitro cellular bioactivity: more than platelets. Int J Mol Sci. 2023 Mar 10;24(6):5367. doi: 10.3390/ijms24065367
52. Ren M, Yao S, Chen T, et al. Connective tissue growth factor: regulation, diseases, and drug discovery. Int J Mol Sci. 2024 Apr 25;25(9):4692. doi: 10.3390/ijms25094692
53. Istvánffy R, Vilne B, Schreck C, et al. Stroma-derived connective tissue growth factor maintains cell cycle progression and repopulation activity of hematopoietic stem cells in vitro. Stem Cell Reports. 2015 Nov 10;5(5):702-715. doi: 10.1016/j.stemcr.2015.09.018
54. Yang H, Chen X, Chen J, et al. The pathogenesis and targeted therapies of intervertebral disc degeneration induced by cartilage endplate inflammation. Front Cell Dev Biol. 2024 Dec 2;12:1492870. doi: 10.3389/fcell.2024.1492870
55. Fu M, Peng D, Lan T, et al. Multifunctional regulatory protein connective tissue growth factor (CTGF): a potential therapeutic target for diverse diseases. Acta Pharm Sin B. 2022 Apr;12(4):1740-1760. doi: 10.1016/j.apsb.2022.01.007
56. Gentile P, Garcovich S. Systematic review—The potential implications of different platelet-rich plasma (PRP) concentrations in regenerative medicine for tissue repair. Int J Mol Sci. 2020;21(16):5702. doi:10.3390/ijms21165702.
57. Havis E, Duprez D. EGR1 transcription factor is a multifaceted regulator of matrix production in tendons and other connective tissues. Int J Mol Sci. 2020 Feb 28;21(5):1664. doi: 10.3390/ijms21051664
58. Lu L, Xu A, Gao F, et al. Mesenchymal stem cell-derived exosomes as a novel strategy for the treatment of intervertebral disc degeneration. Front Cell Dev Biol. 2022 Jan 24;9:770510. doi: 10.3389/fcell.2021.770510
59. Cavallo C, Filardo G, Mariani E, et al. Comparison of platelet-rich plasma formulations for cartilage healing: an in vitro study. J Bone Joint Surg Am. 2014 Mar 5;96(5):423-9. doi: 10.2106/JBJS.M.00726
60. Itsuji T, Tonomura H, Ishibashi H, et al. Hepatocyte growth factor regulates HIF-1α-induced nucleus pulposus cell proliferation through MAPK-, PI3K/Akt-, and STAT3-mediated signaling. J Orthop Res. 2021 Jun;39(6):1184-1191. doi: 10.1002/jor.24679
61. Tratnig-Frankl M, Luft N, Magistro G, et al. Hepatocyte growth factor modulates corneal endothelial wound healing in vitro. Int J Mol Sci. 2024 Aug 29;25(17):9382. doi: 10.3390/ijms25179382
62. Yang F, Deng L, Li J, et al. Emodin retarded renal fibrosis through regulating HGF and TGFβ-Smad signaling pathway. Drug Des Devel Ther. 2020 Sep 3;14:3567-3575. doi: 10.2147/DDDT.S245847
63. Everts PA, Lana JF, Alexander RW, et al. Profound properties of protein-rich, platelet-rich plasma matrices as novel, multi-purpose biological platforms in tissue repair, regeneration, and wound healing. Int J Mol Sci. 2024 Jul 19;25(14):7914. doi: 10.3390/ijms25147914
64. Kataria S, Wijaya JH, Patel U, et al. The role of platelet rich plasma in vertebrogenic and discogenic pain: a systematic review and meta-analysis. Curr Pain Headache Rep. 2024 Aug;28(8):825-833. doi: 10.1007/s11916-024-01274-y
65. Kawabata S, Hachiya K, Nagai S, et al. Autologous platelet-rich plasma administration on the intervertebral disc in low back pain patients with Modic type 1 change: report of two cases. Medicina (Kaunas). 2023 Jan 5;59(1):112. doi: 10.3390/medicina59010112
66. Chang Y, Yang M, Yu S, Zhan K. Effect of platelet-rich plasma on intervertebral disc degeneration in vivo and in vitro: a critical review. Oxid Med Cell Longev. 2020;2020:8893819. doi: 10.1155/2020/8893819
67. Kanehisa M, Furumichi M, Sato Y, Kawashima M, Ishiguro-Watanabe M. KEGG for taxonomy-based analysis of pathways and genomes. Nucleic Acids Res. 2023;51(D1):D587–D592. doi:10.1093/nar/gkac963.

Review article

Ukrainian Neurosurgical Journal. 2025;31(4):20-25
doi: 10.25305/unj.333267

Post-concussion syndrome: Part 1. Overview of the epidemiology and pathophysiology of mild blast-related traumatic brain injury

Vadym V. Biloshytsky [1,2], Yurii V. Zavaliy [3], Alisa V. Pachevska [4], Illia V. Biloshytskyi [5]

[1] Pain Management Center SPRAVNO, Kyiv, Ukraine
[2] Scientific and Organizational Department, Romodanov Neurosurgery Institute, Kyiv, Ukraine
[3] Department of Neurosurgery, National Military Medical Clinical Center "Main Military Clinical Hospital", Kyiv, Ukraine
[4] Department of Pediatric Stomatology, National Pirogov Memorial Medical University, Vinnytsia, Ukraine
[5] Medical Faculty No. 2, Bogomolets National Medical University, Kyiv, Ukraine

Received: 21 June 2025
Accepted: 19 July 2025

Address for correspondence:
Vadym V. Biloshytsky, Pain Management Center SPRAVNO, Mezhyhirska St., 28, Kyiv, 04071, Ukraine, e-mail: dr.biloshytsky@spravno.clinic

This article provides a review of current data on the epidemiology and pathophysiology of mild blast-related traumatic brain injury (mbTBI), which has become the leading type of injury in modern military conflicts. The prevalence of mbTBI among U.S. military personnel during operations in Afghanistan and Iraq is described, with emphasis on the cumulative effect of repeated injuries that increases the risk of chronic traumatic encephalopathy. The paper discusses the main mechanisms of blast wave impact on the brain, including direct and indirect effects, pathomorphological changes, and differences from "civilian" mild traumatic brain injury (TBI). Current insights into molecular and cellular alterations underlying mbTBI are summarized, along with data from experimental and clinical studies. These findings are crucial for developing effective diagnostic approaches, treatment strategies, and rehabilitation programs for service members and veterans.

Keywords: *post-concussion syndrome; mild blast-related traumatic brain injury; pathophysiology; epidemiology; military medicine*

Epidemiology of mild blast-related traumatic brain injury

In countries involved in modern military conflicts, blast-related TBI has taken the leading position among injuries sustained by service members [1]. During the military operations in Iraq and Afghanistan—where the intensity of hostilities was lower compared to the current Russian-Ukrainian war, and regular Western forces often faced paramilitary groups—at least 10–20% of U.S. military personnel sustained TBI [2]. From the beginning of American involvement in military operations in 2000 through 2014, approximately 320,000 cases of TBI were registered [3]. According to the Defense and Veterans Brain Injury Center (DVBIC), between 2000 and the first quarter of 2016, about 348,000 active-duty service members sustained TBI. The annual number of such injuries increased from 10,958 in 2000 to a peak of 32,907 in 2011, subsequently decreasing to 22,594 in 2015. The majority of these injuries (82%) were classified as mild. Blast exposure accounted for 80% of mild TBI cases [4, 5].

In 2014, 7% of Iraq and Afghanistan war veterans receiving care within the U.S. Department of Veterans Affairs (VA) healthcare system had a TBI diagnosis [6]. A more detailed screening of one million veterans for head injuries between 2007 and 2015 revealed TBI in 8.4% of them. Given that an additional 45,000 service members had already been diagnosed with mild TBI, the total number of individuals with this type of injury reached 137,841, representing 13.8% of all those examined [7].

According to U.S. researchers, blast-related injuries—including those caused by explosive shells, landmines, and rocket-propelled grenades—accounted for 56–78% of all combat injuries sustained during operations in Iraq and Afghanistan [8]. These changes in the injury structure observed during recent military campaigns give reason to consider blast-related TBI to be the marker injuries sustained by soldiers in modern warfare [1]. Due to the prolonged nature of the conflicts in Afghanistan and Iraq and the frequent use of blast devices by enemy combatants, clinical and research attention has increasingly focused on blast-related TBI, especially its mild form [9]. It is noteworthy that only about 2.8% of blast-related head injuries were classified as severe, while the majority were mild. The true prevalence is believed to be underestimated, as mbTBI often remains undiagnosed and untreated due to the limitations of current screening tools, vague diagnostic criteria, and the lack of objective or imaging-based verification methods [10].

Reports indicating the frequent occurrence of repeated blast injuries among military personnel are alarming. A literature review [11] described a case of a U.S. Marine Corps Explosive Ordnance Disposal technician who sustained 50 significant blast exposures over 14 years of service. Other reports have documented groups of patients with an average of 13–14 blast exposures per individual during active combat deployment [11]. The high incidence of recurrent mbTBI increases the risk of developing chronic traumatic encephalopathy (a condition believed to result from multiple mild TBIs) as well as other forms of dementia [12].

The treatment and rehabilitation of service members who have sustained TBI are associated with substantial economic costs. In 2014, the average medical cost per injured service member diagnosed with TBI in the United States was USD 15,161, which was significantly higher than the cost for those without such a diagnosis (USD 5,058) [6].

Studies of blast-related TBI based on data from military campaigns in Iraq and Afghanistan concluded that, although many medical principles and treatment protocols used in the civilian sector for the assessment and management of TBI can be applied to wounded service members, there are several distinctive factors specific to this injury in military and veteran populations. These include the combat-related mechanisms of injury, unique blast dynamics, comorbid psychiatric conditions, and the influence of military culture, which often minimizes the perceived significance of mild injuries [9].

The military operations in Ukraine, ongoing since 2014 as a result of Russian aggression, are characterized by the simultaneous use of modern personal protective equipment and advanced weaponry, including barrel and rocket artillery, rocket-propelled grenades, and landmines. This has led to a growing number of blast injury cases and an urgent need for effective medical care and rehabilitation for the affected service members [13]. Accurate epidemiological data on the prevalence and long-term consequences of mbTBI will only be available after the war concludes. However, based on international research findings, it is evident that the long-term rehabilitation of a large number of affected individuals will become one of the major challenges for Ukraine's healthcare system.

Pathophysiology of mild blast-related traumatic brain injury

The mechanisms underlying blast-related TBI differ fundamentally from those of "civilian" TBI (hereinafter, the term civilian TBI is used in a nonstandard sense to distinguish injuries sustained in non-combat conditions from blast-related TBI). In peacetime injuries, brain damage typically results from rotational and inertial forces as well as from local traumatic impact. In contrast, blast-related injuries are caused by a pressure wave transmitted over a distance through the air [14]. According to the classical definition by C.J. Clemedson (1956), a blast injury represents the biophysical and pathophysiological changes resulting from direct exposure to an explosion or its associated shock wave [15]. Although blast-related TBI may present with the clinical features of mild TBI, it can be accompanied by significant morphological alterations, including cerebral edema, neuroinflammation, vasospasm, diffuse axonal injury, neuronal death, and secondary astrogliosis. At the cellular level, blast-related brain injury is characterized by multiple heterogeneous disturbances, such as increased accumulation of β-amyloid precursor protein, upregulated expression of proto-oncogenes c-Myc, c-Fos, and c-Jun, enhanced nitric oxide synthesis leading to oxidative stress, disruption of axonal transport, and elevated levels of TBI biomarkers including neuron-specific enolase (NSE), ubiquitin C-terminal hydrolase-L1 (UCH-L1), and glial fibrillary acidic protein (GFAP) [1].

Blast-related TBI represents a distinct form of traumatic injury resulting from direct or indirect exposure to an explosion, most commonly under combat conditions. Injury caused by excessive blast pressure occurs as a result of the rapid release of energy over a short time interval and within a limited volume, generating a nonlinear wave of shock and pressure. The resulting "shock wave" consists of a high-pressure front that compresses the surrounding air within submillisecond–millisecond timeframes, followed by an abrupt pressure drop, often below atmospheric levels (negative pressure)—before returning to ambient conditions. The zone of negative pressure then rapidly expands and is replaced by an equivalent volume of air. This air displacement produces the so-called "blast wind," a powerful stream of superheated air constituting a large mass of gas capable of propelling the victim's body against surrounding objects. The blast wind, together with the shock wave, forms the primary components of the "blast wave." Blast waves exert complex effects on the head–brain system, and the severity of blast-related TBI depends on both the magnitude and the duration of the pressure cycle [1, 16, 17].

From a physical standpoint, tissue injury resulting from the primary blast effect occurs through several mechanisms, including spallation, implosion, inertial effects, and cavitation. Spallation arises when a shock wave transitions from a denser to a less dense medium, causing the fragmentation of the denser material into the less dense one. A relatively simple example is an underwater explosion, in which the denser water is dispersed into the less dense air. Cavitation and implosion are interrelated phenomena that occur when the negative pressure phase of the blast wave forces dissolved gases in fluids to form bubbles. These bubbles subsequently collapse under negative pressure (implosion) and then explosively expand once the negative pressure phase passes. Spallation, cavitation, and implosion can lead to primary pulmonary blast injury. Inertial forces develop at the interfaces of tissues with different densities when the blast pressure accelerates materials of varying density at different rates, generating shear stresses [18–20]. Experimental models have demonstrated that cavitation can also result in secondary tissue damage under blast exposure. In particular, cavitation of the cerebrospinal fluid may occur at pressure levels and exposure durations consistent with those observed during real-life explosive events [19, 21].

The U.S. Centers for Disease Control and Prevention (CDC) classifies blast-related injuries into four categories [22]:

1) primary injuries, caused by the direct effect of the initial overpressure wave on body surfaces (primary blast);

2) secondary injuries, resulting from penetrating or blunt trauma caused by fragments and projectiles;

3) tertiary injuries, sustained when the body is propelled by the blast wind;

4) quaternary injuries, encompassing all other explosion-related injuries, illnesses, or diseases not caused by the primary, secondary, or tertiary mechanisms, as well as the exacerbation or complication of pre-existing medical conditions [22].

Although blast injuries are often combined or complex, this study focuses exclusively on mbTBI resulting from the shock wave.

There is a limited number of studies reporting chronic neuropathological changes associated with blast-related TBI. The results of such investigations are summarized in a literature review [23], which notes that these reports began to emerge after 2011. Notably, in the brain tissue of a former U.S. Marine, neurofibrillary tangles and tau protein pathology were identified, resembling the pattern characteristic of chronic traumatic encephalopathy (CTE). Similar pathological alterations were observed at autopsy in four military veterans exposed to blasts. In another series of pathohistological studies (five blast-exposed servicemen, four of whom survived longer than two months after the incident), axonal pathology was described. In five additional cases of chronic blast-related TBI (with survival beyond six months post-injury), the authors reported pronounced astroglial pathology (astrogliosis), indicating the presence of reactive gliosis, as well as tau protein abnormalities in two of the five cases. In addition to these limited human studies investigating both acute and chronic neuropathological outcomes, a considerable number of animal models have been developed. However, these models have inherent limitations in accurately replicating the pathophysiological mechanisms and neuropathological features of blast-related TBI observed in humans.

The blast wave can affect the brain through several mechanisms. First, as kinetic energy passes through the skull, it can directly induce acceleration or rotational motion of the brain, leading to diffuse axonal injury (DAI) followed by secondary axonal degeneration. Although these injury types may initially appear similar to non-blast, "civilian" TBI, recent evidence indicates that the axonal injury pattern caused by blast exposure is unique to blast-related TBI. Neuroimaging studies of military personnel using diffusion tensor magnetic resonance imaging (DT-MRI) after blast exposure have demonstrated that axonal injury in blast-related TBI is more widespread and spatially variable compared to non-blast "civilian" trauma. Affected brain regions include the superior corona radiata of the frontal cortex, the cerebellum, and the optic tracts [24, 25]. These findings are consistent with results obtained from rat models of blast-related TBI, which showed that rotational brain injury (analogous to "civilian" trauma) produces distinct behavioral disturbances compared with blast-induced neurotrauma [26]. Collectively, these data support the notion that blast-induced axonal injury should be regarded as a separate subtype of diffuse axonal injury. This is further supported by the more pronounced inflammatory response observed in blast-related TBI relative to non-blast trauma, including increased expression of pro-inflammatory cytokines and heightened neuroglial activation [27, 28]. Additionally, in rat models of blast-related TBI, brain edema and vasospasm are more prevalent due to primary arterial constriction and compromised vascular integrity, leading to secondary neuronal tissue damage [29].

According to K.J. Dixon (2017), in addition to the direct mechanical impact on brain tissue, the blast wave may also act indirectly through two possible mechanisms. First, a blast can cause compression and subsequent expansion of gas-containing compartments within the brain, resulting in damage to surrounding tissues. Second, the blast wave may generate pressure waves within the blood or cerebrospinal fluid, which propagate to the brain within seconds. Such a shock wave can accelerate tissue components from rest to a velocity dependent on medium density, potentially causing deformation and injury of the affected neural structures [30]. These indirect effects of blast exposure are thought to result both from the transmission of explosive energy through the blood vessels of the thoracic and abdominal cavities and from vagus-mediated bradycardia, arterial hypotension, and possibly cerebral hypoperfusion [31].

The described effects of blast waves on the central nervous system have been confirmed in experimental studies. Following a single sublethal blast exposure generating overpressure levels of 48.9–77.3 kPa in open-field conditions (a model of mbTBI), rat brains examined one day post-injury exhibited "darkened", shrunken cortical neurons and spastic blood vessels. Histological analyses revealed apoptotic oligodendrocytes and astrocytes (TUNEL-positive staining) within the white matter, along with acute axonal injury (increased amyloid precursor protein immunoreactivity) but without evidence of macrophage or microglial activation. Signs of recovery were observed on days 4 and 7 post-blast, indicating the mild nature of the cellular injury and white matter alterations [32].

Several anatomophysiological prerequisites may underlie the mechanisms described above. These include the direct propagation of the blast wave through the skull or paranasal sinuses [33]. Conversely, the indirect action of the blast wave is associated with compression of the abdomen and thoracic cavity, which transmits kinetic energy through the body's biological fluids. This effect generates oscillatory pressure waves that travel from the bloodstream to the brain—remote from the site of maximal explosive energy impact. Such kinetic energy transfer induces functional and morphological alterations within brain structures, constituting a specific feature of blast-induced brain injury, which is not observed in other known forms of TBI. The complex mechanism of blast-related damage also involves the primary blast impact on the autonomic nervous system [1]. In an experimental mouse model, the effects of mbTBI were assessed at overpressures of 68, 103, and 183 kPa generated by a shock tube on parenchymal organs and the brain. The principal injuries to extracerebral organs included pulmonary hemorrhages and hemorrhagic infarctions of the liver, spleen, and kidneys. Multifocal axonal injury was observed in the cerebellum, corticospinal tracts, and

optic pathways, accompanied by persistent behavioral and motor impairments, such as deficits in social interaction, spatial memory, and motor coordination. Notably, torso protection significantly reduced both axonal damage and behavioral deficits [34]. In another study, mbTBI was modeled in rats using a shock tube producing overpressures of 126 and 147 kPa. The thoracic cage and abdominal region of the animals were protected with a Kevlar vest, which reduced blast-related mortality, as well as the extent of axonal degeneration in the brain and the severity of neurological and behavioral disturbances [35].

Taken together, these findings support the increasingly recognized theory that thoracoabdominal vascular/hydrodynamic transmission of blast waves may represent a primary mechanism of blast-related TBI. Notably, certain patients exposed to blast events exhibit clinical signs of TBI in the absence of direct head trauma [20]. This theory has received experimental confirmation. The authors of the study [36] investigated the effects of a blast wave on rats placed within a shock tube apparatus, where overpressure of 70 and 130 kPa was applied exclusively to the torso, while carotid artery and intracranial pressure were simultaneously measured. The researchers demonstrated that the blast energy transmitted through the torso resulted in a 255% increase in peak bulk blood flow velocity in the basal brain regions and a 289% increase in shear stress within cerebral vessels. They concluded that the indirect mechanism of blast injury provokes a sudden, high-magnitude blood surge that rapidly propagates from the torso through the neck to the cerebral vasculature. This surge markedly increases vascular wall shear stress within the brain's circulatory network, potentially leading to functional and structural alterations of cerebral veins and arteries and, ultimately, to vascular pathology [36]. An increase in cerebral vascular pressure resulting from thoracoabdominal compression compromises the integrity of the blood–brain barrier (BBB), leading to damage of small cerebral vessels. As noted above, blast-related injury to air-filled organs, such as the lungs, may cause air embolism through the spallation mechanism. Air emboli can enter cerebral vessels, resulting in cerebral ischemia and infarction. In addition, blast overpressure may provoke structural alterations of arteries due to blast-relayed vasospasm [20,37–39].

According to researchers [40], experimental models should compare the severity of blast-related TBI using two types of special protective devices. The first device ("iron lungs") allows the blast wave to act exclusively on the head of the animal, while the second directs the blast exposure to the thoracic and abdominal regions. Such experiments would help explain and substantiate the clinical observation that enhanced thoracic protection provided by ballistic body armor likely plays a significant role in mitigating the severity of blast-related TBI by preventing pulmonary injury at blast intensities that would otherwise cause TBI [41]. However, it has been reported [11] that under real combat conditions in the Iraq and Afghanistan wars, body armor and helmets did not protect soldiers from closed blast-related TBI.

Taken together, the literature evidence convincingly demonstrates that the biomechanics and pathophysiology of neurotrauma resulting from blast exposure differ fundamentally from those of civilian peacetime injuries or penetrating ballistic trauma sustained in combat. These findings are of critical importance for developing effective diagnostic, therapeutic, and rehabilitation strategies for military personnel and veterans affected by blast-related brain injury.

Disclosure

Conflict of Interest

The authors declare no conflict of interest.

Funding

This research received no external funding.

References

1. Kobeissy F, Mondello S, Tümer N, Toklu HZ, Whidden MA, Kirichenko N, Zhang Z, Prima V, Yassin W, Anagli J, Chandra N, Svetlov S, Wang KK. Assessing neuro-systemic & behavioral components in the pathophysiology of blast-related brain injury. Front Neurol. 2013 Nov 21;4:186. doi: 10.3389/fneur.2013.00186
2. Hoge CW, McGurk D, Thomas JL, Cox AL, Engel CC, Castro CA. Mild traumatic brain injury in U.S. Soldiers returning from Iraq. N Engl J Med. 2008 Jan 31;358(5):453-63. doi: 10.1056/NEJMoa072972
3. Elder GA. Update on TBI and Cognitive Impairment in Military Veterans. Curr Neurol Neurosci Rep. 2015 Oct;15(10):68. doi: 10.1007/s11910-015-0591-8
4. Defense and Veterans Brain Injury Center. DoD Worldwide Numbers for TBI. https://www.biami.org/wp-content/uploads/2017/09/DoD-TBI-Worldwide-Totals_2000-2016_Feb-17-2017_v1.0_2017-04-06.pdf
5. Mac Donald CL, Johnson AM, Wierzechowski L, Kassner E, Stewart T, Nelson EC, Werner NJ, Zonies D, Oh J, Fang R, Brody DL. Prospectively assessed clinical outcomes in concussive blast vs nonblast traumatic brain injury among evacuated US military personnel. JAMA Neurol. 2014 Aug;71(8):994-1002. doi: 10.1001/jamaneurol.2014.1114
6. Taylor B, Campbell E, Nugent S. Fiscal year 2011 VA utilization report for Iraq and Afghanistan war veterans diagnosed with TBI. Minneapolis VA health care system, Affairs DoV. 2015 Nov. https://www.polytrauma.va.gov/TBIReports/FY14-TBI-Diagnosis-HCU-Report.pdf
7. DePalma RG, Hoffman SW. Combat blast related traumatic brain injury (TBI): Decade of recognition; promise of progress. Behav Brain Res. 2018 Mar 15;340:102-105. doi: 10.1016/j.bbr.2016.08.036
8. Owens BD, Kragh JF Jr, Wenke JC, Macaitis J, Wade CE, Holcomb JB. Combat wounds in operation Iraqi Freedom and operation Enduring Freedom. J Trauma. 2008 Feb;64(2):295-9. doi: 10.1097/TA.0b013e318163b875
9. Armistead-Jehle P, Soble JR, Cooper DB, Belanger HG. Unique Aspects of Traumatic Brain Injury in Military and Veteran Populations. Phys Med Rehabil Clin N Am. 2017 May;28(2):323-337. doi: 10.1016/j.pmr.2016.12.008
10. Phipps H, Mondello S, Wilson A, Dittmer T, Rohde NN, Schroeder PJ, Nichols J, McGirt C, Hoffman J, Tanksley K, Chohan M, Heiderman A, Abou Abbass H, Kobeissy F, Hinds S. Characteristics and Impact of U.S. Military Blast-Related Mild Traumatic Brain Injury: A Systematic Review. Front Neurol. 2020 Nov 2;11:559318. doi: 10.3389/fneur.2020.559318
11. Karr JE, Areshenkoff CN, Duggan EC, Garcia-Barrera MA. Blast-related mild traumatic brain injury: a Bayesian random-effects meta-analysis on the

cognitive outcomes of concussion among military personnel. Neuropsychol Rev. 2014 Dec;24(4):428-44. doi: 10.1007/s11065-014-9271-8
12. McKee AC, Stern RA, Nowinski CJ, Stein TD, Alvarez VE, Daneshvar DH, Lee HS, Wojtowicz SM, Hall G, Baugh CM, Riley DO, Kubilus CA, Cormier KA, Jacobs MA, Martin BR, Abraham CR, Ikezu T, Reichard RR, Wolozin BL, Budson AE, Goldstein LE, Kowall NW, Cantu RC. The spectrum of disease in chronic traumatic encephalopathy. Brain. 2013 Jan;136(Pt 1):43-64. doi: 10.1093/brain/aws307
13. Sirko A, Pilipenko G, Romanukha D, Skrypnik A. Mortality and Functional Outcome Predictors in Combat-Related Penetrating Brain Injury Treatment in a Specialty Civilian Medical Facility. Mil Med. 2020 Jun 8;185(5-6):e774-e780. doi: 10.1093/milmed/usz431
14. Kucherov Y, Hubler GK, DePalma RG. Blast induced mild traumatic brain injury/concussion: a physical analysis. Journal of Applied Physics. 2012 Nov 15;112(10):104701. doi: 10.1063/1.4765727
15. Benzinger TL, Brody D, Cardin S, Curley KC, Mintun MA, Mun SK, Wong KH, Wrathall JR. Blast-related brain injury: imaging for clinical and research applications: report of the 2008 st. Louis workshop. J Neurotrauma. 2009 Dec;26(12):2127-44. doi: 10.1089/neu.2009.0885
16. Zhou Y, Wen LL, Wang HD, Zhou XM, Fang J, Zhu JH, Ding K. Blast-Induced Traumatic Brain Injury Triggered by Moderate Intensity Shock Wave Using a Modified Experimental Model of Injury in Mice. Chin Med J (Engl). 2018 Oct 20;131(20):2447-2460. doi: 10.4103/0366-6999.243558
17. Rutter B, Song H, DePalma RG, Hubler G, Cui J, Gu Z, Johnson CE. Shock Wave Physics as Related to Primary Non-Impact Blast-Induced Traumatic Brain Injury. Mil Med. 2021 Jan 25;186(Suppl 1):601-609. doi: 10.1093/milmed/usaa290
18. Wolf SJ, Bebarta VS, Bonnett CJ, Pons PT, Cantrill SV. Blast injuries. Lancet. 2009 Aug 1;374(9687):405-15. doi: 10.1016/S0140-6736(09)60257-9
19. Salzar RS, Treichler D, Wardlaw A, Weiss G, Goeller J. Experimental Investigation of Cavitation as a Possible Damage Mechanism in Blast-Induced Traumatic Brain Injury in Post-Mortem Human Subject Heads. J Neurotrauma. 2017 Apr 15;34(8):1589-1602. doi: 10.1089/neu.2016.4600
20. Yamamoto S, DeWitt DS, Prough DS. Impact & Blast Traumatic Brain Injury: Implications for Therapy. Molecules. 2018 Jan 26;23(2):245. doi: 10.3390/molecules23020245
21. Panzer MB, Myers BS, Capehart BP, Bass CR. Development of a finite element model for blast brain injury and the effects of CSF cavitation. Ann Biomed Eng. 2012 Jul;40(7):1530-44. doi: 10.1007/s10439-012-0519-2
22. Explosions and blast injuries: a primer for clinicians. Centers for Disease Control and Prevention National Center for Injury Prevention and Control. 2016. https://stacks.cdc.gov/view/cdc/28987
23. Kinch K, Fullerton JL, Stewart W. One hundred years (and counting) of blast-associated traumatic brain injury. J R Army Med Corps. 2019 Jun;165(3):180-182. doi: 10.1136/jramc-2017-000867
24. Mu W, Catenaccio E, Lipton ML. Neuroimaging in Blast-Related Mild Traumatic Brain Injury. J Head Trauma Rehabil. 2017 Jan/Feb;32(1):55-69. doi: 10.1097/HTR.0000000000000213
25. Salat DH, Robinson ME, Miller DR, Clark DC, McGlinchey RE. Neuroimaging of deployment-associated traumatic brain injury (TBI) with a focus on mild TBI (mTBI) since 2009. Brain Inj. 2017;31(9):1204-1219. doi: 10.1080/02699052.2017.1327672
26. Zuckerman A, Ram O, Ifergane G, Matar MA, Sagi R, Ostfeld I, Hoffman JR, Kaplan Z, Sadot O, Cohen H. Controlled Low-Pressure Blast-Wave Exposure Causes Distinct Behavioral and Morphological Responses Modelling Mild Traumatic Brain Injury, Post-Traumatic Stress Disorder, and Comorbid Mild Traumatic Brain Injury-Post-Traumatic Stress Disorder. J Neurotrauma. 2017 Jan 1;34(1):145-164. doi: 10.1089/neu.2015.4310
27. Muneer PMA, Schuetz H, Wang F, Skotak M, Jones J, Gorantla S, Zimmerman MC, Chandra N, Haorah J. Induction of oxidative and nitrosative damage leads to cerebrovascular inflammation in an animal model of mild traumatic brain injury induced by primary blast. Free Radic Biol Med. 2013 Jul;60:282-91. doi: 10.1016/j.freeradbiomed.2013.02.029
28. Tompkins P, Tesiram Y, Lerner M, Gonzalez LP, Lightfoot S, Rabb CH, Brackett DJ. Brain injury: neuro-inflammation, cognitive deficit, and magnetic resonance imaging in a model of blast induced traumatic brain injury. J Neurotrauma. 2013 Nov 15;30(22):1888-97. doi: 10.1089/neu.2012.2674
29. Elder GA, Gama Sosa MA, De Gasperi R, Stone JR, Dickstein DL, Haghighi F, Hof PR, Ahlers ST. Vascular and inflammatory factors in the pathophysiology of blast-induced brain injury. Front Neurol. 2015 Mar 16;6:48. doi: 10.3389/fneur.2015.00048
30. Dixon KJ. Pathophysiology of Traumatic Brain Injury. Phys Med Rehabil Clin N Am. 2017 May;28(2):215-225. doi: 10.1016/j.pmr.2016.12.001
31. Rodriguez UA, Zeng Y, Deyo D, Parsley MA, Hawkins BE, Prough DS, DeWitt DS. Effects of Mild Blast Traumatic Brain Injury on Cerebral Vascular, Histopathological, and Behavioral Outcomes in Rats. J Neurotrauma. 2018 Jan 15;35(2):375-392. doi: 10.1089/neu.2017.5256
32. Mishra V, Skotak M, Schuetz H, Heller A, Haorah J, Chandra N. Primary blast causes mild, moderate, severe and lethal TBI with increasing blast overpressures: Experimental rat injury model. Sci Rep. 2016 Jun 7;6:26992. doi: 10.1038/srep26992
33. Säljö A, Arrhén F, Bolouri H, Mayorga M, Hamberger A. Neuropathology and pressure in the pig brain resulting from low-impulse noise exposure. J Neurotrauma. 2008 Dec;25(12):1397-406. doi: 10.1089/neu.2008.0602
34. Koliatsos VE, Cernak I, Xu L, Song Y, Savonenko A, Crain BJ, Eberhart CG, Frangakis CE, Melnikova T, Kim H, Lee D. A mouse model of blast injury to brain: initial pathological, neuropathological, and behavioral characterization. J Neuropathol Exp Neurol. 2011 May;70(5):399-416. doi: 10.1097/NEN.0b013e3182189f06
35. Long JB, Bentley TL, Wessner KA, Cerone C, Sweeney S, Bauman RA. Blast overpressure in rats: recreating a battlefield injury in the laboratory. J Neurotrauma. 2009 Jun;26(6):827-40. doi: 10.1089/neu.2008.0748
36. Rubio JE, Skotak M, Alay E, Sundaramurthy A, Subramaniam DR, Kote VB, Yeoh S, Monson K, Chandra N, Unnikrishnan G, Reifman J. Does Blast Exposure to the Torso Cause a Blood Surge to the Brain? Front Bioeng Biotechnol. 2020 Dec 17;8:573647. doi: 10.3389/fbioe.2020.573647
37. Alford PW, Dabiri BE, Goss JA, Hemphill MA, Brigham MD, Parker KK. Blast-induced phenotypic switching in cerebral vasospasm. Proc Natl Acad Sci U S A. 2011 Aug 2;108(31):12705-10. doi: 10.1073/pnas.1105860108
38. Chodobski A, Zink BJ, Szmydynger-Chodobska J.

Blood-brain barrier pathophysiology in traumatic brain injury. Transl Stroke Res. 2011 Dec;2(4):492-516. doi: 10.1007/s12975-011-0125-x
39. Gupta RK, Przekwas A. Mathematical Models of Blast-Induced TBI: Current Status, Challenges, and Prospects. Front Neurol. 2013 May 30;4:59. doi: 10.3389/fneur.2013.00059
40. Chen H, Constantini S, Chen Y. A Two-Model Approach to Investigate the Mechanisms Underlying Blast-Induced Traumatic Brain Injury. In: Kobeissy FH, editor. Brain Neurotrauma: Molecular, Neuropsychological, and Rehabilitation Aspects. Boca Raton (FL): CRC Press/Taylor & Francis; 2015. Chapter 17.
41. Bass CR, Panzer MB, Rafaels KA, Wood G, Shridharani J, Capehart B. Brain injuries from blast. Ann Biomed Eng. 2012 Jan;40(1):185-202. doi: 10.1007/s10439-011-0424-0

Original article

Ukrainian Neurosurgical Journal. 2025;31(4):26-36
doi: 10.25305/unj.328442

Comprehensive assessment of surgical, clinical, and radiological outcomes in craniovertebral junction anomalies with basilar invagination and atlantoaxial dislocation: An initial experience of 5 cases

Dharmikkumar Velani, Varshesh Shah, Krushi Soladhra, Renish Padshala, Nazar Imam, Jaimin Modh, Arvind Verma

Department of Neurosurgery, Smt. NHL Municipal Medical College, Ahmedabad, Gujrat, India

Received: 30 April 2025
Accepted: 27 June 2025

Address for correspondence*:* *Dharmikkumar Velani, Department of Neurosurgery, Smt. NHL Municipal Medical College, 2H9C+2FR, Pritan Rai Cross Road, Ellise Bridge, Paldi, Ahmedabad, Gujarat 380006, India, e-mail: dharmikvelani@yahoo.com*

Objective: The craniovertebral junction (CVJ) plays a pivotal role in stabilizing and facilitating movement within the craniospinal axis. This study aimed to evaluate the clinical, radiological characteristics and surgical outcomes in patients with CVJ anomalies associated with basilar invagination and atlantoaxial dislocation.

Materials and methods: A retrospective analysis of five patients with CVJ anomalies, who underwent surgical management at Sardar Vallabhbhai Patel (SVP) Hospital, Ahmedabad, Gujarat, India. They were analyzed for clinical characteristics, radiological parameters and various surgical procedures. Patient's clinical and radiological status was assessed pre- and postoperatively at discharge and at 6 months of follow-up. Nurick grading system and Modified Japanese Orthopedic Association (mJOA) score was used. Radiological assessment was done by atlantodental interval (ADI), craniobasal angle, and craniometric lines.

Results: Most patients presented with neck pain, followed by motor weakness as the second most common symptom, while sensory deficits were the least frequent. Congenital atlantoaxial dislocation was the most prevalent CVJ anomaly observed. Clinically, significant postoperative improvements were observed in both Nurick grade and Modified Japanese Orthopedic Association (mJOA) score. Radiological findings showed a reduction in the atlanto-dens interval (ADI), a less acute clivus-canal angle, and downward movement of the odontoid process in the postoperative period. All cases had favorable postoperative outcomes, with no mortality reported at the one-year follow-up, and the condition of all patients stabilized.

Conclusion: Favorable outcomes were achieved through posterior fixation without anterior exposure in selected cases. The key to achieving excellent clinical and radiological outcomes with minimal complications lay in a thorough preoperative evaluation, timely surgical intervention, and the selection of an individualized surgical technique.

Keywords*: craniovertebral junction; basilar invagination; atlantoaxial dislocation; posterior fixation; surgical clinical; outcomes; case series*

Introduction

The craniovertebral junction (CVJ) plays a critical role in maintaining both mobility and biomechanical stability. Common developmental anomalies in this region include irreducible atlantoaxial dislocation (AAD) and basilar invagination (BI), which are frequently seen alongside occipital fusion of the C1 arch. Basilar invagination refers to the congenital upward shift of the upper cervical spine, particularly the odontoid process, into the foramen magnum, and it is often associated with AAD [1].

The aim of treatment is to stabilize the craniovertebral junction, correct any deformities or misalignments, and relieve pressure on the neural structures. The purpose of using instrumentation is to achieve immediate stability, enhance fusion outcomes, minimize postoperative external immobilization, and shorten rehabilitation periods. Common complications that may arise include dural tears, CSF leakage, infections at the surgical site, nerve or cord damage, vertebral artery damage, and failure of fusion at the bone or screw interface [2].

The progress made in neuroradiology and surgical techniques has led to improved safety, increased fusion success, fewer complications, and better clinical outcomes [3, 4]. Nevertheless, the posterior approach, including occipitocervical fusion or C1-2 fusion with or without bony decompression — remain a complex procedure due to the intricate bony and neurovascular anatomy at the CVJ [5, 6].

This case report series presents our institutional experience with posterior surgical approaches in five patients diagnosed with congenital BI and AAD.

This study sought to analyze the clinical characteristics, Nurick grading, Modified Japanese Orthopedic Association (mJOA) score and the outcomes

of patients with craniovertebral instability who underwent posterior surgical treatment, either with or without decompression. It also aimed to assess the radiological results, including the measurement of craniometric and craniobasal angles, atlanto-dental interval (ADI), and bony fusion.

Material and methods

Study participants

A retrospective review was conducted on 5 patients with developmental craniovertebral junction anomalies operated on at the Neurosurgery Department SVP Hospital, Ahmedabad.

Inclusion criteria

Patients with developmental CVJ anomalies managed surgically through a posterior approach either occipitocervical or atlantoaxial fixation and fusion who had developmental irreducible BI with AAD with minimum 6 months' follow-up were included in our study.

Exclusion criteria

The following conditions led to exclusion from the study:

1. Traumatic AADs with fractures of the C1 or C2 arches or facet joints,

2. Polytrauma involving other areas of the cervical spine.

3. Rheumatoid arthritis.

Preoperative Assessment

Cases followed our inclusion criteria and they were analyzed for age, sex, clinical characteristics, radiological diagnosis, and treatment given. Patient's clinical status was assessed pre- and postoperatively (at 6 months) by the Nurick grading system and Modified Japanese Orthopedic Association (mJOA) score.

Nurick grades 0, I, and II have been considered as good and III to V as poor Nurick grade. Various craniometric lines (McRae, McGregor, Wackenheim Line, Chamberlain, Modified Ranawat Line and clivus canal line), craniobasal angle (clivus canal angle), and ADI were recorded. Standard definition exists for all the parameters mentioned.

The atlantodental interval was measured to evaluate the horizontal dislocation of C1 over C2 or C2 over assimilated C1.

The following measurements were used to assess the BI

Chamberlain Line (CL): The normal range was considered as dens being about 2.3 - 2.6 mm below this line.

Wackenheim Line: The normal value was considered being about 0.9 –2.2 mm below this line.

McRae Line (ML): The normal value was considered being about 5.8±1.6 mm below this line.

Modified Ranawat Line: From the midpoint of the base of C2, a line was drawn to meet the line drawn from the center of the anterior arch of C1 to the center of the posterior arch. The distance between the 2 lines along the long axis of C2 was measured (normal value is about 17 +-2.6 mm; a value less than this indicates BI).

The realignment was measured using the clivus canal angle (normal value ~ 150°).

CT angiogram was performed in patients to explore the size and course of the vertebral arteries between C1 and C2 segments.

Associated Chiari malformation, syringomyelia, or other intramedullary signal changes were also evaluated. Associated syringomyelia was found in 3 patients.

Postoperatively at 1 year follow-up, dynamic computerized tomography (CT) scan CVJ region was done in each case and we reassessed the various craniometric lines, ADI, craniobasal angles, and bone fusion between C1 and C2.

The posterior margin of the foramen magnum was removed in all cases, making it impossible to directly draw the cranial line (CL) and mandibular line (ML) on the postoperative images. To circumvent this, a technique based on the approach by Jian et al. was applied. A reference line was drawn from the posterior edge of the hard palate to the anterior edge of the foramen magnum. Then the angles between this reference line and CL (hard palate to posterior foramen magnum) and ML (anterior to posterior foramen magnum) were measured. On the postoperative CT scans, the reference line was drawn first, and then the CL and ML were reconstructed by transferring the measured angles.

Operative technique

All cases underwent posterior fixation and decompression. Out of 5 cases of posterior fixation, one case underwent C1 lateral mass and C2 pars screw fixation for reducible atlantoaxial dislocation (AAD) (see ***Fig. 1, Fig. 2***). O-C2 fixation (***Fig. 3, Fig. 4***) was performed in one case of C1-C2 subluxation was associated with C1 defects (assimilation, absent posterior arch) and abnormal C1-C2 joint anatomy (vertically oriented or deformed C1-C2 joint). O-C2-C3-C4 fixation was performed in three cases.

Intraoperatively, vertebral artery rupture leading to bleeding, had occurred in one case during C2 screw placement. Postoperatively, a wound infection was noticed in the same case. Both complications were managed conservatively and the patient was subsequently discharged.

Statistical analysis

Descriptive statistics were used to summarize demographic data, clinical characteristics, radiological parameters, and outcome measures. Continuous variables such as age, ADI (atlanto-dental interval), clivus canal angle, and mJOA scores were expressed as mean ± standard deviation (SD) or median where appropriate. Categorical variables such as Nurick grades and presence of associated anomalies were reported as frequencies and percentages.

Results

Neck pain was the most common presenting symptom in our study. Other frequent manifestations were motor weakness, sensory disturbances, and restricted neck movement. Additional clinical findings are given in ***Table 1***. The majority of cases presented with symptoms duration longer than 12 months.

This article contains some figures that are displayed in color online but in black and white in the print edition.

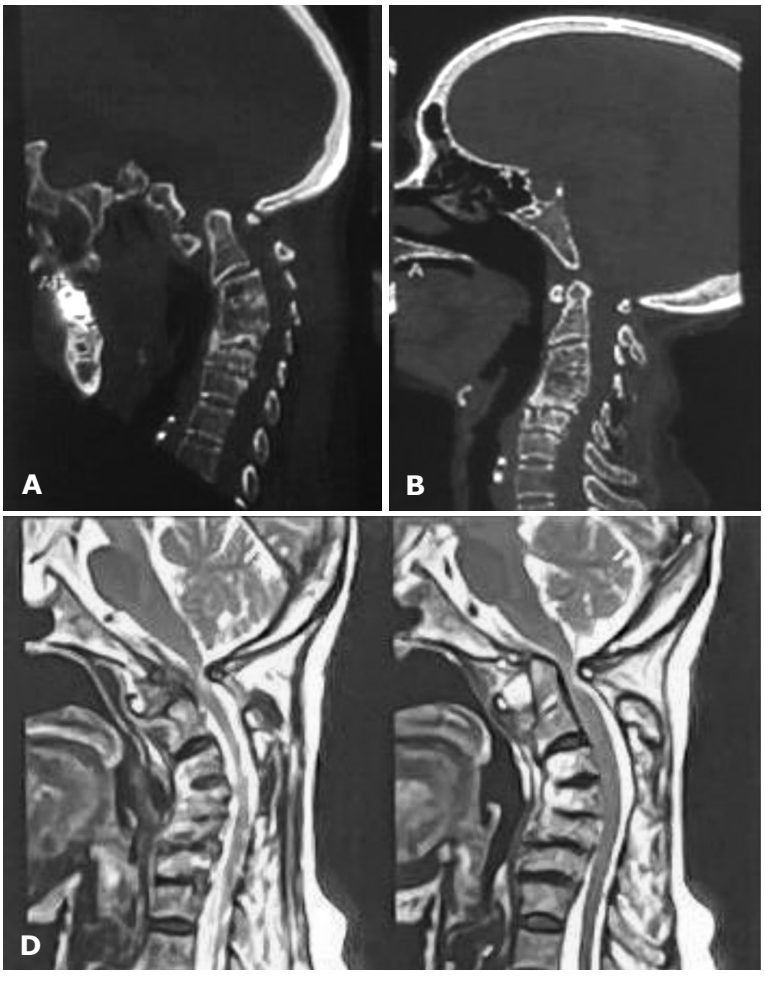

Fig. 1. Preoperative non-contrast computed tomography (CT) of craniovertebral junction (CVJ).

A - sagittal view showing atlantoaxial dislocation (AAD) in flexion

B - sagittal view showing in neutral position

C - reduction of AAD in extension

D - T2-weighted (T2W) magnetic resonance imaging (MRI) of CVJ in sagittal view

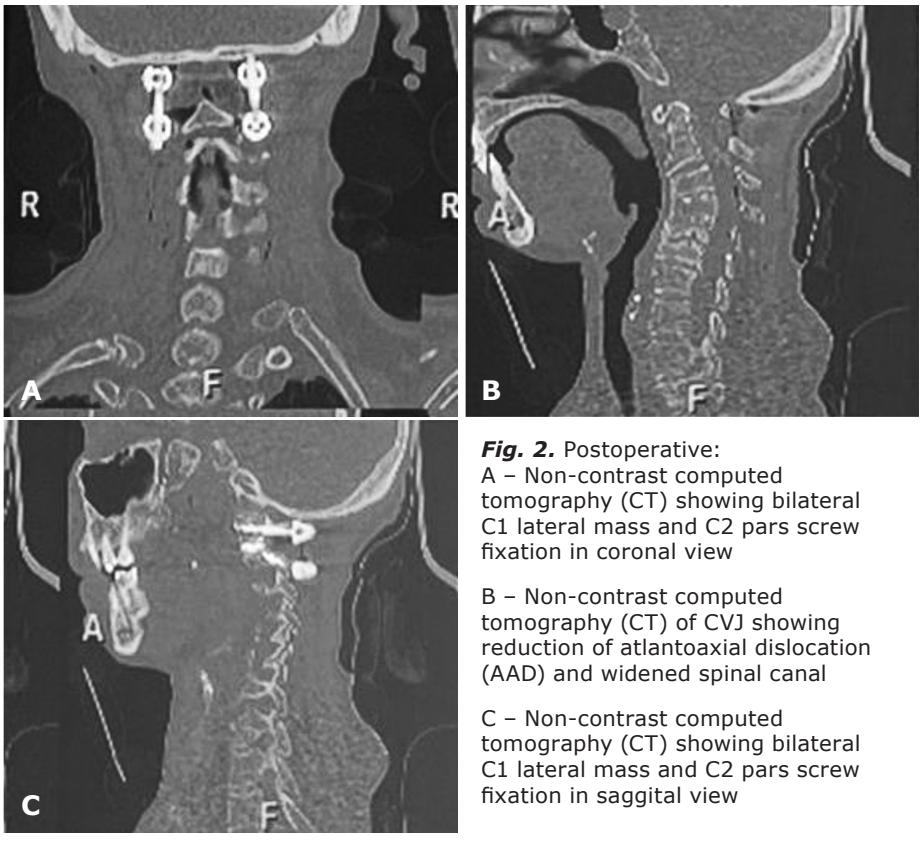

Fig. 2. Postoperative:
A – Non-contrast computed tomography (CT) showing bilateral C1 lateral mass and C2 pars screw fixation in coronal view

B – Non-contrast computed tomography (CT) of CVJ showing reduction of atlantoaxial dislocation (AAD) and widened spinal canal

C – Non-contrast computed tomography (CT) showing bilateral C1 lateral mass and C2 pars screw fixation in saggital view

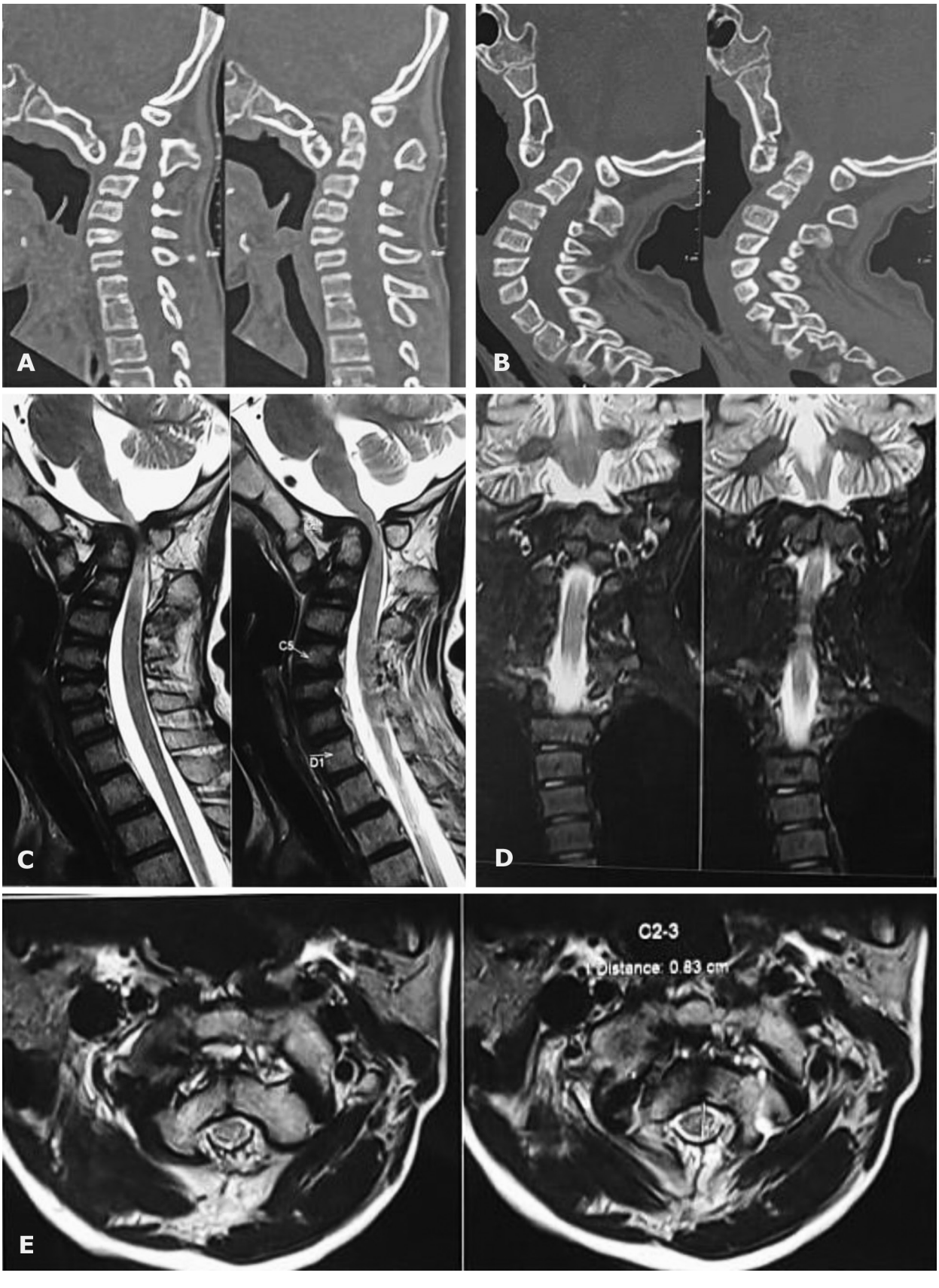

Fig. 3. Preoperative non-contrast computed tomography (CT) of craniovertebral junction (CVJ).
A - sagittal view showing in flexion position
B - sagittal view showing in extension position
C,D,E - T2-weighted (T2W) magnetic resonance imaging (MRI) CVJ sagittal view and axial cuts, showing cord compression with hyperintense changes in the cord at the CVJ region.

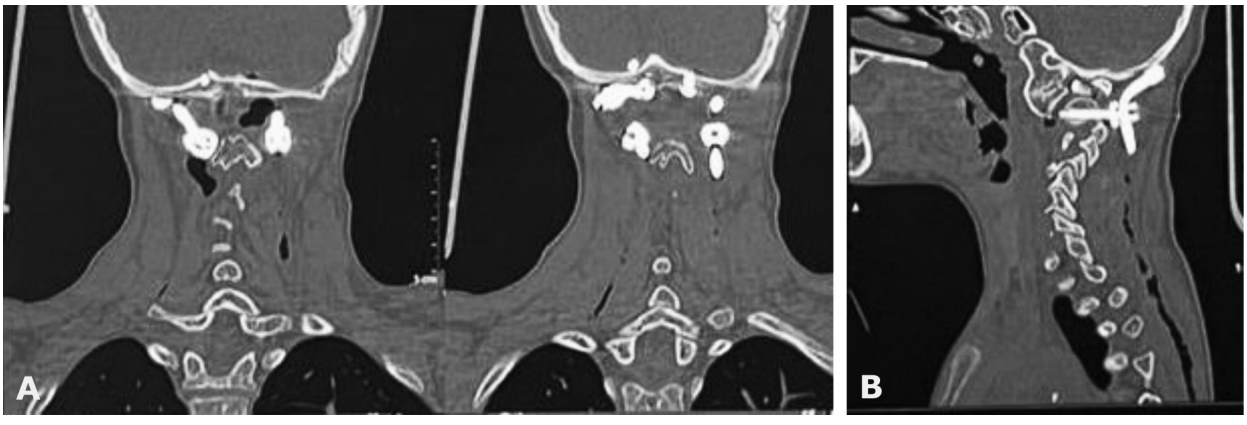

Fig. 4. Postoperative computed tomography (CT) of craniovertebral junction (CVJ).
A - Coronal view showing occipital plate and C2 pars screw
B - Sagittal view showing occipital plate and C2 pars screw

Table 1. Clinical findings and duration of symptoms

Clinical findings		Number
Neck pain		4
Restricted neck movement		2
Motor weakness	Quadriparesis	0
	Hemiparesis	4
Sensory disturbances	Posterior column involvement	3
	Spinothalamic tract involvement	2
Cerebellovestibular disturbances		0
Lower cranial nerve palsy		0
Sphincter disturbances		0
Respiratory involvements		0
Neck tilt, low hair line, short neck		4
Thenar/hypothenar muscle wasting		1
Duration of symptoms (in months)	Up to 6	1
	7–12	1
	13–24	2
	≥ 25	1

Congenital AAD was the most common congenital CVJ anomaly. Other common congenital CVJ anomalies are given in ***Table 2***.

In preoperative period, all patients were classified as having poor Nurick grades and low mJOA scores. In the postoperative period, all patients had improved in Nurick and m-JOA grading as compared with preoperative scores. (***Table 3***).

In the postoperative period, there was a significant shortening of distance of the odontoid process above the defined craniometric lines. Radiologically, a significant decrease in the ADI was observed postoperatively. Preoperatively, clivus canal angle was more acute as compare to the postoperative period (***Table 4***). Both, the decrease in ADI and the increase in clivus canal angle, suggest a reduction in the ventral compression of the cord postoperatively.

Various radiological craniometric lines were calculated. Some of examples are given in the image below (***Fig. 5, Fig. 6***).

Table 2. Distribution of congenital anomaly

Congenital anomaly	Number
Atlantoaxial dislocation	5
Basilar invagination	4
Chiari malformation	2
Assimilation of atlas	4
Unilateral deficient posterior arch of atlas	0
Block vertebrae	1
Klippel–Feil syndrome	0
Platybasia	0

Table 3. Associated radiological anomalies, surgery performed, clinical outcomes

No	Age	Sex	Radiology	Surgery	Nurick grading		m-JOA grading	
					pre-op	post-op	pre-op	post-op
1	29	F	C1A,Syr	Oc- C2-3-4	4	1	14	16
2	57	M	C1A	Oc-C2-3-4	3	0	15	17
3	52	F	C1A,Syr	Oc-C2-3-4	4	2	11	10
4	11	M	C1A	Oc-C2	4	2	10	14
5	61	F	C1A	C1-C2	4	1	15	18

Notes. M=male; F=female; C1A=C1 arch assimilated with occiput; C1NA=C1 arch not assimilated with occiput; Ch=Chiari malformation; Syr=syringomyelia; Oc-C2= occipito-C2 distractive compressive reduction performed; C1/C2=C1 and C2 distractive compressive reduction performed; preop=preoperative; postop=postoperative, Syr=syringomyelia

Table 4. Pre- and postoperative radiological findings

Patient No.	Age,Y	Sex	ADI, mm		CL (Normal = 2.3±2.6 mm)		ML (Normal = 5.8±1.6 mm)		WL (Normal = 0.9±2.2 mm)		CCA (Normal.150°)		RL (Normal = 17±2.6 mm)	
			pre-op	post-op	pre-op	post-op	pre-op	post-op	pre-op	post-op	pre-op	post-op	pre-op	post-op
1	29	F	3.9	2.2	-8.9	3.3	-3.2	4.8	26.4	1	115	155	7	17
2	57	M	2.1	1.8	-7.1	3.8	-3.58	4.5	22.4	1.2	106	130	3	19
3	52	F	3.1	1.4	-9.8	0.2	-4.5	1.2	25.4	1.1	141	135	10	23
4	11	M	5	1	-12.9	3.6	-15.3	1.1	-11.3	1.5	138	156	3.5	23
5	61	F	4	0	-6.1	2.2	-7.4	1.9	-6.5	-1.2	116	134	9	20

Notes. ADI, atlantodental interval; CL, Chamberlain line; ML, McRae line; WL, Wackenheim line; CCA, clivus canal angle; RL, modified Ranawat line; M, male; F, female; preop, preoperative; postop, postoperative.

Negative value indicates that the dens is placed above this line.

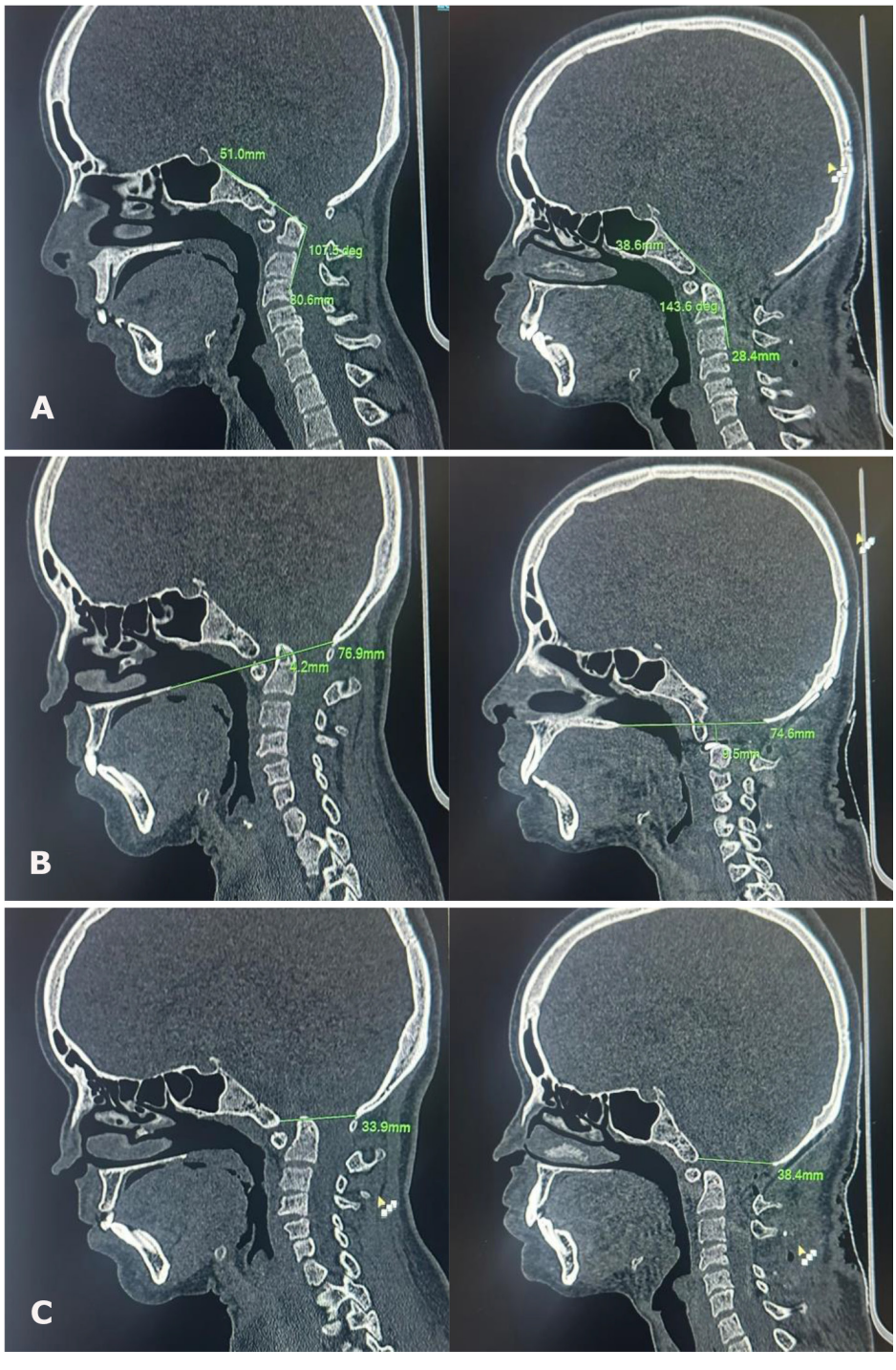

Fig. 5. A - pre-op and post op clivus canal angle
B - pre and post op chamberlain line
C - pre and post op McRae line

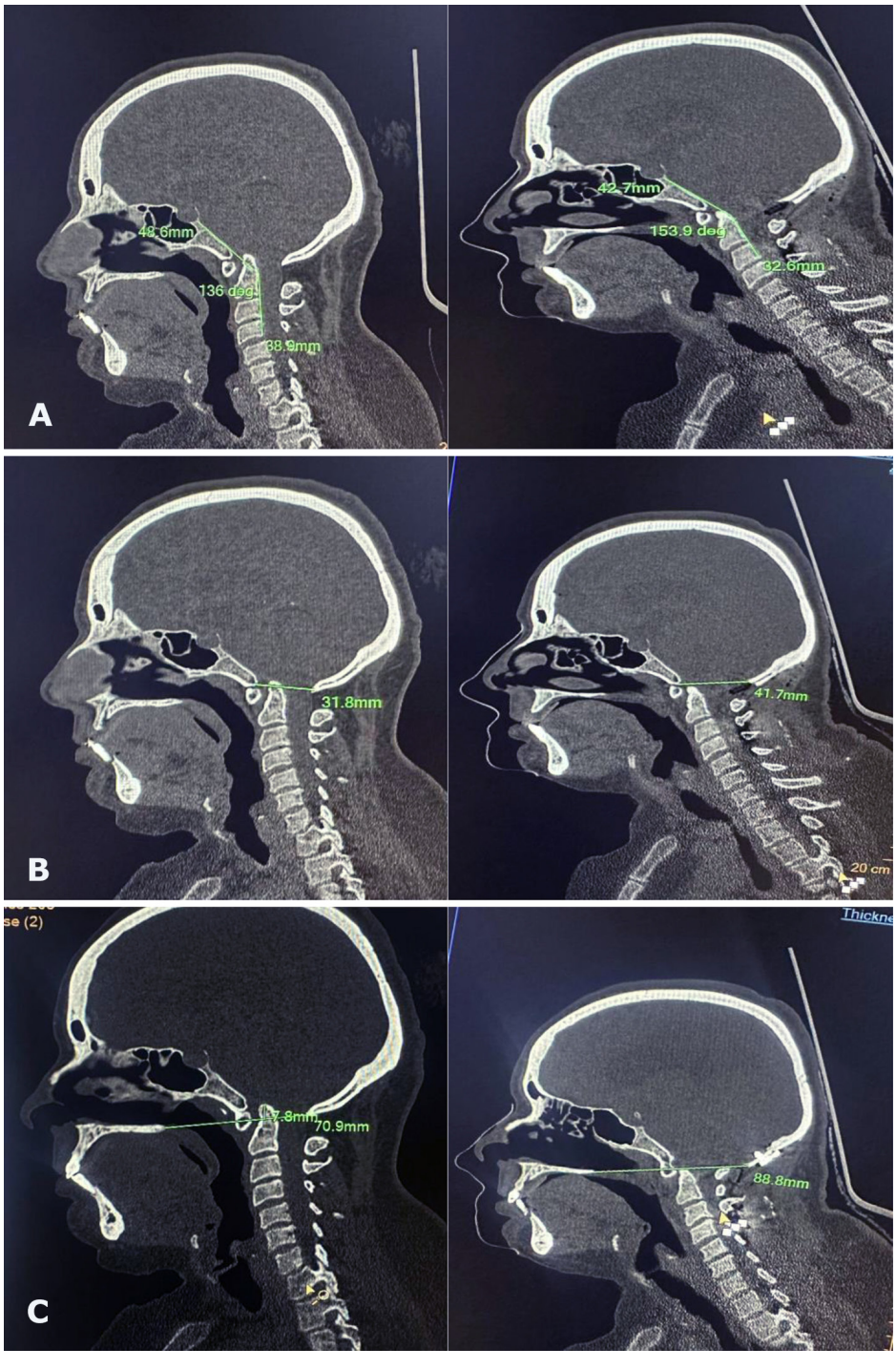

Fig. 6. A - pre and post op clivus canal angle
B - pre and post op McRae line
C - pre and post op Chamberlain line

Discussion

The main objectives of surgery in CVJ anomalies are to alleviate compression and stabilize the CVJ. In most cases, both of these goals can be effectively achieved through a single posterior midline approach. While posterior approaches have gained popularity due to lower morbidity and improved instrumentation, ventral decompression techniques remain crucial in managing rigid anatomical constraints and severe ventral cord compression.

Previously, semi-rigid wire and loop fixation devices were used for stabilization [7]. However, recent studies have shown that rigid screw fixation provides superior results [8, 9].

Atlantoaxial dislocation (AAD) and basilar invagination (BI) are complex conditions that lead to progressive cervicomedullary compression and neurological deficits. The primary goal of treatment is to alleviate compression, provide adequate stability, and correct any deformities. These congenital anomalies

typically cannot be reduced using cervical traction with dynamic X-rays. Most cases are associated with atlas assimilation to the occiput. Notably, most of our patients had irreducible AAD and BI. Traditionally, BI with AAD was managed through an anterior transoral approach to remove the odontoid process, followed by posterior instrumented fixation.

The common clinical presentations in our study were neck pain, motor weakness, sensory disturbances, restricted neck motion. A study done by Goel has similar presentations except lower number of cases presenting with cerebellovestibular disturbances and respiratory involvement [10]. The differences may be due to less number of cases in our study.

Goel compared the ADI preoperatively and postoperatively and achieved a satisfactory decrease in ADI in more than 80% of the patients [10]. In our study, we also attained a satisfactory decrease in ADI in all cases.

After fixation, the bone fusion rate of CVJ anomalies has been reported to be highly successful (75–100%) as described by previous studies regardless of fixation material used and underlying pathologies [11, 12]. In our study, 6 months after surgery solid bone fusion was achieved in all cases, this is comparable to other studies. Excellent results have been reported by Grob et al (100%) and Wertheim et al (100%) [13, 14].

Complications such as dural tear was noted in one case. Intraoperative verterbral artery rupture, wound infection had occurred in one case in our study.

Distraction, compression, extension, and reduction. Chandra et al [15, 16] described an innovative technique for reducing BI with AAD via a single-stage posterior approach. This approach avoids the need for an anterior transoral procedure and involves both the use of an interarticular spacer to distract the C1-C2 joints and the application of horizontal occipito-cervical manipulation to address the CVJ deformity secondary to AAD. The technique is especially suited for cases where C1 is fused with the occiput.

Non-reducible basilar invagination is classified into three types based on the sagittal inclination (SI) angle, which is the angle between a line parallel to the axis of the odontoid process (tangential to its posterior border) and a line parallel to the C1-C2 joint surface. The normal range of the SI angle is 87.15 ± 5.65°. The classification is as follows: type I for SI angles <100°, Type II for 100–160°, and Type III for >160°. Chandra et al. advised particular surgical interventions for each type, and further details can be found in their manuscript.:

Type I: DCER

Type II: Joint remodeling+DCER

Type III: Extra-articular distraction+DCER

Two main approaches have emerged for the management of non-reducible BI and AAD:

1. Posterior decompression and reduction with occipitocervical fixation.

2. The DCER procedure that includes the application of a C1–C2 facet joint spacer.

Both recent methods resulted in complete fusion. The techniques including the C1–C2 joint spacer and vertical reduction yielded significantly better outcomes in terms of index correction and reduction rates. Although it is difficult to compare major complications in detail due to the limited number of cases, vertebral artery injury was the most serious complication reported in both techniques, with a slightly higher incidence in DCER procedures. In accordance with current literature and the findings from Chandra et al., we successfully applied the DCER technique for the first time at our institution to treat individuals with BI and AAD.

Ventral decompression techniques in irreducible BI and AAD:

When dealing with fixed deformities and non-reducible basilar invagination (BI) or atlantoaxial dislocation (AAD), direct anterior decompression is often required to relieve pressure on the brainstem and upper cervical spinal cord. In such cases, the transoral odontoidectomy, as described and popularized by Alan Crockard and colleagues, remains the gold standard for direct ventral decompression [17–19].

Crockard's work laid the foundation for modern transoral approaches, particularly in patients with significant ventral compression due to an upwardly displaced odontoid process. His studies demonstrated that transoral odontoidectomy allows for safe and effective removal of the odontoid process through an intraoral route, thereby relieving ventral pressure without the need for extensive brain retraction or dural manipulation [17]. This approach is especially beneficial in cases where the sagittal inclination (SI) angle exceeds 160° (Type III deformity), making posterior reduction inadequate or impossible.

Combined anterior-posterior approach: Crockard's legacy. One of the most important contributions of Alan Crockard to CVJ surgery was his advocacy for a combined anterior-posterior approach — particularly in complex cases involving irreducible BI and AAD. He emphasized that while anterior decompression addresses the immediate threat to neural structures, posterior stabilization provides the biomechanical support necessary for durable outcomes.

In his seminal work, Crockard described a two-stage procedure:

1. Anterior transoral odontoidectomy to remove the offending bony structure causing ventral compression

2. Posterior occipitocervical or C1–C2 fixation to stabilize the CVJ and maintain alignment post-decompression

This combined strategy has since become the benchmark for managing severe, non-reducible CVJ pathologies, especially in the context of congenital anomalies, rheumatoid arthritis, and post-traumatic instability.

Comparison with Posterior Approaches:

While anterior decompression remains the gold standard in certain scenarios, posterior-only approaches have shown promising results in carefully selected patients. As highlighted by Goel and Chandra et al., patients with reducible or semi-reducible BI and AAD can achieve satisfactory outcomes using posterior fixation alone, avoiding the morbidity associated with transoral surgery [10, 15, 16].

In our series, we observed satisfactory clinical and radiological outcomes following posterior decompression and fixation without anterior exposure. Our findings align with those of Goel and Chandra et al., who have demonstrated that carefully selected patients with reducible or semi-reducible BI and AAD can benefit from posterior-only strategies [10, 15, 16]. Specifically, we noted a consistent reduction in the atlantodental interval (ADI) and improvement in clivus-canal angles postoperatively, indicating effective reduction and decompression of the cervicomedullary junction.

As highlighted by Crockard and others, ventral compression in the presence of rigid anatomical constraints or severe fixed deformities often necessitates anterior decompression to avoid catastrophic complications such as tetraplegia or respiratory compromise [17, 18]. Therefore, preoperative imaging—particularly dynamic MRI and CT angiography—is essential to assess reducibility, vertebral artery course, and the degree of ventral cord compression.

Although, the anterior transoral approach remains the gold standard for definitive ventral decompression in non-reducible BI with AAD, our experience suggests that selected patients with certain morphological characteristics may benefit from a posterior-only strategy. Meticulous patient selection, accurate radiological assessment, and intraoperative neuromonitoring are imperative to ensure safe and effective outcomes.

Future studies with larger cohorts and comparative analyses between anterior and posterior approaches are warranted to further refine surgical indications and optimize patient care.

Conclusion

We noted satisfactory clinical improvement and vertical reduction. Congenital CVJ anomalies were the most common lesions found. The majority of patients presented with neck pain, motor weakness, and sensory deficits. Favorable outcomes, both clinically and radiologically, were seen in most cases. Proper preoperative evaluation and careful selection of individualized surgical techniques are crucial for minimizing complications. Our case series supports the use only posterior fixation without anterior exposure in patients with reducible or semi-reducible anomalies. The findings of this study may be subject to revision in the future with a more streamlined, single-stage approach, given the small sample size and potential selection bias.

Disclosure

Conflict of interest

The authors declare no conflicts of interest.

Funding

The study was not sponsored.

Informed consent

Informed and voluntary written consent to participate in the study and publication of data was obtained from all patients.

References

1. Nakajima K, Onomura T, Tanida Y, Ishibashi I. Factors related to the severity of myelopathy in atlantoaxial instability. Spine (Phila Pa 1976). 1996 Jun 15;21(12):1440-5. doi: 10.1097/00007632-199606150-00008
2. Vender JR, Houle PJ, Harrison S, McDonnell DE. Occipital-cervical fusion using the Locksley intersegmental tie bar technique: long-term experience with 19 patients. Spine J. 2002 Mar-Apr;2(2):134-41. doi: 10.1016/s1529-9430(01)00273-x
3. Goel A. Atlantoaxial joint jamming as a treatment for atlantoaxial dislocation: a preliminary report. Technical note. J Neurosurg Spine. 2007 Jul;7(1):90-4. doi: 10.3171/SPI-07/07/090
4. Grob D, Magerl F. Operative Stabilisierung bei Frakturen von C1 und C2 [Surgical stabilization of C1 and C2 fractures]. Orthopade. 1987 Feb;16(1):46-54. German.
5. Hong JT, Lee SW, Son BC, Sung JH, Yang SH, Kim IS, Park CK. Analysis of anatomical variations of bone and vascular structures around the posterior atlantal arch using three-dimensional computed tomography angiography. J Neurosurg Spine. 2008 Mar;8(3):230-6. doi: 10.3171/SPI/2008/8/3/230
6. Sardhara J, Behari S, Mohan BM, Jaiswal AK, Sahu RN, Srivastava A, Mehrotra A, Lal H. Risk stratification of vertebral artery vulnerability during surgery for congenital atlanto-axial dislocation with or without an occipitalized atlas. Neurol India. 2015 May-Jun;63(3):382-91. doi: 10.4103/0028-3886.158218
7. Reilly TM, Sasso RC, Hall PV. Atlantoaxial stabilization: clinical comparison of posterior cervical wiring technique with transarticular screw fixation. J Spinal Disord Tech. 2003 Jun;16(3):248-53. doi: 10.1097/00024720-200306000-00004
8. Ahmed R, Traynelis VC, Menezes AH. Fusions at the craniovertebral junction. Childs Nerv Syst. 2008 Oct;24(10):1209-24. doi: 10.1007/s00381-008-0607-7
9. Anderson RC, Ragel BT, Mocco J, Bohman LE, Brockmeyer DL. Selection of a rigid internal fixation construct for stabilization at the craniovertebral junction in pediatric patients. J Neurosurg. 2007 Jul;107(1 Suppl):36-42. doi: 10.3171/PED-07/07/036
10. Goel A. Posterior atlantoaxial 'facetal' instability associated with cervical spondylotic disease. J Craniovertebr Junction Spine. 2015 Apr-Jun;6(2):51-5. doi: 10.4103/0974-8237.156039
11. Oda I, Abumi K, Sell LC, Haggerty CJ, Cunningham BW, McAfee PC. Biomechanical evaluation of five different occipito-atlanto-axial fixation techniques. Spine (Phila Pa 1976). 1999 Nov 15;24(22):2377-82. doi: 10.1097/00007632-199911150-00015
12. Vale FL, Oliver M, Cahill DW. Rigid occipitocervical fusion. J Neurosurg. 1999 Oct;91(2 Suppl):144-50. doi: 10.3171/foc.1999.6.6.11
13. Grob D, Dvorak J, Panjabi M, Froehlich M, Hayek J. Posterior occipitocervical fusion. A preliminary report of a new technique. Spine (Phila Pa 1976). 1991 Mar;16(3 Suppl):S17-24.
14. Wertheim SB, Bohlman HH. Occipitocervical fusion. Indications, technique, and long-term results in thirteen patients. J Bone Joint Surg Am. 1987 Jul;69(6):833-6.
15. Chandra PS, Goyal N, Chauhan A, Ansari A, Sharma BS, Garg A. The severity of basilar invagination and atlantoaxial dislocation correlates with sagittal joint inclination, coronal joint inclination, and craniocervical tilt: a description of new indexes for the craniovertebral junction. Neurosurgery. 2014 Dec;10 Suppl 4:621-9; discussion 629-30. doi: 10.1227/NEU.0000000000000470
16. Chandra PS, Kumar A, Chauhan A, Ansari A, Mishra NK, Sharma BS. Distraction, compression, and extension reduction of basilar invagination and atlantoaxial dislocation: a novel pilot technique. Neurosurgery.

2013 Jun;72(6):1040-53; discussion 1053. doi: 10.1227/NEU.0b013e31828bf342
17. Crockard HA, Pozo JL, Ransford AO, Stevens JM, Kendall BE, Essigman WK. Transoral decompression and posterior fusion for rheumatoid atlanto-axial subluxation. J Bone Joint Surg Br. 1986 May;68(3):350-6. doi: 10.1302/0301-620X.68B3.3733795
18. Crockard HA. The transoral approach to the base of the brain and upper cervical cord. Ann R Coll Surg Engl. 1985 Sep;67(5):321-5.
19. Crockard HA. Ventrale Zugänge zur oberen Halswirbelsäule [Ventral approaches to the upper cervical spine]. Orthopade. 1991 Apr;20(2):140-6. German.

Original Article

Ukrainian Neurosurgical Journal. 2025;31(4):37-43
doi: 10.25305/unj.333521

Low temporal muscle thickness is an independent poor prognostic factor in patients with brain metastases treated with radiosurgery

Kiril Z. Zhelev [1], Emilia A. Barsha [1], Maria I. Mihaylova-Hristova [2], Nikolay V. Conev [3], Rostislav R. Manev [3]

[1] Department of Radiotherapy, University Hospital "Deva Maria", Vetren, Burgas, Bulgaria
[2] Department of Radiotherapy, National Oncological Hospital, Sofia, Bulgaria
[3] Clinic of Medical Oncology, UMHAT "St. Marina", Varna, Bulgaria

Received: 24 June 2025
Accepted: 17 July 2025

Address for correspondence: *Rostislav Manev, Clinic of Medical Oncology, UMHAT "St. Marina", 1 Hristo Smirnenski str., Varna, Bulgaria, Postal Code 9000, email: rostislav.manev1991@gmail.com*

Objective: The aim of this Bulgarian study was to determine the impact of temporal muscle thickness (TMT), a prognostic factor for sarcopenia, in patients with brain metastases (BMs) treated with radiosurgery.

Methods: A retrospective analysis was conducted using TMT values from planning brain magnetic resonance imaging (MRI) studies for 232 patients diagnosed with brain metastases originating from various histological solid tumors. These measurements were taken prior to their initial radiosurgery procedure, conducted between January 2021 and December 2022. The total TMT for both the left and right sides was calculated by summing them and then dividing by two to determine the average TMT. The cut-off value was determined for TMT based on the median of the measured values among all participants. Additionally, sarcopenia was assessed as an independent prognostic factor through Cox regression models that accounted for other relevant prognostic variables.

Results: In sarcopenia patients with a TMT below the cut-off values, specifically the median TMT (5.42 mm), the risk of death was significantly increased (HR = 6.310, 95% CI: 4.161–9.568, $p < 0.001$). In addition, sarcopenia was revealed to be an independent prognostic factor even after adjusting for gender, number of BMs, cancer type, and ECOG Performance Status (HR = 5.757, 95% CI: 3.717–8.915, $p < 0.001$). Patients with sarcopenia had a significantly shorter mean OS (5.46 months, 95% CI = 5.00–5.91) compared to those without sarcopenia (23.40 months, 95% CI = 20.62–26.18) (log-rank test $P < 0.001$).

Conclusions: In patients with BMs treated with radiosurgery, TMT from planning MRI studies serves as an independent prognostic marker and may help with patient stratification in future clinical trials.

Keywords: *sarcopenia; temporal muscle thickness; radiosurgery; brain metastases*

Introduction

Primary brain tumors and metastatic brain lesions from various extracranial malignancies are both classified as types of brain cancer [1]. Despite the implementation of comprehensive treatment strategies—including surgery, radiation therapy, and systemic chemotherapy, the rate of morbidity and mortality remains high. The median overall survival (OS) for these patients is about 12 months [2]. Various factors—such as age, Eastern Cooperative Oncology Group (ECOG) performance status (PS), tumor location and size, along with molecular and histological features—can serve as prognostic indicators [3]. In individuals diagnosed with brain tumors, evaluations related to sarcopenia and skeletal muscle mass may enhance prognostic predictions and help refine treatment plans.

Sarcopenia is a progressive and generalized loss of skeletal muscle mass and strength [4], and it has been identified as a prognostic factor in several extracranial cancer types [5-7]. Assessing skeletal muscle mass and function requires additional examinations, which may result in increased radiation exposure, healthcare costs, and/or a prolonged hospital stay.

Skeletal muscle mass is most often calculated from the volume of the third lumbar vertebrae musculature on cross-sectional abdominal computed tomography (CT) imaging [8-9]. In the case of brain tumors, radiologic images of the abdomen are not routinely available. To address this limitation, researchers have introduced the temporal muscle thickness (TMT), measured on magnetic resonance imaging (MRI), as a novel surrogate biomarker of muscle mass [10-11]. In clinical settings cranial MRI is routinely performed on patients with brain tumors. Researchers have proposed measuring TMT as an alternative method to evaluate muscle mass and identify sarcopenia in patients with brain tumors. There is no universally used threshold for determining low muscle mass.

The aim of this Bulgarian study was to ascertain whether TMT is an independent prognostic factor for overall survival (OS) in patients with brain metastases.

Materials and Methods

Patient selection

In this retrospective study conducted in Bulgaria, we evaluated 232 patients diagnosed with brain metastases who received radiosurgery between January 2021 to December 2022. Institutional records were reviewed to obtain demographic, pathological, radiological, and treatment-related information. The procedure was approved by the scientific research ethics committee of the hospital.

The eligibility criteria were established as follows:

1) A primary tumor diagnosis confirmed by pathology.

2) Confirmation of brain metastasis through magnetic resonance imaging (MRI) by blinded neuroradiologists.

3) Patients who are inoperable.

4) No prior history of brain radiotherapy or surgery.

5) Individuals must be over 18 years old.

6) An Eastern Cooperative Oncology Group (ECOG) performance status (PS) ranging from 0 to 2.

The TMT measurements were performed by blinded specialists (neuroradiologists). However, patients lacking survival data or those with a history of primary brain tumors before the onset of brain metastasis were excluded from the analysis.

Temporal Muscle Thickness (TMT)

The day prior to radiosurgery, the TMT was assessed using a 1 mm axial slice from contrast-enhanced T1-weighted MRI. The axial plane of the MRI was aligned parallel to the line connecting the anterior and posterior commissures. Anatomical landmarks including the Sylvian fissure (in an anterior-posterior orientation) and the orbital roof (in a cranio-caudal direction), were used to create a perpendicular reference line relative to the long axis of the temporal muscle. The mean TMT value was calculated as the average of bilateral measurements. The cut-off value for TMT was established as the median measurement among all patients included in this study [12-14].

Statistical design and analysis

Data was processed and analyzed with IBM SPSS Statistics software version 23. The demographic details were presented as frequencies and percentages for categorical variables, while medians and means, accompanied by standard deviations, represented quantitative variables. To compare and assess the relationships between TMT and various clinicopathological characteristics of patients — including age, gender, tumor volume, and hematologic inflammation markers—the $\chi 2$ test was employed. The diagnostic performance of biomarkers was evaluated by calculating the maximum area under the curve (AUC) from receiver operating characteristic curve analysis. AUC values were classified as follows: ≥ 0.9 were considered excellent; ≥ 0.80 good; ≥ 0.7 fair, whereas values below 0.70 indicated poor accuracy. Survival curves based on treatment response were estimated using the Kaplan–Meier method, with differences tested through the log-rank test methodology. Additionally, multinomial logistic regression analyses were conducted to determine how TMT influenced treatment responses. Two-tailed p-values < 0.05 were considered statistically significant.

Ethical approval

All procedures conducted in studies involving human participants adhered to the ethical guidelines established by the relevant institutional and/or national research committees, as well as the 1964 Declaration of Helsinki, along with its subsequent amendments or equivalent ethical standards. Approval was secured from the local ethics committee.

Results

Baseline characteristics and their relationship with temporal muscle thickness (TMT)

This single-center retrospective study included 232 patients with brain metastases (133 males and 99 females) receiving radiosurgery treatment. At the time of diagnosis, the mean age of the patients was 63 ± 10.1 years. The primary tumors included 122 non-small cell lung cancers (NSCLC), 22 small cell lung cancers (SCLC), 30 breast cancers, 29 melanomas, 12 renal cancers, and 18 gastrointestinal (GI) cancers. The number of patients with brainstem metastases was 63, and those with brain edema were 129. After radiosurgery, 39 patients developed brain progression. The aforementioned cut-off value of TMT was used as the median TMT value (5.42 mm) for the included patients. Low TMT was observed in 56.5% of those patients, and high TMT was observed in 43.5%. Clinical characteristics of the patients and their relationship with TMT were summarized in ***Table 1***.

A Chi-squared analysis was performed to assess associations between the levels of TMT and the clinicopathological characteristics of the patients. The age of the patients at diagnosis ($p=0.148$) and the number of metastases ($p=0.147$) did not correlate with the TMT levels ***(Table 1)***. There were no significant differences between the values of PLR, SII, and TMT (***Table 1***). However, the levels of TMT were significantly related to gender ($p=0.008$), ECOG (PS) ($p<0.001$), cancer type ($p = 0.022$), tumor volume ($p<0.001$), brainstem metastases ($p=0.002$), brain edema ($p<0.001$), NLR ($p=0.024$), and brain progression ($p<0.001$) *(**Table 1**).*

Clinical outcomes and prognostic role of the TMT

The median duration of the follow-up was 32 months. Patients with sarcopenia had a significantly shorter mean OS than those without sarcopenia (log-rank test $p<0.001$). (***Fig. 1***).

In a univariate Cox regression analysis, high levels of TMT were associated with longer OS (HR = 6.310, 95% CI: 4.161–9.568, $p<0.001$; ***Table 2***). The multivariate analysis confirmed this association (HR = 5.757, 95% CI: 3.717–8.915, $p=0.001$; ***Table 2***).

TMT as a non-invasive biomarker for the discrimination between patients with or without sarcopenia

A receiver operating characteristic (ROC) curve analysis was conducted to investigate the predictive capacity of TMT as a non-invasive biomarker for distinguishing between responders and non-responders. At the established optimal cut-off value for TMT, this biomarker was able to effectively distinguish between these groups, achieving a sensitivity of 84.1% and a specificity of 73.6% (***Fig. 2***).

Table 1. Relationship between the baseline clinicopathological characteristics of patients and temporalis muscle thickness (TMT)

Characteristics	TMT≤ median (n=131)	TMT>median n=101	p-value
Age			**0.148**
≤63y	64 (27.6%)	59 (25.4%)	
>63y	67 (28.9%)	42 (18.1%)	
Gender			**0.008**
Male	85 (36.6%)	48 (20.7%)	
Female	46 (19.8%)	53 (22.9%)	
ECOG (PS)			**<0.001**
0	36 (15.5%)	55 (23.7%)	
1	63 (27.2%)	39 (16.8%)	
2	32 (13.8%)	7 (3.0%)	
Cancer type			**0.022**
NSCLC	74 (31.8%)	47 (20.3%)	
SCLC	14 (6.0%)	8 (3.5%)	
Breast cancer	8 (3.4%)	22 (9.5%)	
Melanoma	16 (6.9%)	13 (5.6%)	
Renal cancer	7 (3.0%)	5 (2.2%)	
GI	12 (5.2%)	6 (2.6%)	
Tumor volume			**<0.001**
≤median	50 (21.5%)	66 (28.4%)	
>median	81 (35.0%)	35 (15.1%)	
Number metastasis			**0.147**
≤3	77 (33.2%)	69 (29.7%)	
4-9	35 (15.1%)	25 (10.8%)	
≥10	19 (8.2%)	7 (3.0%)	
Brainstem metastasis			**0.002**
Yes	46 (19.8%)	17 (7.4%)	
No	85 (36.6%)	84 (36.2%)	
Brain edema			**<0.001**
Yes	90 (38.8%)	39 (16.8%)	
No	41 (17.7%)	62 (26.7%)	
NLR			**0.024**
≤median	57 (24.7%)	59 (25.4%)	
>median	74 (31.8%)	42 (18.1%)	
PLR			**0.691**
≤median	67 (28.9%)	49 (21.1%)	
>median	64 (27.6%)	52 (22.4%)	
SII			**0.659**
≤600×109 cells/L	25 (10.8%)	17 (7.4%)	
>600×109 cells/L	106 (45.6%)	84 (36.2%)	
Brain progression			**<0.001**
Yes	11 (4.8%)	28 (12.1%)	
No	120 (51.7%)	73 (31.4%)	

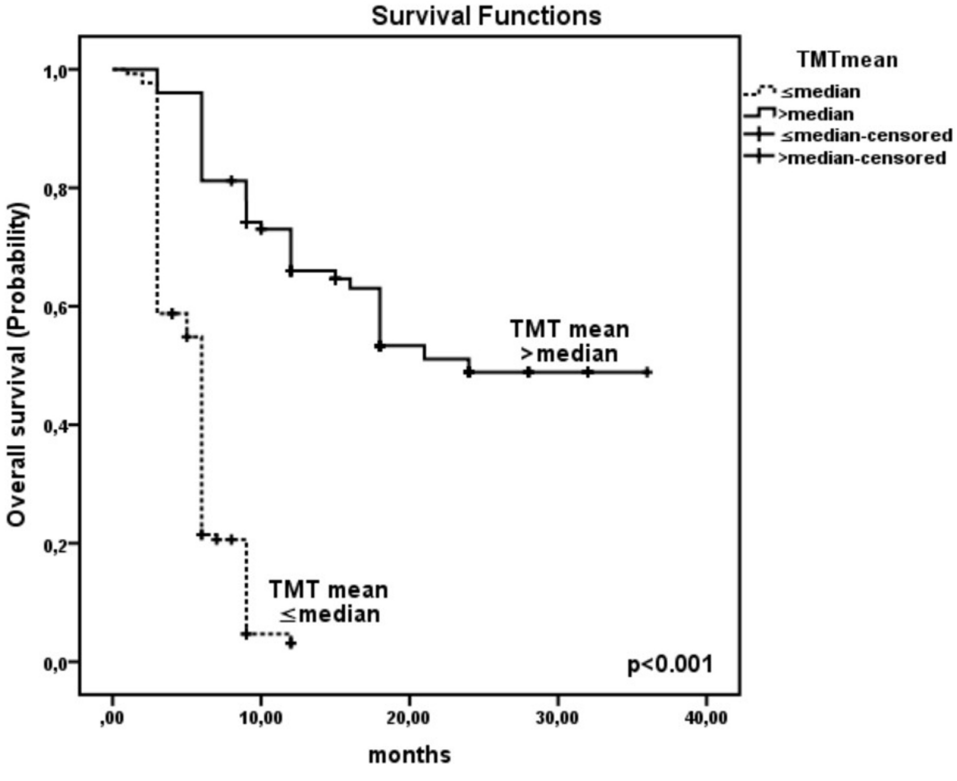

Fig. 1. Kaplan–Meier estimates of overall survival (OS) in patients with sarcopenia and non-sarcopenia. Patients with TMT ≤ median had a significantly shorter mean OS than patients with TMT > median

Table 2. Results of the Cox regression analysis for predicting overall survival

	Univariate Analysis			Multivariate Analysis		
Variable	**Hazard ratio**	**95%CI**	***p*-value**	**Hazard ratio**	**9%CI**	***p*-value**
TMT ≤median vs. >median	6.310	4.161-9.568	<0.001	5.757	3.717-8.915	<0.001
Age ≤63y. vs >63y.	0.793	0.582-1.079	0.140			
Gender Male vs Female	1.387	1.009-1.906	0.044	1.030	0.743-1.427	0.861
ECOG 0 vs 1 and 2	0.538	0.386-750	<0.001	0.833	0.524-1.324	0.439
Number metastasis ≤3 vs > 4	0.700	0.512-0.957	0.025	0.778	0.544-1.112	0.168
Brainstem metastasis Yes vs. No	1.703	1.220-2.378	0.002	1.237	0.856-1.789	0.258
Tumor volume ≤median vs >median	1.569	1.149-2.143	0.005	1.096	0.738-1.628	0.649
Brain edema Yes vs. No	1.926	1.395-2.660	<0.001	1.247	0.863-1.801	0.240
NLR ≤median vs >median	0.678	0.497-0.924	0.014	0.822	0.599-1.126	0.222
PLR ≤median vs >median	0.987	0.725-1.342	0.932			
SII ≤600×109 cells/L vs >600×109 cells/L	1.038	0.686-1.571	0.860			
Cancer type NSCLC vs other type	1.211	0.889-1.650	0.225			

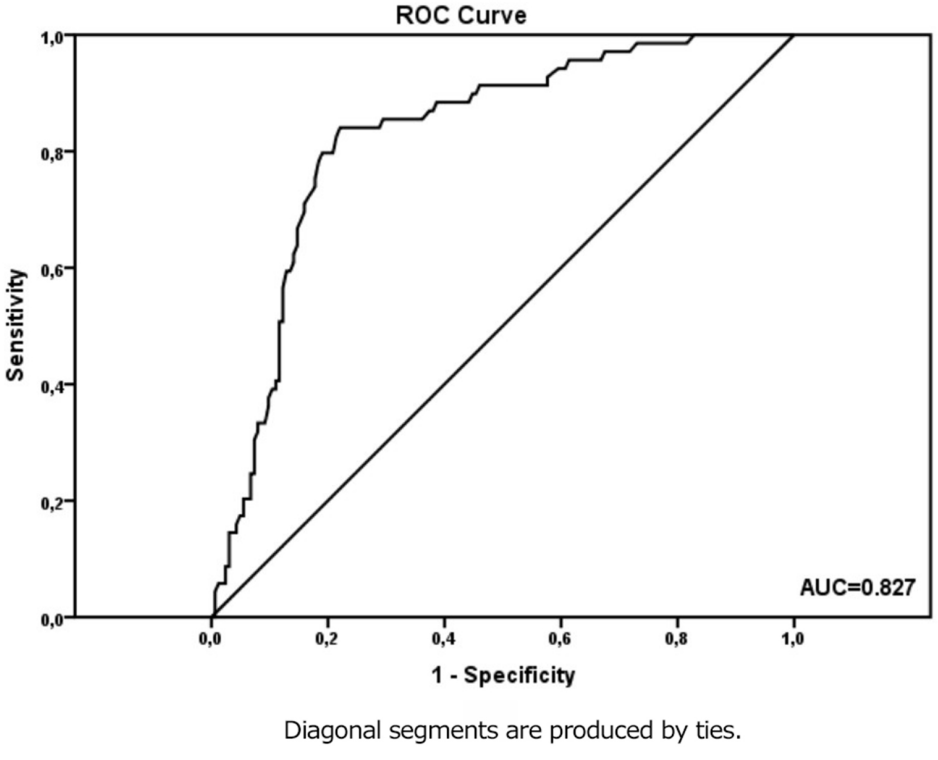

Fig. 2. ROC analysis demonstrates the predictive capacity of TMT as a non-invasive biomarker in responders and non-responders (AUC = 0.827, 95% CI: 0.770–0.884; $p < 0.001$), achieving a sensitivity of 84.1% and a specificity of 73.6%.

Discussion

This research aimed to explore the predictive significance of TMT assessed through standard MRI scans of the brain in individuals with brain metastases, conducted on the day prior to initiating radiosurgery. We focused on patient groups from prevalent tumor types known for central nervous system dissemination and included only those patients who had complete clinical follow-up data. Our findings revealed a robust association between initial TMT levels and patient outcomes within this cohort. Notably, this relationship remained significant regardless of established prognostic indicators. Therefore, we believe that measuring TMT can enhance survival predictions for patients with brain metastases in clinical practice and may facilitate better patient selection and stratification during clinical trials. Various factors such as age, heterogeneity of the different primary tumors, and exclusion of patients due to loss of follow-up were the main limitations of this retrospective single-center study.

The gold standard for evaluating sarcopenia includes not only the loss of skeletal muscle mass but also the decline in muscle function, such as gait speed and grip strength, according to the European Working Group on Sarcopenia in Older People (EWGSOP) [4], EWGSOP2 [15], and the Asian Working Group for Sarcopenia [16]. However, measuring muscle functions such as grip strength and gait speed sometimes cannot be accomplished because patients with brain tumors often have problems with motor proficiency or a decrease in muscle strength due to the neuromuscular dysfunction caused by the brain tumor itself [17].

MRI is the gold standard for the non-invasive assessment of muscle mass [18]. Patients with cancer commonly use CT images of the third lumbar vertebra (L3) to measure skeletal muscle mass, which significantly correlates with whole-body muscle and predicts prognosis [19]. A meta-analysis of 38 studies demonstrated that sarcopenia obtained from CT imaging is associated with worse survival in patients with extracranial solid tumors [9]. However, for brain tumors, using lumbar paravertebral muscles to calculate skeletal muscle is not feasible in clinical settings.

Routinely performed cranial imaging allows for full delineation of the temporal muscle, which is preferable for estimating muscle mass loss. Its thickness remains unaffected by muscular edema or radiation-related atrophy, only by oral disease or previous surgery. Regular cranial MRIs in patients with brain tumors allow for monitoring the TMT skeletal muscle status throughout the disease course. Therefore, we can use TMT to evaluate the musculoskeletal condition of these patients [20]. Several studies have demonstrated an excellent correlation between TMT and total skeletal muscle mass [16, 21].

In comparison to the plane or volume of muscle segmentation, TMT measurement on MRIs takes approximately 30 seconds per patient [10, 12, 22]. Therefore, we believe that TMT assessment, once validated in a prospective setting, could serve as a suitable parameter for integration into the clinical workflow.

Our research did not investigate the specific pathobiology associated with atrophy of the temporal

muscles; however, we believe this condition likely indicates a broader cancer-related sarcopenic syndrome. Supporting this idea, prior research [20] has shown a significant correlation between skeletal muscle mass and TMT measurements. While corticosteroids are known to lead to considerable muscle loss over time due to their side effects, they are often prescribed by physicians for managing symptomatic brain edema in patients diagnosed with brain metastases. In our investigation, baseline TMT was measured before commencing radiosurgery treatment, which minimizes the chance of extended corticosteroid exposure among participants.

Correlations with various patient characteristics were conducted, and the results of these analyses indicate that the TMT measurement offers insights not captured by other clinical parameters. Initially, we observed a weak inverse correlation between TMT and patient age. This suggests that assessing sarcopenia as an indicator of a patient's physical condition may provide more valuable information for clinical decision-making than relying solely on chronological age [23]. The variation in median TMT across different cancer types within the patient cohort could be attributed to differences in gender predominance.

Furthermore, recognizing the link between sarcopenia and cancer could encourage additional research and lead to new therapeutic targets. Interventions such as nutritional support, including omega-3 fatty acids, exercise training, or pharmacological strategies like myostatin inhibitors, could potentially aid in preventing muscle loss [12, 24-26]. Consequently, integrating muscle mass assessment into standard clinical practice for cancer patients is crucial; this allows for the early detection of muscle mass decline enabling prompt implementations to prevent or slow down its progression.

Disclosure

Conflict of interest

The authors declare no conflicts of interest.

Funding

This study received no financial support or sponsorship.

References

1. Cagney DN, Martin AM, Catalano PJ, Redig AJ, Lin NU, Lee EQ, Wen PY, Dunn IF, Bi WL, Weiss SE, Haas-Kogan DA, Alexander BM, Aizer AA. Incidence and prognosis of patients with brain metastases at diagnosis of systemic malignancy: a population-based study. Neuro Oncol. 2017 Oct 19;19(11):1511-1521. doi: 10.1093/neuonc/nox077
2. Passiglia F, Caglevic C, Giovannetti E, Pinto JA, Manca P, Taverna S, Listì A, Gil-Bazo I, Raez LE, Russo A, Rolfo C. Primary and metastatic brain cancer genomics and emerging biomarkers for immunomodulatory cancer treatment. Semin Cancer Biol. 2018 Oct;52(Pt 2):259-268. doi: 10.1016/j.semcancer.2018.01.015
3. Ostrom QT, Bauchet L, Davis FG, Deltour I, Fisher JL, Langer CE, Pekmezci M, Schwartzbaum JA, Turner MC, Walsh KM, Wrensch MR, Barnholtz-Sloan JS. The epidemiology of glioma in adults: a "state of the science" review. Neuro Oncol. 2014 Jul;16(7):896-913. doi: 10.1093/neuonc/nou087
4. Cruz-Jentoft AJ, Baeyens JP, Bauer JM, Boirie Y, Cederholm T, Landi F, Martin FC, Michel JP, Rolland Y, Schneider SM, Topinková E, Vandewoude M, Zamboni M; European Working Group on Sarcopenia in Older People. Sarcopenia: European consensus on definition and diagnosis: Report of the European Working Group on Sarcopenia in Older People. Age Ageing. 2010 Jul;39(4):412-23. doi: 10.1093/ageing/afq034
5. Mintziras I, Miligkos M, Wächter S, Manoharan J, Maurer E, Bartsch DK. Sarcopenia and sarcopenic obesity are significantly associated with poorer overall survival in patients with pancreatic cancer: Systematic review and meta-analysis. Int J Surg. 2018 Nov;59:19-26. doi: 10.1016/j.ijsu.2018.09.014
6. Ubachs J, Ziemons J, Minis-Rutten IJG, Kruitwagen RFPM, Kleijnen J, Lambrechts S, Olde Damink SWM, Rensen SS, Van Gorp T. Sarcopenia and ovarian cancer survival: a systematic review and meta-analysis. J Cachexia Sarcopenia Muscle. 2019 Dec;10(6):1165-1174. doi: 10.1002/jcsm.12468
7. Simonsen C, de Heer P, Bjerre ED, Suetta C, Hojman P, Pedersen BK, Svendsen LB, Christensen JF. Sarcopenia and Postoperative Complication Risk in Gastrointestinal Surgical Oncology: A Meta-analysis. Ann Surg. 2018 Jul;268(1):58-69. doi: 10.1097/SLA.0000000000002679
8. McGovern J, Dolan RD, Horgan PG, Laird BJ, McMillan DC. Computed tomography-defined low skeletal muscle index and density in cancer patients: observations from a systematic review. J Cachexia Sarcopenia Muscle. 2021 Dec;12(6):1408-1417. doi: 10.1002/jcsm.12831
9. Shachar SS, Williams GR, Muss HB, Nishijima TF. Prognostic value of sarcopenia in adults with solid tumours: A meta-analysis and systematic review. Eur J Cancer. 2016 Apr;57:58-67. doi: 10.1016/j.ejca.2015.12.030
10. Leitner J, Pelster S, Schöpf V, Berghoff AS, Woitek R, Asenbaum U, Nenning KH, Widhalm G, Kiesel B, Gatterbauer B, Dieckmann K, Birner P, Prayer D, Preusser M, Furtner J. High correlation of temporal muscle thickness with lumbar skeletal muscle cross-sectional area in patients with brain metastases. PLoS One. 2018 Nov 29;13(11):e0207849. doi: 10.1371/journal.pone.0207849
11. Cho J, Park M, Moon WJ, Han SH, Moon Y. Sarcopenia in patients with dementia: correlation of temporalis muscle thickness with appendicular muscle mass. Neurol Sci. 2022 May;43(5):3089-3095. doi: 10.1007/s10072-021-05728-8
12. Furtner J, Berghoff AS, Albtoush OM, Woitek R, Asenbaum U, Prayer D, Widhalm G, Gatterbauer B, Dieckmann K, Birner P, Aretin B, Bartsch R, Zielinski CC, Schöpf V, Preusser M. Survival prediction using temporal muscle thickness measurements on cranial magnetic resonance images in patients with newly diagnosed brain metastases. Eur Radiol. 2017 Aug;27(8):3167-3173. doi: 10.1007/s00330-016-4707-6
13. Furtner J, Berghoff AS, Schöpf V, Reumann R, Pascher B, Woitek R, Asenbaum U, Pelster S, Leitner J, Widhalm G, Gatterbauer B, Dieckmann K, Höller C, Prayer D, Preusser M. Temporal muscle thickness is an independent prognostic marker in melanoma patients with newly diagnosed brain metastases. J Neurooncol. 2018 Oct;140(1):173-178. doi: 10.1007/s11060-018-2948-8
14. Furtner J, Genbrugge E, Gorlia T, Bendszus M, Nowosielski M, Golfinopoulos V, Weller M, van den Bent MJ, Wick W, Preusser M. Temporal muscle thickness is an independent prognostic marker in patients with progressive glioblastoma: translational imaging analysis of the EORTC 26101 trial. Neuro Oncol. 2019 Dec 17;21(12):1587-1594. doi: 10.1093/neuonc/noz131
15. Cruz-Jentoft AJ, Bahat G, Bauer J, Boirie Y, Bruyère O, Cederholm T, Cooper C, Landi F, Rolland Y, Sayer AA, Schneider SM, Sieber CC, Topinkova E, Vandewoude M, Visser M, Zamboni M; Writing Group for the European Working Group on Sarcopenia in Older People 2 (EWGSOP2), and the Extended Group for EWGSOP2. Sarcopenia: revised European consensus on definition and diagnosis. Age Ageing. 2019 Jan 1;48(1):16-31. doi: 10.1093/ageing/afy169
16. Chen LK, Woo J, Assantachai P, Auyeung TW, Chou MY, Iijima K, Jang HC, Kang L, Kim M, Kim S, Kojima T, Kuzuya M, Lee JSW, Lee SY, Lee WJ, Lee Y, Liang CK, Lim JY, Lim WS, Peng LN, Sugimoto K, Tanaka T, Won CW, Yamada M, Zhang T, Akishita M, Arai H. Asian Working Group for Sarcopenia: 2019 Consensus Update on Sarcopenia Diagnosis and Treatment. J Am Med Dir Assoc. 2020 Mar;21(3):300-307.e2. doi: 10.1016/j.jamda.2019.12.012

17. Keilani M, Krall C, Marosi C, Flechl B, Dieckmann K, Widhalm G, Marhold M, Crevenna R. Strength of skeletal muscle and self-reported physical performance in Austrian glioblastoma-patients. Wien Klin Wochenschr. 2012 Jun;124(11-12):377-83. doi: 10.1007/s00508-012-0186-1
18. Beaudart C, McCloskey E, Bruyère O, Cesari M, Rolland Y, Rizzoli R, Araujo de Carvalho I, Amuthavalli Thiyagarajan J, Bautmans I, Bertière MC, Brandi ML, Al-Daghri NM, Burlet N, Cavalier E, Cerreta F, Cherubini A, Fielding R, Gielen E, Landi F, Petermans J, Reginster JY, Visser M, Kanis J, Cooper C. Sarcopenia in daily practice: assessment and management. BMC Geriatr. 2016 Oct 5;16(1):170. doi: 10.1186/s12877-016-0349-4
19. Jones K, Gordon-Weeks A, Coleman C, Silva M. Radiologically Determined Sarcopenia Predicts Morbidity and Mortality Following Abdominal Surgery: A Systematic Review and Meta-Analysis. World J Surg. 2017 Sep;41(9):2266-2279. doi: 10.1007/s00268-017-3999-2
20. Furtner J, Weller M, Weber M, Gorlia T, Nabors B, Reardon DA, Tonn JC, Stupp R, Preusser M; EORTC Brain Tumor Group. Temporal Muscle Thickness as a Prognostic Marker in Patients with Newly Diagnosed Glioblastoma: Translational Imaging Analysis of the CENTRIC EORTC 26071-22072 and CORE Trials. Clin Cancer Res. 2022 Jan 1;28(1):129-136. doi: 10.1158/1078-0432.CCR-21-1987
21. Ranganathan K, Terjimanian M, Lisiecki J, Rinkinen J, Mukkamala A, Brownley C, Buchman SR, Wang SC, Levi B. Temporalis muscle morphomics: the psoas of the craniofacial skeleton. J Surg Res. 2014 Jan;186(1):246-52. doi: 10.1016/j.jss.2013.07.059
22. Steindl A, Leitner J, Schwarz M, Nenning KH, Asenbaum U, Mayer S, Woitek R, Weber M, Schöpf V, Berghoff AS, Berger T, Widhalm G, Prayer D, Preusser M, Furtner J. Sarcopenia in Neurological Patients: Standard Values for Temporal Muscle Thickness and Muscle Strength Evaluation. J Clin Med. 2020 Apr 28;9(5):1272. doi: 10.3390/jcm9051272
23. Fearon K, Strasser F, Anker SD, Bosaeus I, Bruera E, Fainsinger RL, Jatoi A, Loprinzi C, MacDonald N, Mantovani G, Davis M, Muscaritoli M, Ottery F, Radbruch L, Ravasco P, Walsh D, Wilcock A, Kaasa S, Baracos VE. Definition and classification of cancer cachexia: an international consensus. Lancet Oncol. 2011 May;12(5):489-95. doi: 10.1016/S1470-2045(10)70218-7
24. Argilés JM, Busquets S, López-Soriano FJ, Costelli P, Penna F. Are there any benefits of exercise training in cancer cachexia? J Cachexia Sarcopenia Muscle. 2012 Jun;3(2):73-6. doi: 10.1007/s13539-012-0067-5
25. Di Girolamo FG, Situlin R, Mazzucco S, Valentini R, Toigo G, Biolo G. Omega-3 fatty acids and protein metabolism: enhancement of anabolic interventions for sarcopenia. Curr Opin Clin Nutr Metab Care. 2014 Mar;17(2):145-50. doi: 10.1097/MCO.0000000000000032
26. Padhi D, Higano CS, Shore ND, Sieber P, Rasmussen E, Smith MR. Pharmacological inhibition of myostatin and changes in lean body mass and lower extremity muscle size in patients receiving androgen deprivation therapy for prostate cancer. J Clin Endocrinol Metab. 2014 Oct;99(10):E1967-75. doi: 10.1210/jc.2014-1271

Original article

Ukrainian Neurosurgical Journal. 2025;31(4):44-54
doi: 10.25305/unj.331033

Short-segment stabilization techniques for burst fractures of the thoracolumbar junction: a finite element study under lateral flexion

Oleksii S. Nekhlopochyn [1], Vadim V. Verbov [2], Ievgen V. Cheshuk [2], Milan V. Vorodi [2], Michael Yu. Karpinsky [3], Oleksandr V. Yaresko [3]

[1] Spinal Department, Romodanov Neurosurgery Institute, Kyiv, Ukraine
[2] Restorative Neurosurgery Department, Romodanov Neurosurgery Institute, Kyiv, Ukraine
[3] Biomechanics Laboratory, Sytenko Institute of Spine and Joint Pathology, Kharkiv, Ukraine

Received: 27 May 2025
Accepted: 21 July 2025

Address for correspondence*: Oleksii S. Nekhlopochyn, PhD, Spinal Department, Romodanov Neurosurgery Institute, 32 Platon Maiborody st., Kyiv, 04050, Ukraine, e-mail: AlexeyNS@gmail.com*

Introduction: Burst fractures of the thoracolumbar junction (TLJ, T10–L2) are common spinal injuries associated with a high risk of neurological complications. Transpedicular fixation is one of the most effective treatment methods; however, the optimal choice of fixation configuration remains unresolved. This study aims to analyze the stress-strain state of various short-segment transpedicular fixation configurations for Th12 vertebra burst fractures under lateral flexion loading.

Materials and methods: A finite element model of the Th9–L5 spinal segment with a simulated Th12 burst fracture was created. Four fixation configurations were considered: M1 – short screws in Th11 and L1 (without intermediate screws), M2 – long screws in Th11 and L1 (without intermediate screws), M3 – short screws in Th11 and L1 with intermediate screws in Th12, and M4 – long screws in Th11 and L1 with intermediate screws in Th12.

The models were analyzed using *CosmosM* software, assessing equivalent von Mises stress at 18 control points. Loads simulated physiological lateral trunk bending.

Results: Models with long screws (M2, M4) demonstrated lower maximum stresses in connecting rods (315.5–321.0 MPa) compared to short screws (324.8–324.9 MPa). The inclusion of intermediate screws (M3, M4) significantly reduced stress in the fractured Th12 vertebra (by up to 28%), in adjacent vertebral endplates (by 18–25%), and at screw entry points into vertebral arches (up to 28%). The lowest fixation screw stresses were observed in the model with long and intermediate screws (up to 38% lower compared to the baseline model M1). However, intermediate screws minimally influenced stresses in the connecting rods (up to 1.2%).

Conclusions: The optimal short-segment transpedicular fixation configuration is the use of long screws in adjacent vertebrae combined with intermediate fixation in the fractured vertebra (M4). This approach provides optimal load distribution, reduces the risk of construct failure, and preserves mobility of adjacent segments. Long screws improve overall system stiffness, while intermediate screws effectively stabilize the damaged segment and significantly unload critical areas of the construct and adjacent anatomical structures.

Keywords: *burst fractures; thoracolumbar junction; transpedicular fixation; short-segment stabilization; finite element modeling; lateral flexion; intermediate screws*

Introduction

Injuries of the thoracolumbar junction (TLJ) are among the most common spinal traumas. Approximately 50% of all vertebral fractures occur in the Th10–L2 segment [1].

The biomechanical characteristics of the TLJ—specifically, the transition from the relatively rigid thoracic to the more flexible lumbar segment—predispose this region to a higher risk of injury [2]. Such traumas carry considerable clinical significance, as a substantial proportion of patients (20–50%) experience associated neurological deficits [3]. Given the risk of spinal cord injury and subsequent disability, TLJ injuries warrant special attention and timely management.

Among TLJ injuries, burst fractures of the vertebral bodies are of particular concern. A burst fracture constitutes a severe form of spinal trauma characterized by fragmentation of the vertebral body with disruption of the anterior and middle spinal columns and retropulsion of bony fragments into the spinal canal [4]. These

fractures typically result from high-energy mechanisms, such as falls from height or motor vehicle accidents, and frequently lead to compression of neural structures [5]. Burst fractures are prone to progressive kyphotic deformity and neurological complications; therefore, surgical treatment is often indicated. This includes spinal stabilization through internal fixation and, when necessary, decompression of the spinal canal (direct or indirect) [6, 7].

Transpedicular fixation is a widely accepted method for surgical stabilization of TLJ fractures [8]. Two principal strategies are employed: long-segment fixation (involving two or more vertebrae above and below the fracture level) and short-segment fixation (involving only one vertebra above and below the fracture) [9]. Long-segment constructs provide superior initial stability and more effectively prevent post-traumatic kyphosis [10]. However, they require immobilization of a greater portion of the spine, resulting in reduced mobility of additional segments and increased surgical invasiveness [11]. Short-segment constructs are less invasive and help preserve motion in a larger portion of the spine, but have historically been associated with a higher risk of fixation failure (such as rod breakage, screw migration, or pullout) and secondary deformity [12]. According to the literature, conventional short-segment fixation of thoracolumbar burst fractures results in loss of kyphotic correction >10° or other stabilization-related complications in approximately half of the cases [13].

To enhance the reliability of short-segment transpedicular fixation systems, various technical methods have been employed to strengthen the construct. In particular, the additional use of transverse connectors increases the rigidity of the system under rotational loads. However, the placement of intermediate screws directly into the body of the injured vertebra is considered a more effective method for reinforcing short fixation [14]. As early as 1987, it was demonstrated that including the injured vertebra in the fixation construct significantly increases its stiffness: resistance to bending and axial loading rises by 84–160% compared with the standard configuration that does not include such screws [15]. Numerous biomechanical studies have confirmed that the presence of an intermediate screw improves construct stability and protects the anterior spinal column by reducing the load on the implants [14]. Clinical observations also indicate the advantages of fixation involving the damaged vertebra. This approach allows for better maintenance of deformity correction and reduces the incidence of stabilization failure during the postoperative period compared to traditional short fixation without intermediate screws [16].

Most biomechanical analyses of transpedicular fixation systems have focused on the behavior of constructs under flexion/extension and axial loading. However, lateral bending (lateroflexion) is an equally important component of implant loading, since lateral forces generate pronounced asymmetric deformations within the construct and stress concentration in certain fixation elements [17]. The limited data regarding fixation system behavior during lateroflexion do not allow for a precise assessment of their strength reserve under such conditions. Therefore, the study of the stress–strain state of fixation elements under lateral spinal bending remains a relevant and important research direction.

The authors conducted a comparative analysis of short-segment transpedicular fixation variants for burst fractures in the TLJ, using intermediate screws inserted into the body of the injured vertebra and without them. In addition, the length of the main screws inserted into the adjacent intact vertebrae (monocortical versus bicortical fixation) was also taken into account.

The study examined only one model of burst fracture with short-segment transpedicular fixation without reconstruction of the anterior supporting column. This approach was chosen because other methods of surgical stabilization—such as corpectomy with a telescopic cage or hybrid techniques—had been previously analyzed and partially published by the authors. The presented findings constitute a component of a large, multi-stage study devoted to the biomechanical evaluation of various stabilization strategies for traumatic injuries in the TLJ region.

Objective: to analyze the stress–strain state of various options for transpedicular fixation in a T12 burst fracture under conditions of lateroflexion (lateral bending).

Materials and methods

Model of the spine and fixation options

A finite element model of the thoracolumbar spine segment (Th9–L5) with a burst fracture of the T12 vertebra was developed. The T12 vertebral body was modeled with a destructive defect to represent the presence of bone fragments and structural damage. For this purpose, a region of reduced stiffness was incorporated into the model to simulate the interfragmentary regenerate. Transpedicular fixation was used to stabilize the injured segment. Four fixation configurations were considered:

- **model 1 (M1)**: short (monocortical) screws inserted into the Th11 and L1 vertebral bodies without intermediate screws in the fractured T12 body (standard four-screw fixation).
- **model 2 (M2):** long (bicortical) screws inserted into the Th11 and L1 vertebral bodies without intermediate screws in the T12 body.
- **model 3 (M3):** short (monocortical) screws inserted into the Th11 and L1 vertebral bodies with intermediate screws placed in the T12 body (six-screw fixation).
- **model 4 (M4):** long (bicortical) screws inserted into the Th11 and L1 vertebral bodies with intermediate screws in the T12 body.

Short screws were confined within the vertebral body, whereas long screws penetrated the anterior cortical wall to enhance fixation rigidity (bicortical placement).

It is well established that the use of transverse connectors positively influences the load distribution within the fixation system by reducing stress

This article contains some figures that are displayed in color online but in black and white in the print edition.

concentration and increasing overall construct stiffness. Their application is justified in cases where biomechanical studies or clinical observations indicate a risk of reaching the mechanical strength limit of certain components of the stabilization system — both metallic and bone structures.

However, in the framework of this study, a fixation configuration corresponding to a minimally invasive (percutaneous) surgical procedure was simulated. In such interventions, the placement of transverse connectors is technically infeasible. Therefore, the effect of transverse connectors was not evaluated.

Materials and their properties

All biological tissues and implant elements in the model were considered homogeneous and isotropic. The mechanical characteristics of the materials — Young's modulus (E) and Poisson's ratio (ν) — were selected based on literature data and technical documentation [18–20]. The mechanical properties of the materials used in the simulation are summarized in ***Table 1.***

Finite element network and software

The geometric model of the spine was constructed using the computer-aided design (CAD) system SolidWorks (Dassault Systèmes). For the strength analysis, the CosmosM software package was employed, which implements the finite element method (FEM) [21]. The discretization of the model was performed using solid tetrahedral elements with 10 nodes (quadratic displacement field approximation). This level of mesh refinement ensures more accurate calculations of the stress–strain state of both the spinal structure and the implants [22].

Loading and boundary conditions

The model was loaded according to a scheme simulating a lateral bending of the torso. To achieve this, a bending moment was applied to the upper part of the model (the region of the Th9 vertebral body and its corresponding articular processes) through a lateral force of 350 N. This value approximately corresponds to the weight of the upper half of the human torso, creating a physiological load on the thoracolumbar region of the spine during lateral bending. The lower base of the model—specifically, the caudal (inferior) surface of the L5 intervertebral disc—was rigidly fixed (immovable support condition) to reproduce the influence of pelvic support. Thus, the simulation reproduced realistic boundary conditions: the upper vertebrae were subjected to gravitational loading during flexion, while the lower end of the model remained stationary [23].

Evaluation of the stress–strain state

The analysis of stresses and deformations in the models was performed using the von Mises equivalent stress criterion [24,25]. This approach enables the evaluation of maximum stress intensity in both bone structures and fixation elements for each stabilization method. To compare the effectiveness of the constructs, the stress levels were determined in 18 control points within key areas of the model — including the bodies of vertebrae adjacent to the fracture and the elements of the metal fixation system ***(Fig. 1)***:

- ***vertebral bodies*** Th9, Th10, Th11, Th12, L1, L2, L3, L4, L5 (control points 1–9, respectively);
- **endplates of the vertebrae adjacent to the damaged one**: the inferior endplate of Th11 (point 10) and the superior endplate of L1 (point 11);
- **entry zones of the screws** into the vertebral arches Th11 (point 12), Th12 (point 13), and L1 (point 14);
- **screws** within the vertebral bodies Th11 (point 15), Th12 (point 16), and L1 (point 17) (for models without intermediate fixation, points 13 and 16 are absent, as no screws were inserted into Th12);
- **connecting rods** (fixation system bars) (point 18).

This approach made it possible to identify stress concentration zones for each fixation configuration and to compare them, which is important for the biomechanical assessment of stabilization reliability [26].

A separate modeling of the unfixed state was not performed, since in the case of a burst fracture without stabilization, the structure loses its mechanical integrity, making an accurate stress calculation impossible.

Table 1. Mechanical characteristics of materials used in the simulation

Material	Young's modulus, MPa	Poisson's ratio
Compact bone tissue	10 000	0,30
Cancellous (spongy) bone tissue	450	0,20
Articular cartilage	10,5	0,49
Intervertebral disc	4,2	0,45
Interfragmentary regenerate	1,0	0,45
Titanium (VT-16 alloy)	110 000	0,30

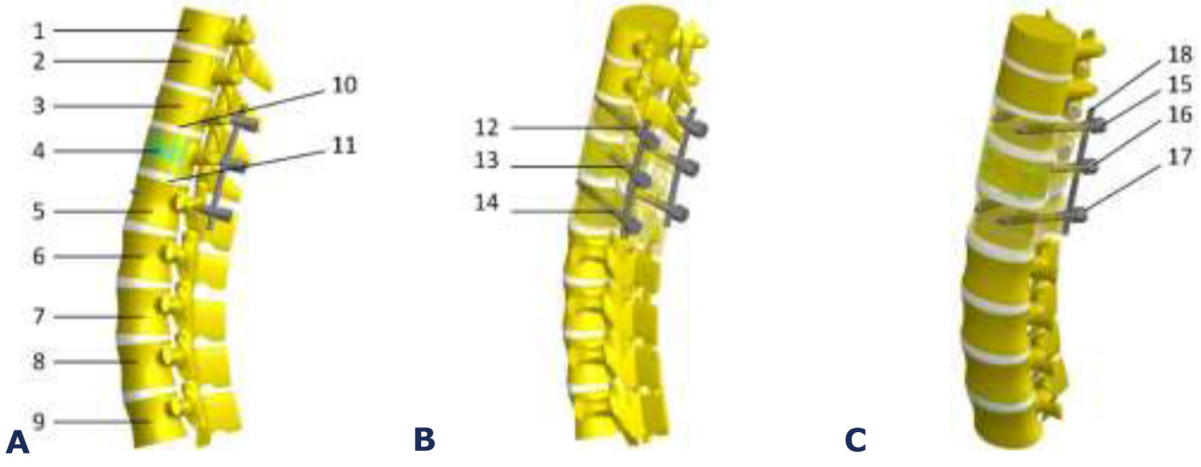

Fig. 1. Schematic arrangement of the control points of the models (description in the text): A – lateral projection; B – posterior-lateral projection; C – anterior-lateral projection

Results

For each control point, we analyzed how the stress level changes when transitioning from one fixation model to another.

Stress in vertebral bodies (control points 1–9)

Upper and lower segments (Th9, Th10, L2–L5). In vertebrae distant from the fixation zone, stresses remain low and nearly identical across all configurations. Specifically, in the vertebral bodies Th9 and Th10, the stress values range from 1.0 to 1.4 MPa and show negligible differences between the models. In the lumbar L2–L5 vertebrae, the stresses range from 12.1 to 17.5 MPa, decreasing when longer and intermediate screws are used (for example, in the body of vertebra L3 — down to 12.1 MPa). This is an expected result, as regions far from the site of injury and implantation are influenced mainly by external loading and depend little on the configuration of the fixation device.

Vertebrae adjacent to the fracture (Th11 and L1). In the vertebrae adjacent to the injured Th12, where screws were placed, a moderate reduction in stress was observed as the fixation was improved. The baseline model (short screws without intermediate ones) shows stress values of 7.9 MPa in the Th11 vertebral body and 18.9 MPa in the L1 body. The use of longer screws (without intermediate ones) reduces these stresses to 7.8 MPa (Th11) and 18.0 MPa (L1). Adding intermediate screws into the Th12 vertebral body (short screws with intermediates) further unloads the Th11 vertebra (down to 7.0 MPa), but slightly increases the stress in L1 (up to 19.0 MPa). The lowest stress levels in adjacent vertebrae were recorded when combining long screws with intermediate ones: 6.8 MPa in Th11 and 17.1 MPa in L1.

Overall, the use of longer screws and intermediate fixation contributes to a reduction of stress in the bodies of the adjacent vertebrae. The effect of intermediate screws is more pronounced for Th11 (~ 14% reduction) than for L1. When both factors—long and intermediate screws—are combined, a cumulative effect occurs, providing the lowest stress levels in Th11 and L1.

Injured Th12 vertebra. The affected Th12 vertebral body exhibited the most pronounced differences among all bony structures across the tested models. Without intermediate fixation, the Th12 vertebral body experienced maximum stresses of 12.3 MPa (short screws) and 12.1 MPa (long screws). The use of intermediate screws significantly reduced the load on the vertebra: stresses decreased to 9.1 MPa (short screws with intermediates) and 8.8 MPa (long screws with intermediates). Thus, intermediate fixation of the Th12 vertebra reduces stress by 27–28%. The screw length alone, without intermediate fixation, had a relatively minor effect (a decrease of only 1–2%), but when combined with intermediate screws, the maximum reduction reached 28%. Summary data on stress distribution in the bodies of the main vertebrae for all fixation models are presented in ***Table 2.***

A visual representation of the stress distribution on the model elements, depending on the type of fixation system, is shown in ***Fig. 2.***

Stress on the endplates (points 10–11)

Changes in stress within the endplates of the Th11 (caudal) and L1 (cranial) vertebrae exhibit smaller amplitudes and less consistent trends, as the cartilaginous tissue of the intervertebral discs partially compensates for differences between fixation schemes due to a similar load transfer mechanism.

The inferior endplate of the Th11 vertebra (point 10) without intermediate fixation demonstrates stresses of 4.3 MPa (short screws, M1) and 4.2 MPa (long screws, M2). The presence of screws in the Th12 vertebral body leads to a distinct reduction in load on the inferior endplate of Th11 — to 3.8 MPa (short screws with intermediate fixation, M3) and to a minimum of 3.2 MPa (long screws with intermediate fixation, M4). This difference indicates effective load reduction in this area due to stabilization of the injured Th12 segment with intermediate screws. Compared with the baseline model (M1), the maximal load decrease amounts to approximately 25.6% (from 4.3 to 3.2 MPa).

Table 2. Equivalent stress (MPa) in the vertebral bodies of T11, Th12, and L1 for four fixation models under lateral flexion

Control point	Short screws without intermediates	Long screws without intermediates	Short screws with intermediates	Long screws with intermediates
Th11 vertebral body	7,9	7,8	7,0	6,8
Th12 vertebral body	12,3	12,1	9,1	8,8
L1 vertebral body	18,9	18,0	19,0	17,1

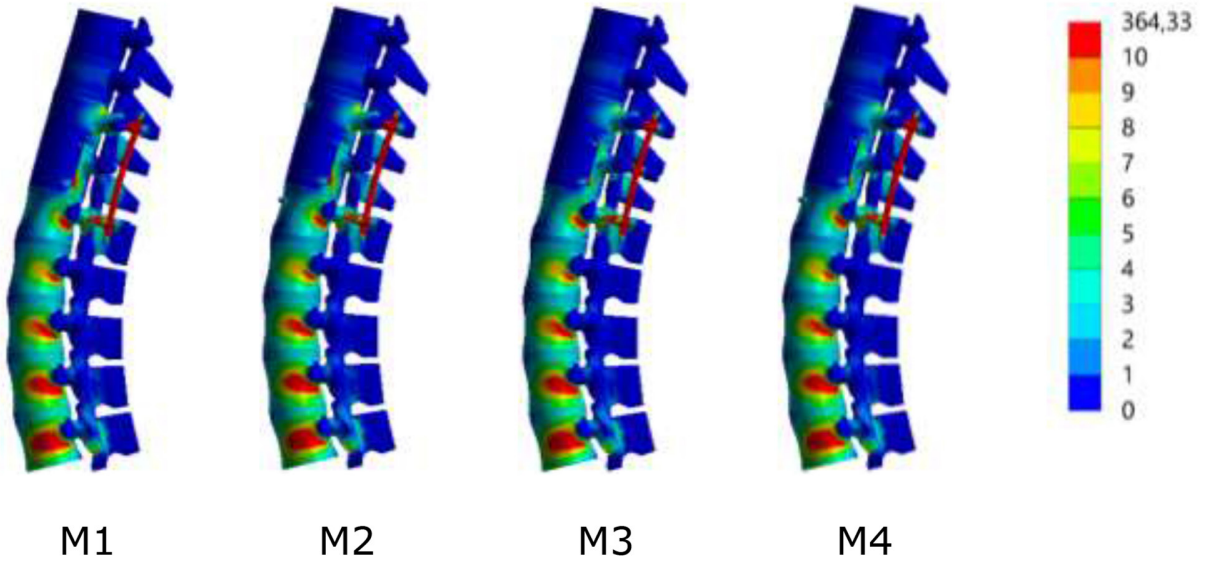

Fig. 2. Stress distribution in models (M1–M4) of the thoracolumbar spine with a burst fracture of the Th12 vertebral body during lateral flexion

The superior endplate of the L1 vertebra (point 11) shows a slightly smaller amplitude of stress variation, though the downward trend is clearly evident. The highest load was recorded in the model without intermediate screws and with short screws (M1) — 8.2 MPa; slightly lower in the model with long screws without intermediate fixation (M2) — 8.1 MPa. The addition of intermediate screws significantly reduced the load on the superior endplate of L1: in the model with short and intermediate screws (M3), the load decreased to 7.0 MPa. In the configuration with long and intermediate screws (M4), the lowest value was recorded — 6.7 MPa, corresponding to an 18.3% reduction compared with the baseline configuration (M1). Thus, the use of intermediate screws substantially decreases the load on the superior endplate of the L1 vertebra, improving structural stability and reducing the risk of cartilage tissue damage.

Overall, endplate stress varied by 1.1–1.5 MPa depending on the model. The most effective load reduction was observed in the model with long screws combined with intermediate fixation.

Stress distribution in screw entry zones (points 12–14)

Arch of the Th11 vertebra (point 12). At the screw entry site in the Th11 vertebral arch (the point of load transfer from the screw to the bone), a gradual decrease in stress was observed when transitioning from short screws without intermediate fixation (7.5 MPa, M1) to long screws without intermediates (7.3 MPa, M2). A more pronounced reduction in stress was recorded with the use of intermediate screws: for short screws with intermediate fixation (M3), the stress decreased to 5.8 MPa (a 22.7% reduction compared to M1). The model with long screws and intermediate fixation (M4) demonstrated a slight increase in stress to 6.1 MPa; however, it remained substantially lower (by 18.7%) than in the baseline configuration. Thus, the presence of intermediate screws provides a significant unloading effect on the Th11 vertebral arch, while the screw length moderately affects the stress distribution.

Arch of the Th12 vertebra (point 13). This area was analyzed only in models with intermediate screws (M3, M4). The stress at the entry point of the intermediate screws into the damaged Th12 vertebral arch remained low: 3.7 MPa for short screws (M3) and slightly lower (3.5 MPa) for long screws (M4). These findings indicate that additional intermediate screws do not generate significant local overstress in the fractured segment, confirming their safety and effectiveness for stabilizing the injured vertebra.

Arch of the L1 vertebra (point 14). The stress in the screw entry zone of the L1 vertebral arch showed a downward trend when moving from short screws without intermediates (14.9 MPa, M1) to long screws without intermediates (13.2 MPa, M2). The inclusion of intermediate screws in the Th12 vertebral body further reduced the stress: in the model with short and intermediate screws (M3), it reached 13.4 MPa, close to

the M2 value. The lowest stress level was recorded in the configuration with long and intermediate screws (M4) — 10.7 MPa, which is 28.2% lower than in the baseline model (M1). This demonstrates that the combination of long and intermediate screws provides the most effective unloading of the screw entry zone in the inferior adjacent vertebra, which is crucial for preventing bone tissue damage.

Stress in screws (control points 15–17)

Screws in the Th11 vertebral body (point 15). In the model with short screws and without intermediates (baseline model), the stress value was 47.5 MPa. The use of long screws without intermediate fixation resulted in a slight reduction in stress (to 46.9 MPa), likely due to improved screw anchorage in the bone. The addition of intermediate screws (short screws with intermediates) further reduced the stress in the Th11 vertebral body screws to 39.2 MPa, while the combination of long and intermediate screws achieved the minimum value of 29.3 MPa — 38% lower than in the baseline model. Therefore, the use of intermediate screws ensures the most substantial reduction of stress in the screws of the Th11 vertebral body, particularly when combined with long screws.

Screws in the Th12 vertebral body (point 16). Data for this point were analyzed only for models that included intermediate screws. The stress in the intermediate screws was the lowest among all screws in the construct: 12.6 MPa (short screws with intermediate fixation) and 10.3 MPa (long screws with intermediate fixation). The low stress values can be explained by the fact that these screws primarily serve a stabilizing function for the injured vertebral fragments, bearing a smaller portion of the overall torque. The length of the main screws in the adjacent vertebrae had only a minor effect on the load of the intermediate screws in the Th12 vertebral body, although longer screws demonstrated slightly better (by about 18%) unloading of these intermediate structural elements.

Screws in the L1 vertebral body (point 17). The screws in the lower adjacent vertebra (L1) also exhibited considerable variation in loading depending on the fixation configuration. In the baseline model (short screws without intermediate fixation), the stress reached a maximum of 50.1 MPa. The use of long screws without intermediate fixation reduced the stress to 45.3 MPa (a decrease of approximately 10%). The addition of intermediate screws further reduced the stress on the screws in the L1 vertebral body—to 48.6 MPa (short screws with intermediate fixation) and a minimum of 39.9 MPa (long screws with intermediate fixation), which is 20% lower than in the baseline configuration. Thus, as in the case of the Th11 vertebral screws, the lowest stress levels were recorded for the combination of long screws with intermediate fixation.

Baseline values of equivalent stress in the main structural elements and in the "metal–bone tissue" contact zones are presented in ***Table 3.***

Stress in the connecting rods (point 18)

The connecting rods (longitudinal bars of the fixation system) experience the highest stress among all structural elements, as they effectively bear a significant portion of the load by bypassing the damaged spinal segment. The durability of the entire construct depends on how efficiently the rods are unloaded since exceeding the fatigue limit may lead to metal fatigue fractures.

Without intermediate fixation (only 4 screws): The maximum stress (σ) in the rods during lateral flexion reached 324.9 MPa in the model with short screws (M1). This was the highest recorded stress among all analyzed configurations, typically concentrated between the screws where the bending moment is maximal. Using longer screws (M2) slightly reduced the stress peak to 315.5 MPa, a decrease of about 2.9% compared to M1. Thus, in the absence of an intermediate support point, screw length has only a minor influence on rod stress.

With intermediate screws into the Th12 vertebral body, the changes were modest. Adding an intermediate support in the short-screw model (M3) did not significantly alter rod stress, yielding a maximum of 324.8 MPa, practically identical to the baseline model M1 (difference <0.1%). The configuration with long screws and an intermediate support (M4) reduced the maximum stress to 321.0 MPa, or 1.2% lower than the baseline (M1). The difference between models M3 and M4 was minimal (≈1.2%), indicating that in this configuration, the main contribution to rod unloading is provided by the screw length rather than the presence of an intermediate support.

Table 3. Equivalent stress (MPa) in the main structural elements and "metal–bone tissue" contact zones (screw entry points, screws, rods) for the four models

Structural element	Short screws without intermediates	Long screws without intermediates	Short screws with intermediates	Long screws with intermediates
Screw entry in Th11 (arch)	7,5	7,3	5,8	6,1
Screw entry in Th12 (arch)	–	–	3,7	3,5
Screw entry in L1 (arch)	14,9	13,2	13,4	10,7
Screws in Th11	47,5	46,9	39,2	29,3
Screws in Th12	–	–	12,6	10,3
Screws in L1	50,1	45,3	48,6	39,9
Connecting rods	324,9	315,5	324,8	321,0

From the standpoint of construct longevity, the most reliable configurations were those with long screws—regardless of intermediate screw presence—since the maximum rod stresses were lowest (315.5–321.0 MPa). Given the typical yield strength range for Ti-6Al-4V titanium alloy implants (760–800 MPa), the observed stress levels (315.5–324.9 MPa) account for only about 40% of this threshold [27]. This aligns with international standards (ASTM F136, ISO 5832-3) and literature data on the mechanical properties of this material, confirming a substantial safety margin. Even relatively small differences in absolute stress values can positively affect long-term structural integrity and fatigue resistance, enhancing overall reliability during prolonged clinical use.

An alternative rod material is the cobalt–chromium (CoCr) alloy, characterized by greater stiffness compared to titanium. Its use may be appropriate when maximum construct rigidity is required—particularly in cases of severe anterior column destruction. However, the higher rigidity of CoCr rods is potentially associated with increased contact stresses at fixation sites and a risk of stress concentration within the bone tissue, which may have clinical implications.

In the context of the present model, Ti-6Al-4V was selected as a more "compliant" and physiologically compatible material to simulate a standard surgical stabilization scenario in the TLJ.

In summary, within the analyzed models, intermediate screws did not contribute significantly to rod unloading (stress reduction <1%), unlike their substantial positive effect on other control points (injured Th12 vertebral body, endplates, and screw entry zones in Th11 and L1). This indicates that the primary role of intermediate screws lies in local stabilization of the injured segment and redistribution of local loads, whereas the global load on the rods is predominantly influenced by the main screw length. Therefore, the combined use of long and intermediate screws provides the most optimal balance of stress distribution across all structural control points.

Discussion

Effectiveness of intermediate screws in a fractured vertebra

The addition of intermediate screws into the body of the fractured vertebra significantly increases the rigidity and stability of short-segment fixation. Biomechanical studies have demonstrated that six-screw constructs (one level above and one level below the fracture, plus screws inserted into the fractured vertebra) markedly limit the mobility of the injured segment compared to the standard four-screw configuration [28]. In particular, modeling studies have shown a reduction in flexion and lateral bending angles with the inclusion of "index-level" screws in short constructs, resulting in approximately a 25% increase in stiffness [29]. In contrast, the difference for long-segment (two-level above/below fracture) osteosynthesis was minimal, indicating that the addition of intermediate screws is most effective in short-segment systems. Therefore, incorporating the fracture level into fixation substantially reinforces the construct and reduces the risk of angular correction loss even under flexion loads.

The improvement in fixation achieved through intermediate screws has also been clinically confirmed. A prospective study involving 80 patients found that short-segment fixation including the fractured vertebra provided better correction and maintenance of kyphotic deformity, whereas "skipping" the fractured level resulted in progression of kyphosis (a mean difference of 29% compared to constructs including the injured level) [14]. The incidence of implant breakage was higher in the group without screws placed in the fractured vertebral body. A recent meta-analysis further confirmed that the addition of screws into the fractured vertebra enhances biomechanical stability, facilitates better height restoration, reduces loss of correction, and decreases the rate of implant failure and fragmentation [30]. Consequently, many authors recommend supplementing short-segment transpedicular fixation with screws inserted into the fractured vertebra in cases of unstable wedge or burst fractures. This approach reduces the likelihood of recurrent vertebral collapse and hardware failure [28]. Although intermediate screws significantly strengthen short constructs, in cases of highly unstable injuries (AO type C fracture-dislocations), even enhanced short fixation may still provide inferior rigidity compared to long-segment constructs [13]. Therefore, for multi-column fractures with pronounced instability, the use of longer fixation is advisable, while for most burst fractures in the TLJ region, short-segment fixation reinforced with screws at the fracture level remains an effective and biomechanically justified approach.

Effect of screw length

The length of pedicle screws, particularly the use of bicortical (long) screws with perforation of the anterior cortical plate, influences both the fixation strength and the distribution pattern of mechanical loads. Bicortical anchorage is traditionally considered stronger due to the engagement of the opposite vertebral wall. Experimental studies have demonstrated that the pullout force required for screw extraction may be ~ 40% higher with bicortical fixation compared to shorter screws [31]. This effect is especially relevant in cases of osteoporosis, where longer screws significantly improve implant retention within the bone [32]. A "stiffer" anchor, represented by a long screw, alters the stress distribution within the construct. Finite element modeling of lateral flexion has shown that short (monocortical) screws generate lower peak stresses in the fixation system compared to long bicortical screws — at all control points, the applied load was slightly higher when longer screws were used. Therefore, a longer screw, by more firmly "linking" the rod to the vertebra, bears a greater share of the bending moment, which may lead to higher localized stress around its entry point. In contrast, shorter screws exhibit a degree of compliance, redistributing part of the load through the connecting rods. Importantly, although the difference in stress distribution is not critical, it does exist and may become significant under extreme loading conditions.

The use of bicortical screws, however, is associated with an increased risk of injury to adjacent anatomical structures (vessels, organs) in the event of perforation of the anterior cortical wall. Therefore, when selecting screw length, the surgeon must consider the patient's individual anatomy and the necessary balance between fixation stability and procedural safety [33].

Changes in stress distribution in rods, screws, and adjacent vertebrae

The analysis of the stress–strain state of the construct under lateral flexion revealed a characteristic pattern of load distribution among its elements. Maximum stresses typically occurred in the terminal (especially caudal) screws, as they bear the greatest portion of the bending load. For instance, in a short-segment fixation model of an L1 vertebral fracture, the highest equivalent stress was concentrated in the lower screws of the construct [34]. Similar findings were obtained in our study. The addition of intermediate screws altered the pattern: the load was partially redistributed from the terminal screws to the fracture level and the rods. According to modeling data, the inclusion of screws in the fractured vertebra reduced stress in other screws of the construct. Thus, in a six-screw model, lower equivalent stresses were recorded in the transpedicular screws compared with a four-screw system [28]. At the same time, the stress in the rods slightly increased, as the stiffer "coupling" of the segment required the rod to absorb more of the bending moment. Hongwei Wang et al. reported that the stress in the connecting rods with intermediate screws reached a level similar to that observed in long-segment fixation, whereas without intermediate screws, the load on the rod was slightly lower [35]. The reduction of stress in screws when intermediate screws are used is a positive factor, since overstressing of these elements and their surrounding bone often leads to fatigue failure or implant loosening.

An important aspect is the load distribution in the body of the injured and adjacent vertebrae depending on the fixation configuration. If the affected vertebra is not included in the construct (i.e., screws are inserted only into the neighboring vertebrae), a portion of the bending moment is still transmitted through its body despite its minimal contribution to load transfer. In cases where intermediate screws are used, the load on the damaged vertebra is further reduced, resulting in moderate stress formation [34]. This not only decreases the load on the injured segment and thereby the likelihood of secondary deformation but also stimulates bone remodeling in accordance with Wolff's law, promoting better fusion and healing [36].

Regarding adjacent, unaffected segments, studies have shown that overly rigid constructs can increase the load on adjacent intervertebral discs. Specifically, the maximum intradiscal pressure in the upper adjacent segment is usually higher than in the lower one [37], which may indicate a potential risk of overloading the superior neighboring disc. Therefore, shorter fixation with intermediate screws, which preserves the mobility of more motion segments, potentially exerts a lesser impact on adjacent levels compared with excessively long and rigid constructs. When selecting the optimal fixation configuration, it is crucial to maintain this balance—ensuring sufficient rigidity for effective stabilization of the fracture while avoiding excessive load "shielding," which could negatively affect both the implants and the surrounding anatomical structures.

Risks of structural overload during lateral flexion

Lateral flexion of the spine creates asymmetric loading on the implanted system: one rod is subjected to compression, the opposite one to tension, while the pedicle screws on the side of inclination experience significant bending and torsional moments. This loading mode is critical for the construct, as it concentrates stress on individual components. If the fixation strength or configuration is insufficient, lateral flexion may lead to local overload, resulting in fatigue cracking of the rod or gradual loosening of screws in the bone. Historically, short four-screw constructs have often been associated with implant failures (such as rod fracture, bending, or screw pullout) under loading, particularly in the lateral projection. The addition of intermediate screws significantly reduces the risk of such complications by redistributing the load: as mentioned above, the stresses on the most loaded screws decrease, while the overall stiffness of the construct increases, thereby limiting excessive displacement and cyclic loading [28]. Clinical series have demonstrated that the use of six-screw constructs substantially lowers the incidence of metalwork failure, although it does not completely eliminate it. For example, Liao et al. reported approximately 11% of implant failure cases even when fracture-level screws were used (3 out of 27 patients) [38, 39]. In another long-term follow-up study of short fixation with intermediate screws, the rate of implant breakage or loosening reached 16.7% [30]. These data suggest that overload may still occur even in reinforced systems, particularly if the patient resumes significant physical activity early or has osteoporotic changes.

Significant loading during lateral flexion occurs on the rod opposite the direction of inclination, which is subjected to tensile forces. In this context, the role of transverse connectors between the rods is crucial. The addition of at least one cross-link enhances the spatial rigidity of the construct and synchronizes the performance of the left and right rods, preventing their excessive divergent bending. Modeling studies have shown that the presence of a transverse connector reduces stress levels in screws and rods under lateral loading. Specifically, the combination of short screws with a transverse link demonstrated the lowest critical stress among tested configurations, making it biomechanically optimal under lateral flexion [17]. Thus, to reduce the risk of construct overload, it is advisable to use intermediate screws and, when possible, equip the system with transverse connectors. These measures improve load distribution and increase the mechanical strength reserve of the implants under lateral loading. This approach, however, involves a certain trade-off between biomechanical efficiency and clinical feasibility, as such procedures are often performed using minimally invasive techniques. The installation of transverse connectors requires an open surgical stage, which may potentially offset the benefits of a minimally invasive approach. Therefore, when selecting the optimal surgical strategy, it is essential to balance the required construct stability with the degree of invasiveness, considering both clinical conditions and patient needs.

Comparison of short and long fixation systems: practical insights

Biomechanical and clinical evidence indicates that a properly configured short-segment transpedicular fixation can provide effective stabilization of burst

fractures in the TLJ while preserving more motion segments. A short construct (four screws) with the addition of screws into the fractured vertebra achieves stiffness comparable to a long-segment system and significantly exceeds that of a standard short construct without intermediate fixation points [29]. This configuration demonstrates a favorable stress distribution — minimal critical stress in the screws among fixation options, acceptable load sharing in the rods, and inclusion of the fractured vertebral body in bearing the load, which potentially enhances osteogenesis [34]. Clinically, this results in better preservation of vertebral height and less progression of deformity without increasing complication rates [14]. Thus, reinforced short-segment fixation allows limiting the number of instrumented levels, which is especially important in younger patients to maintain spinal mobility and prevent unnecessary disability of adjacent segments.

Long-segment systems (extending at least two levels above and below the fracture) provide maximum stability due to multiple fixation points and wide load distribution. They remain the method of choice in cases of extreme fracture instability, significant osteoporotic bone involvement, or multilevel injuries, where short fixation—even with intermediate screws—may not ensure adequate correction retention. However, this stability comes at the cost of losing motion in additional spinal segments and potentially increasing stress on uninvolved adjacent levels.

Comparative analyses of treatment outcomes reveal that, in the absence of indications for extensive stabilization, short constructs that include the fractured vertebra are not inferior to long systems in clinical results, while offering the advantage of reduced surgical invasiveness and better preservation of the spine's anatomic and functional integrity.

Therefore, according to contemporary approaches to managing burst fractures in the TLJ, preference should be given to the most conservative yet sufficiently stable fixation methods. Short-segment transpedicular systems with intermediate screws represent a balanced strategy that ensures adequate stability under lateral bending and other load conditions, while minimizing the risks of implant overloading and adjacent-segment degeneration. This approach is supported by both biomechanical research (including numerical modeling and cadaveric testing) and clinical observations with adequate postoperative follow-up.

For most type A (burst) injuries in the Th10–L2 region, short-segment transpedicular fixation involving the fractured vertebra provides the necessary stability with a smaller fixation span. Only in cases of extreme instability or insufficient bone quality should long-segment constructs be preferred to protect against mechanical overload under all conditions.

Conclusions

Based on the analysis of stresses at 18 control points across four models, the following conclusions can be drawn:

1. **Intermediate fixation of the fractured vertebra (Th12)** plays a decisive role in load redistribution during lateral flexion. The addition of two intermediate screws into the Th12 vertebral body significantly reduces stresses in the critical elements of both the fixation construct and the spine itself.

2. **Long transpedicular screws** (inserted deeper into the adjacent vertebral bodies) generally improve the biomechanical performance of the fixation system, although their effect is less pronounced than that of the intermediate screws.

3. **The combined use of long screws and intermediate fixation (M4)** provides the most optimal stress distribution. This model demonstrated the lowest stress values in nearly all control points. Therefore, M4 can be considered the most balanced option for short-segment spinal fixation in Th12 vertebral injuries, as it combines the advantages of both approaches: intermediate support at the fracture level substantially unloads the construct, while long screws ensure the safe realization of this support through uniform stress distribution.

4. **Practical implications.** The analysis indicates that, in the treatment of burst fractures in the TLJ, preference should be given to short-segment fixation involving the fractured vertebra (use of intermediate screws). This approach provides mechanical stability comparable to traditional long-segment fixation (two levels above and below the fracture) while requiring fewer implants. The length of the transpedicular screws should be maximized within the patient's anatomical limits, particularly when using intermediate screws, to prevent local overstressing. Both factors contribute to reducing loads on implants and bone structures, potentially improving clinical outcomes—such as a lower risk of implant failure, better conditions for fracture healing, and preservation of spinal segment mobility.

Disclosure

Conflict of interest

The authors declare no conflict of interest.

Funding

This research received no external funding or sponsorship.

References

1. Wang H, Zhang Y, Xiang Q, Wang X, Li C, Xiong H, Zhou Y. Epidemiology of traumatic spinal fractures: experience from medical university-affiliated hospitals in Chongqing, China, 2001-2010. J Neurosurg Spine. 2012;17(5):459-468. doi: 10.3171/2012.8.SPINE111003
2. Bruno AG, Burkhart K, Allaire B, Anderson DE, Bouxsein ML. Spinal Loading Patterns From Biomechanical Modeling Explain the High Incidence of Vertebral Fractures in the Thoracolumbar Region. Journal of bone and mineral research : the official journal of the American Society for Bone and Mineral Research. 2017;32(6):1282-1290. doi: 10.1002/jbmr.3113
3. Vaccaro AR, Lim MR, Hurlbert RJ, Lehman RA, Jr., Harrop J, Fisher DC, et al. Surgical decision making for unstable thoracolumbar spine injuries: results of a consensus panel review by the Spine Trauma Study Group. J Spinal Disord Tech. 2006;19(1):1-10. doi: 10.1097/01.bsd.0000180080.59559.45
4. Rosenthal BD, Boody BS, Jenkins TJ, Hsu WK, Patel AA, Savage JW. Thoracolumbar Burst Fractures. Clin Spine Surg. 2018;31(4):143-151. doi: 10.1097/bsd.0000000000000634
5. Shin SR, Lee SS, Kim JH, Jung JH, Lee SK, Lee GJ, et al. Thoracolumbar burst fractures in patients with neurological deficit: Anterior approach versus posterior percutaneous fixation with laminotomy. J Clin Neurosci. 2020;75:11-18.

doi: 10.1016/j.jocn.2020.03.046
6. Goulet J, Richard-Denis A, Petit Y, Diotalevi L, Mac-Thiong JM. Morphological features of thoracolumbar burst fractures associated with neurological outcome in thoracolumbar traumatic spinal cord injury. Eur Spine J. 2020;29(10):2505-2512. doi: 10.1007/s00586-020-06420-9
7. Jaiswal NK, Kumar V, Puvanesarajah V, Dagar A, Prakash M, Dhillon M, Dhatt SS. Necessity of Direct Decompression for Thoracolumbar Junction Burst Fractures with Neurological Compromise. World Neurosurg. 2020;142:e413-e419. doi: 10.1016/j.wneu.2020.07.069
8. Aebi M. Transpedicular fixation: Indication, techniques and complications. Current Orthopaedics. 1991;5(2):109-116. doi: 10.1016/0268-0890(91)90053-3
9. Jindal R, Jasani V, Sandal D, Garg SK. Current status of short segment fixation in thoracolumbar spine injuries. J Clin Orthop Trauma. 2020;11(5):770-777. doi: 10.1016/j.jcot.2020.06.008
10. Verlaan JJ, Diekerhof CH, Buskens E, van der Tweel I, Verbout AJ, Dhert WJ, Oner FC. Surgical treatment of traumatic fractures of the thoracic and lumbar spine: a systematic review of the literature on techniques, complications, and outcome. Spine (Phila Pa 1976). 2004;29(7):803-814. doi: 10.1097/01.brs.0000116990.31984.a9
11. Ugras AA, Akyildiz MF, Yilmaz M, Sungur I, Cetinus E. Is it possible to save one lumbar segment in the treatment of thoracolumbar fractures? Acta orthopaedica Belgica. 2012;78(1):87-93.
12. Alimohammadi E, Bagheri SR, Joseph B, Sharifi H, Shokri B, Khodadadi L. Analysis of factors associated with the failure of treatment in thoracolumbar burst fractures treated with short-segment posterior spinal fixation. Journal of orthopaedic surgery and research. 2023;18(1):690. doi: 10.1186/s13018-023-04190-w
13. Aly TA. Short Segment versus Long Segment Pedicle Screws Fixation in Management of Thoracolumbar Burst Fractures: Meta-Analysis. Asian Spine J. 2017;11(1):150-160. doi: 10.4184/asj.2017.11.1.150
14. Farrokhi MR, Razmkon A, Maghami Z, Nikoo Z. Inclusion of the fracture level in short segment fixation of thoracolumbar fractures. Eur Spine J. 2010;19(10):1651-1656. doi: 10.1007/s00586-010-1449-z
15. Dick W. The "fixateur interne" as a versatile implant for spine surgery. Spine (Phila Pa 1976). 1987;12(9):882-900. doi: 10.1097/00007632-198711000-00009
16. Zhang C, Liu Y. Combined pedicle screw fixation at the fracture vertebrae versus conventional method for thoracolumbar fractures: A meta-analysis. International journal of surgery (London, England). 2018;53:38-47. doi: 10.1016/j.ijsu.2018.03.002
17. Nekhlopochyn OS, Cheshuk YV, Vorodi MV, Tsymbaliuk YV, Karpinskyi MY, Yaresko OV. Biomechanical State of the Operated Thoracolumbar Junction in Lateroflexion. Visnyk Ortopedii Travmatologii Protezuvannia. 2022(2(113)):58-67. doi: 10.37647/0132-2486-2022-113-2-58-67
18. Boccaccio A, Pappalettere C. Mechanobiology of Fracture Healing: Basic Principles and Applications in Orthodontics and Orthopaedics. In: Klika V, editor. Theoretical Biomechanics. Croatia: InTech; 2011. p. 21-48.
19. Cowin SC. Bone Mechanics Handbook. 2nd ed. Boca Raton: CRC Press; 2001. 980 p.
20. Niinomi M. Mechanical biocompatibilities of titanium alloys for biomedical applications. J Mech Behav Biomed Mater. 2008;1(1):30-42. doi: 10.1016/j.jmbbm.2007.07.001
21. Kurowski PM. Engineering Analysis with COSMOSWorks 2007: SDC Publications; 2007. 263 p.
22. Rao SS. The Finite Element Method in Engineering: Elsevier Science; 2005. 663 p.
23. Wiczenbach T, Pachocki L, Daszkiewicz K, Łuczkiewicz P, Witkowski W. Development and validation of lumbar spine finite element model. PeerJ. 2023;11:e15805. doi: 10.7717/peerj.15805
24. Liebschner MA, Kopperdahl DL, Rosenberg WS, Keaveny TM. Finite element modeling of the human thoracolumbar spine. Spine (Phila Pa 1976). 2003;28(6):559-565. doi: 10.1097/01.Brs.0000049923.27694.47
25. O'Mahony AM, Williams JL, Spencer P. Anisotropic elasticity of cortical and cancellous bone in the posterior mandible increases peri-implant stress and strain under oblique loading. Clin Oral Implants Res. 2001;12(6):648-657. doi: 10.1034/j.1600-0501.2001.120614.x
26. Popsuyshapka KO, Teslenko SO, Popov AI, Karpinsky MY, Yaresko OV. Study of the stress-strain state of the spine model for various methods of treatment for fractures of the bodies of the thoracic spine. Trauma. 2022;23(5):53-64. doi: 10.22141/1608-1706.5.23.2022.916.
27. Abd-Elaziem W, Darwish MA, Hamada A, Daoush WM. Titanium-Based alloys and composites for orthopedic implants Applications: A comprehensive review. Materials & Design. 2024;241:112850. doi: 10.1016/j.matdes.2024.112850
28. Xu C, Bai X, Ruan D, Zhang C. Comparative finite element analysis of posterior short segment fixation constructs with or without intermediate screws in the fractured vertebrae for the treatment of type a thoracolumbar fracture. Comput Methods Biomech Biomed Engin. 2024;27(11):1398-1409. doi: 10.1080/10255842.2023.2243360
29. Baaj AA, Reyes PM, Yaqoobi AS, Uribe JS, Vale FL, Theodore N, et al. Biomechanical advantage of the index-level pedicle screw in unstable thoracolumbar junction fractures. J Neurosurg Spine. 2011;14(2):192-197. doi: 10.3171/2010.10.SPINE10222
30. Nguyen NQ, Phan TH. The Radiological Complications of Short-Segment Pedicle Screw Fixation Combined with Transforaminal Interbody Fusion in the Treatment of Unstable Thoracolumbar Burst Fracture: A Retrospective Case Series Study in Vietnam. Orthop Res Rev. 2022;14:91-99. doi: 10.2147/orr.S356296
31. Bezer M, Ketenci IE, Saygi B, Kiyak G. Bicortical versus unicortical pedicle screws in direct vertebral rotation: an in vitro experimental study. J Spinal Disord Tech. 2012;25(6):E178-182. doi: 10.1097/BSD.0b013e31825dd542
32. Shibasaki Y, Tsutsui S, Yamamoto E, Murakami K, Yoshida M, Yamada H. A bicortical pedicle screw in the caudad trajectory is the best option for the fixation of an osteoporotic vertebra: An in-vitro experimental study using synthetic lumbar osteoporotic bone models. Clin Biomech (Bristol, Avon). 2020;72:150-154. doi: 10.1016/j.clinbiomech.2019.12.013
33. Xu C, Hou Q, Chu Y, Huang X, Yang W, Ma J, Wang Z. How to improve the safety of bicortical pedicle screw insertion in the thoracolumbar vertebrae: analysis base on three-dimensional CT reconstruction of patients in the prone position. BMC Musculoskelet Disord. 2020;21(1):444. doi: 10.1186/s12891-020-03473-1
34. Limthongkul W, Wannaratsiri N, Sukjamsri C, Benyajati CN, Limthongkul P, Tanasansomboon T, et al. Biomechanical Comparison Between Posterior Long-Segment Fixation, Short-Segment Fixation, and Short-Segment Fixation With Intermediate Screws for the Treatment of Thoracolumbar Burst Fracture: A Finite Element Analysis. International journal of spine surgery. 2023;17(3):442-448. doi: 10.14444/8441
35. Wang H, Mo Z, Han J, Liu J, Li C, Zhou Y, et al. Extent and location of fixation affects the biomechanical stability of short- or long-segment pedicle screw technique with screwing of fractured vertebra for the treatment of thoracolumbar burst fractures: An observational study using finite element analysis. Medicine (Baltimore). 2018;97(26):e11244. doi: 10.1097/md.0000000000011244
36. Frost HM. Wolff's Law and bone's structural adaptations to mechanical usage: an overview for clinicians. Angle Orthod. 1994;64(3):175-188. doi: 10.1043/0003-3219(1994)064<0175:Wlabsa>2.0.Co;2
37. Liu H, Wang H, Liu J, Li C, Zhou Y, Xiang L. Biomechanical comparison of posterior intermediate screw fixation techniques with hybrid monoaxial and polyaxial pedicle

screws in the treatment of thoracolumbar burst fracture: a finite element study. Journal of orthopaedic surgery and research. 2019;14(1):122. doi: 10.1186/s13018-019-1149-2
38. Liao JC, Chen WJ. Short-Segment Instrumentation with Fractured Vertebrae Augmentation by Screws and Bone Substitute for Thoracolumbar Unstable Burst Fractures. BioMed research international. 2019;2019:4780426. doi: 10.1155/2019/4780426
39. Liao JC, Chen WP, Wang H. Treatment of thoracolumbar burst fractures by short-segment pedicle screw fixation using a combination of two additional pedicle screws and vertebroplasty at the level of the fracture: a finite element analysis. BMC Musculoskelet Disord. 2017;18(1):262. doi: 10.1186/s12891-017-1623-0

Original article

Ukrainian Neurosurgical Journal. 2025;31(4):55-60
doi: 10.25305/unj.330969

External ventricular drainage for spontaneous intracerebral hemorrhage with intraventricular hemorrhage: mortality and outcomes in Mali

Youssouf Sogoba [1], Olufemi Bankole [2], Jean Marie Kisito Quenum [3], Seybou Hassane Diallo [4], Boubacar Sogoba [1], Moussa Diallo [1], Moustapha Issa Mangané [5], Almeimoune Hamidou [5], Thierno Madane Diop [5], Oumar Coulibaly [1], Housseini Dolo [6], Mahamoud M Koureissi [6], Drissa Kanikomo [1]

[1] Departement of Neurosurgery, Gabriel Toure Teaching University Hospital, Bamako, Mali
[2] Departement of Neurosurgery, Lagos Teaching University Hospital, Lagos, Nigeria
[3] Departement of Neurosurgery, Parakou Teaching University Hospital, Parakou, Benin
[4] Departement of Neurology, Gabriel Toure Teaching University Hospital, Bamako, Mali
[5] Departement of ICU, Gabriel Touré Teaching University Hospital, Bamako, Mali
[6] Departement of epidemiology USTTB, Bamako, Mali

Received: 27 May 2025
Accepted: 21 July 2025

Address for correspondence: *Youssouf Sogoba, Departement of Neurosurgery, Gabriel Toure Teaching University Hospital, Av. Van Vollenhoven, Bamako, Mali, email: sogobayoussouf@yahoo.fr*

Introduction: Intracerebral hemorrhage (ICH) with intraventricular hemorrhage (IVH) is a serious condition associated with high morbidity and mortality. External ventricular drainage (EVD) is a major tool in the treatment of IVH to manage elevated intracranial pressure and may reduce short-term mortality.

The aim of this study was to determine the impact of EVD placement in the acute phase on mortality and short-term neurologic outcomes in patients with spontaneous ICH associated with IVH.

Materials and methods: We conducted a prospective observational study including adult patients admitted to Gabriel Toure University Hospital over a five year period between January 2019 and December 2023. Demographic, clinical and radiographic characteristics of patients were recorded. All patients who underwent EVD for primary diagnosis of ICH and radiographic evidence of IVH were included. The Graeb score was used to assess the severity of IVH. Outcomes were evaluated using the Glasgow Coma Scale (GCS) and the modified Rankin score (mRS). Statistical analysis was performed to determine independent predictor factors of 30-day mortality using Wilcoxon rank sum test and Fisher's exact test. *P* value ≤ 0.05 was considered statistically significant.

Results: During the study period, a total of 63 patients were admitted for spontaneous ICH and IVH was associated in 24 (38.1%) patients. Among them, EVDs were placed in 17 patients. The mean age was 49 years with range of 27 to 66 years. There were 11 males and 6 females. The main risk factors of stroke were hypertension in 13 patients and diabetes in 7 patients. The initial GCS ranged from 5 and 8. Unilateral pupillary dilatation was found in 8 patients. The duration of EVD ranged from 1 to 8 days. The short term mortality rate was 70.5 % at 30 days. The functional outcomes were poor in 4 patients with mRS score of 4 and 5. The independent predictor factors for 30-day mortality were poor GCS (p=0.319), Mydriasis (p=0.245) and poor Graeb score (p=0.004).

Conclusion: The placement of EVD in patient with IVH remains controversial. Our study reveals the high mortality rate in patients with ICH despite this procedure, raising questions about the usefulness of this procedure in our setting. Although our study demonstrated a high mortality rate, patients with appropriate indications undoubtedly require EVD. Complementary and randomized studies are necessary in the future.

Key words: *intracerebral hemorrhage; intraventricular hemorrhage; external ventricular drainage; Glasgow Coma Score; functional outcomes*

Introduction

Intraventricular hemorrhage (IVH) accounts for 40% of intracerebral hemorrhage (ICH) patients and 10% to 15% of all strokes. IVH is predictor of high mortality and poor outcomes [1, 2, 3]. According to the literature the 30-day mortality rate can reach 52 %. Half of those deaths occur in the first 2 days [4, 5, 6]. ICH with IVH causes increased intracranial pressure (ICP). External ventricular drainage (EVD) remains a major tool in the treatment of IVH to manage ICP and may reduce short-term mortality [7, 8, 9]. There is less evidence to guide the management of the EVD in the setting of ICH with IVH and its impact on outcome remains controversial. The aim of this study was to determine the impact of EVD placement in the acute phase on mortality and short-term neurologic outcomes in patients with spontaneous ICH associated with IVH.

Materials and methods

Study participants

We conducted a prospective observational study of adult patients admitted to Gabriel Toure University Hospital between January 2019 and December 2023.

Inclusion criteria

All patients with a primary diagnosis of ICH and radiographic evidence of IVH were included.

Exclusion criteria

Patients with aneurysmal subarachnoid hemorrhage or ICH related to trauma or underlying lesions were excluded as well as patients with Glasgow Coma Scale 3 (GCS) at presentation and bilateral fixed pupillary dilatation.

Group characteristics

Demographic, clinical and radiographic characteristics of patients were recorded. Graeb score was used to assess the severity of IVH. EVDs are considered in patients with GCS ≤ 8. The EVD placement procedure was carried out in the operating room in all cases. EVDs were placed into the frontal horn of the lateral ventricle according to the localization of hematoma in the right or left ventricle. Postoperative CT scan was performed to confirm intraventricular position of the catheter tip.

Study design

Short-term mortality was recorded and outcomes were evaluated using the GCS and the modified Rankin score (mRS).

Statistical analysis

Statistical analysis was performed to determine independent predictor factors of 30-day mortality using Wilcoxon rank sum test and Fisher's exact test. *P* value ≤ 0.05 was considered statistically significant.

Results

During the study period, a total of 63 patients were admitted for spontaneous ICH and IVH was associated in 24 (38.1%) patients. Among them, EVDs were placed in 17 patients. The mean age was 49 years with range of 27 to 66 years. There were 11 males and 6 females. The main risk factors of stroke were hypertension in 13 patients and diabetes in 7 patients. The initial GCS was between 5 and 8. Unilateral pupillary dilatation was found in 8 patients (***Table 1***). EVD was placed in frontal horn in the lateral ventricle in all cases (***Fig. 1, 2***) and continuous CSF drainage was indicated leading to ventricle size and blood clot removal (***Fig. 2, 3***). The duration of EVD was 1 to 8 days. Four (23.5%) patients experienced infection as a complication. The short-term mortality rate was 70.5 % at 30 days including 8 males and 4 females with a mean age of 53 years. The functional outcomes were poor in 4 patients with mRS sore of 4 and 5 (***Table 2***). The independent predictor factors for 30-day mortality (***Table 3***) were poor GCS (p=0.319), mydriasis (p=0.245) and poor Graeb score (p=0.004).

Table 1. Demographic, clinical and CT scan (Graeb score) characteristics of 17 patients with EVD for IVH

Patients	Gender	Age (Years)	Risk factors	Initial GCS	Pupillary abnormalities	Graeb score
1	Female	51	Hypertension	6	Unilateral mydriasis	8
2	Male	60	Hypertension Diabetes	5	Bilateral mydriasis	10
3	Male	27		7	Normal	5
4	Female	49	Diabetes	8	Unilateral mydriasis	8
5	Female	38	Hypertension	8	Normal	7
6	Male	66	Hypertension	7	Normal	9
7	Male	54	Hypertension Diabetes	8	Normal	9
8	Female	61	Hypertension Diabetes	6	Bilateral mydriasis	10
9	Male	40	Hypertension	7	Normal	6
10	Male	32	Hypertension	5	Normal	8
11	Male	65	Hypertension Diabetes	7	Normal	9
12	Male	63	Hypertension Diabetes	8	Normal	6
13	Male	39	Hypertension	7	Normal	9
14	Female	31		7	Normal	4
15	Female	49	Hypertension	5	Normal	6
16	Male	47	Hypertension	8	Unilateral mydriasis	9
17	Male	61	Hypertension Diabetes	8	Normal	5

This article contains some figures that are displayed in color online but in black and white in the print edition.

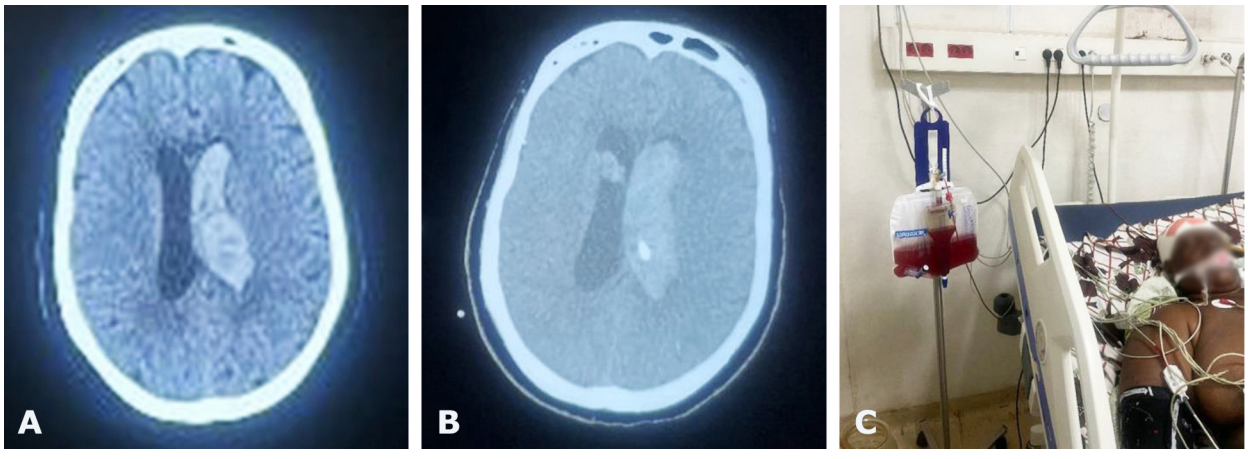

Fig. 1. Preoperative CT scan showing IVH (A), postoperative CT scan showing intraventricular location of the catheter tip (B) and photograph of Patient with EVD in-situ ICU (C)

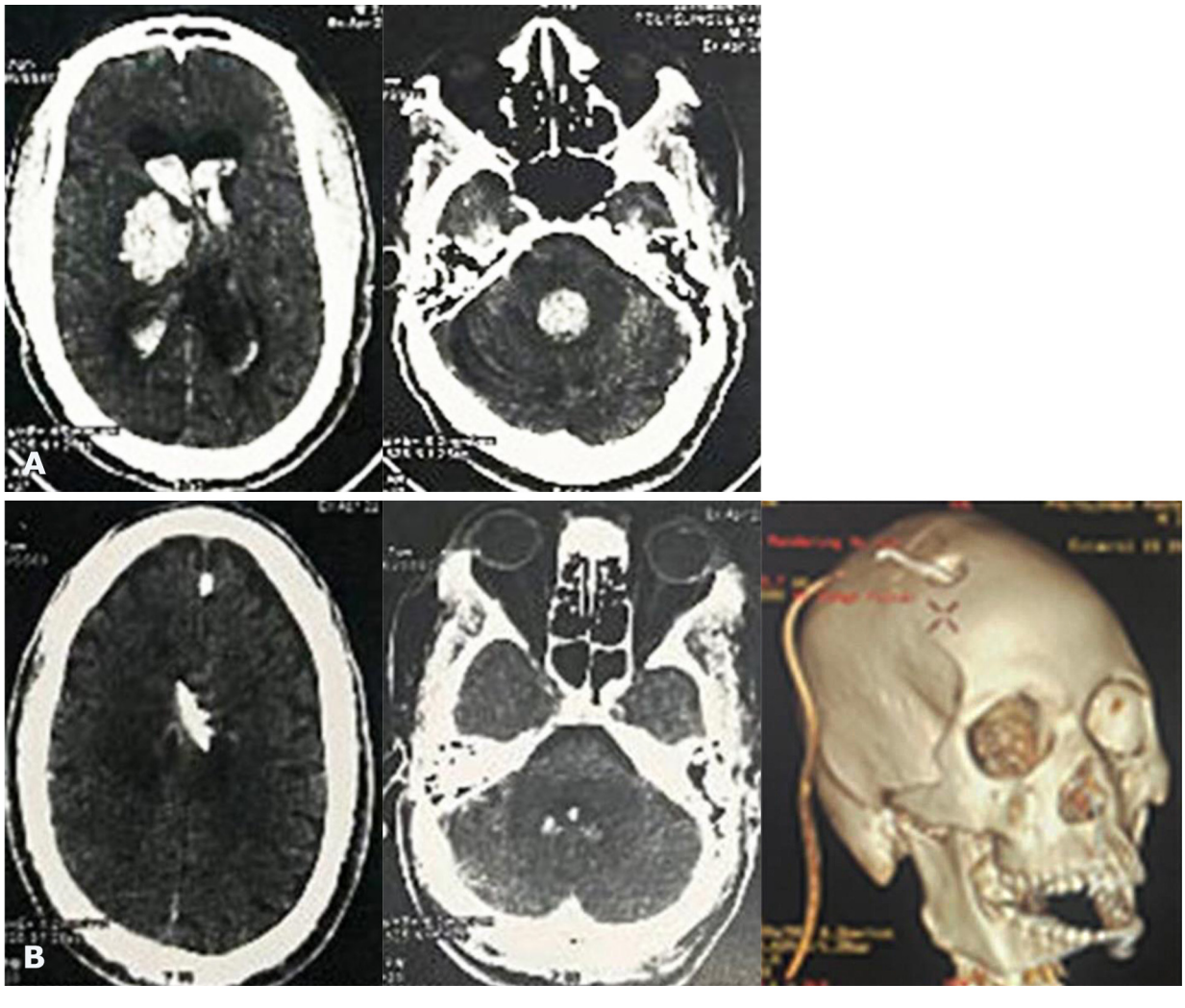

Fig. 2. Preoperative CT scan showing ICH with IVH (A), and postoperative CT scan showing intraventricular catheter tip in the ventricle as well as the decrease of ventricle size and hematoma (B)

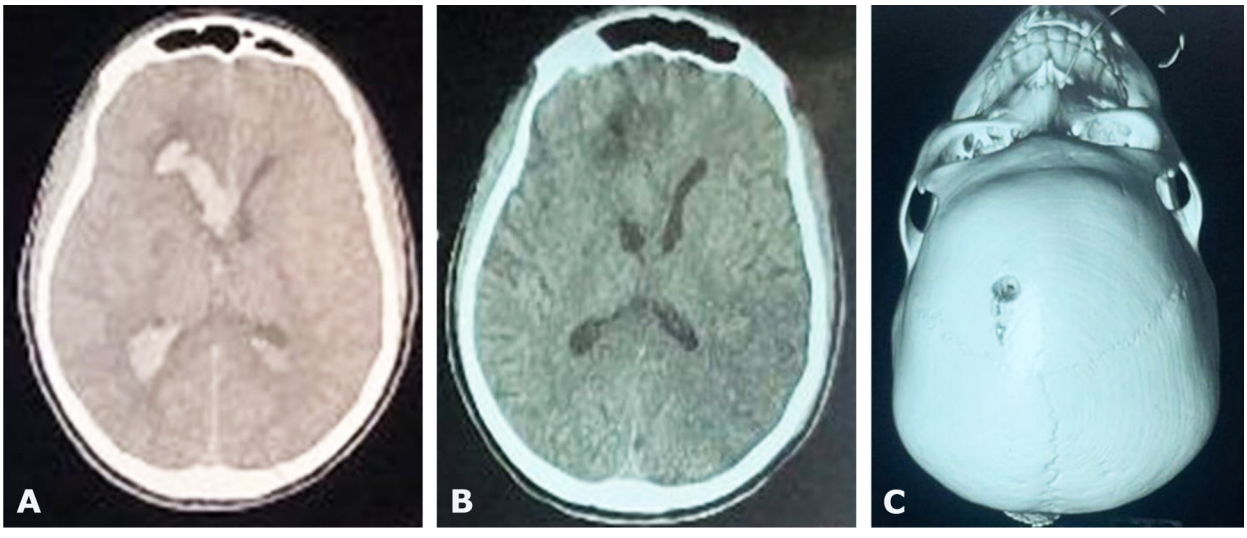

Fig. 3. Preoperative CT scan showing IVH (A) and postoperative CT scan showing the complete evacuation of IVH after EVD (B) with the burr hole in 3D (C)

Table 2. Mortality and mRS after 6 months in 17 patients with EVD for IVH

Patients	Duration of EVD (days)	Mortality (day of death)	mRS
1	4	4	-
2	1	1	-
3	5	Alive	2
4	8	21	-
5	5	Alive	4
6	4	14	-
7	5	5	-
8	3	3	-
9	8	Alive	4
10	3	3	-
11	6	18	-
12	5	27	-
13	6	6	-
14	6	Alive	4
15	6	6	-
16	4	12	-
17	5	Alive	5

Table 3. Statistical analysis to determine independent predictor factors for short-term mortality

		Mortality (30 days)			
Characteristic	**Statistic**	**Died N = 12**	**Alive N = 5**	**Overall N = 17**	**p-value[1]**
Graeb score	Median (Q1 – Q3)	9 (8 – 9)	5 (5 – 6)	8 (6 – 9)	0.004
Gender					>0.999
Female	n (%)	4 (33)	2 (40)	6 (35)	
Male	n (%)	8 (67)	3 (60)	11 (65)	
Age (years)	Median (Q1 – Q3)	53 (48 – 62)	38 (31 – 40)	49 (39 – 61)	0.057
GCS	Median (Q1 – Q3)	7 (6 – 8)	7 (7 – 8)	7 (6 – 8)	0.319
Pupillary abnormalities					0.245
Mydriasis	n (%)	5 (42)	0 (0)	5 (29)	
Normal	n (%)	7 (58)	5 (100)	12 (71)	

[1]Wilcoxon rank sum test; Fisher's exact test

Discussion

IVH occurs in approximately 40 % of all ICH. In this condition management of elevated ICP remains the goal of treatment. EVD is the procedure of choice for the treatment of acute hydrocephalus and increased ICP and it is often placed as a life-saving measure. In 1890, Keen [10] first described the technique of catheter placement in the lateral ventricle and in 1918 Dandy [11] published a technique involving anterior and occipital ventricular horn punctures. EVD is usually indicated in patients with GCS<9. According to the literature, EVD may reduce short-term mortality by reducing ICP [7, 8, 9]. However, there is no evidence that EVD improves functional prognosis. There are no consensus criteria for the indication of EVD in the management of ICH with IVH. We conducted this study using the following criteria: IVH, GCS<9. Patients with a GCS score of 3 and bilateral mydriasis were excluded. Patient's sociodemographic characteristics such as age, sex, comorbidities and risk factors, as well as clinical parameters, including GCS and pupillary abnormalities were taken into account for prognosis. The short-term mortality rate was 70.6% at 30 days. The independent predictor factors of short-term mortality in our study were the mydriasis (p=0.319), the poor GCS (p=0.245) and the poor Graeb score (p=0.004). The decision to place an EVD is multifactorial, including low GCS and the amount of blood in the ventricles. Studies have shown that early intensive care can decrease mortality and improve functional prognosis [12, 13]. Adams et al. [9] concluded that EVD decrease ventricular size but did not affect the level of consciousness of patients. Shapiro et al [14] also concluded that ventriculocisternostomy did not improve prognosis. In a meta-analysis including 7 studies, Nieuwkamp et al. [7] found a slight improvement with EVD, while there was no difference in terms of poor prognosis between EVD and conservative treatment. Staykov et al. [15] reported a mortality of 53% for patients with EVD versus 71% in patients without EVD. There is no prospective and randomized trial addressing the effect of EVD in IVH on clinical outcome. Complications of EVD include complete or partial occlusion and infection. These complications are associated with poor outcome [16]. Infection rate related to EVD was 27.6% in the study of Kirmani et al [17]. In our study, the infection rate was 23.5% despite all EVD placements being performed in the operating room. EVD placement using endoscopy optimizes catheter position and allows aspiration of the blood clot, whereas freehand placement of EVD without the use of imaging guidance may be associated with misplacement of the catheter tip in the ventricle. In their study, Nawabi et al. [18] reported that only 78% of EVDs were placed successfully on the first pass without the use of imaging guidance. All EVDs were placed freehand in our study with accurate placement of the catheter tip in the ventricle confirmed by postoperative CT scan. We do not have access to intraoperative imaging guidance. Nevertheless, freehand placement of EVD is safe as long as the intracranial anatomy is not disfigured to a large extent, surface measurements are carried out precisely and the puncturing is done perpendicularly to the skull [19]. According to a meta-analysis including 680 patients, neuroendoscopy is more effective than EVD combined with intraventricular thrombolysis in terms of both hematoma evacuation and prognosis [20]. Neuroendoscopic evacuation of IVH improves outcomes compared with EVD according to a systematic review with meta-analysis by Mezzacappa et al. [21] Haldrup et al. [22] found that EVD associated with fibrinolysis promoted hematoma clearance and decreased mortality and improved good functional outcomes. Furthermore, EVD combined with continuous lumbar drainage has been reported to improve the prognoses and quality of life in patients with IVH [23]. In our study, there was no endoscopy or thrombolysis associated with EVD placement.

Our study is limited by the relatively small numbers achieved over the period. Additionally, patients were not randomized making it difficult to determine whether the impact of placing the EVD in our setting was positive or negative. Also, being a single institution study, it is difficult to generalize the findings.

Conclusion

The placement of EVD in patient with IVH remains controversial. Our study reveals the high mortality rate in patients with ICH despite this procedure, prompting questions about the usefulness of this procedure in our setting. Although our study demonstrated a high mortality rate, patients with appropriate indications undoubtedly require EVD. Complementary and randomized studies are necessary in the future.

Disclosure

Conflict of interest

The authors declare no conflicts of interest and no personal financial interest in the preparation of this article

Informed consent

Informed and voluntary written consent to participate in the study and publication of data was obtained from all patients.

Funding

Not applicable

References

1. Steiner T, Diringer MN, Schneider D, Mayer SA, Begtrup K, Broderick J, Skolnick BE, Davis SM. Dynamics of intraventricular hemorrhage in patients with spontaneous intracerebral hemorrhage: risk factors, clinical impact, and effect of hemostatic therapy with recombinant activated factor VII. Neurosurgery. 2006 Oct;59(4):767-73; discussion 773-4. doi: 10.1227/01.NEU.0000232837.34992.32
2. Diringer MN, Edwards DF, Zazulia AR. Hydrocephalus: a previously unrecognized predictor of poor outcome from supratentorial intracerebral hemorrhage. Stroke. 1998 Jul;29(7):1352-7. doi: 10.1161/01.str.29.7.1352
3. Tuhrim S, Dambrosia JM, Price TR, Mohr JP, Wolf PA, Heyman A, Kase CS. Prediction of intracerebral hemorrhage survival. Ann Neurol. 1988 Aug;24(2):258-63. doi: 10.1002/ana.410240213
4. Badjatia N, Rosand J. Intracerebral hemorrhage. Neurologist. 2005 Nov;11(6):311-24. doi: 10.1097/01.nrl.0000178757.68551.26
5. Binz DD, Toussaint LG 3rd, Friedman JA. Hemorrhagic complications of ventriculostomy placement: a meta-analysis. Neurocrit Care. 2009;10(2):253-6. doi: 10.1007/s12028-009-9193-0
6. Ehtisham A, Taylor S, Bayless L, Klein MW, Janzen JM. Placement of external ventricular drains and intracranial pressure monitors by neurointensivists. Neurocrit Care. 2009;10(2):241-7. doi: 10.1007/s12028-008-9097-4
7. Nieuwkamp DJ, de Gans K, Rinkel GJ, Algra A. Treatment and outcome of severe intraventricular extension in patients with subarachnoid or intracerebral hemorrhage: a systematic review of the literature. J Neurol. 2000 Feb;247(2):117-21. doi: 10.1007/pl00007792
8. Engelhard HH, Andrews CO, Slavin KV, Charbel FT. Current management of intraventricular hemorrhage. Surg Neurol. 2003 Jul;60(1):15-21; discussion 21-2. doi: 10.1016/s0090-3019(03)00144-7
9. Adams RE, Diringer MN. Response to external ventricular

drainage in spontaneous intracerebral hemorrhage with hydrocephalus. Neurology. 1998 Feb;50(2):519-23. doi: 10.1212/wnl.50.2.519
10. Keen W. Surgery of the lateral ventricles of the brain. Lancet. 1890; 136 (3498):553-5. doi: 10.1016/S0140-6736(00)48676-9
11. Dandy WE. VENTRICULOGRAPHY FOLLOWING THE INJECTION OF AIR INTO THE CEREBRAL VENTRICLES. Ann Surg. 1918 Jul;68(1):5-11. doi: 10.1097/00000658-191807000-00002
12. Mirski MA, Chang CW, Cowan R. Impact of a neuroscience intensive care unit on neurosurgical patient outcomes and cost of care: evidence-based support for an intensivist-directed specialty ICU model of care. J Neurosurg Anesthesiol. 2001 Apr;13(2):83-92. doi: 10.1097/00008506-200104000-00004
13. Becker KJ, Baxter AB, Cohen WA, Bybee HM, Tirschwell DL, Newell DW, Winn HR, Longstreth WT Jr. Withdrawal of support in intracerebral hemorrhage may lead to self-fulfilling prophecies. Neurology. 2001 Mar 27;56(6):766-72. doi: 10.1212/wnl.56.6.766
14. Shapiro SA, Campbell RL, Scully T. Hemorrhagic dilation of the fourth ventricle: an ominous predictor. J Neurosurg. 1994 May;80(5):805-9. doi: 10.3171/jns.1994.80.5.0805
15. Staykov D, Bardutzky J, Huttner HB, Schwab S. Intraventricular fibrinolysis for intracerebral hemorrhage with severe ventricular involvement. Neurocrit Care. 2011 Aug;15(1):194-209. doi: 10.1007/s12028-010-9390-x
16. Gu C, Lind ANR, Haldrup M, Eschen JT, Eskildsen MH, Kjær A, Rasmussen M, Dyrskog S, Meier K, Simonsen CZ, Debrabant B, Korshøj AR. Outcomes and complications of external ventricular drainage in primary and secondary intraventricular hemorrhage: a descriptive observational study. J Neurosurg. 2025 Jan 3;142(6):1599-1605. doi: 10.3171/2024.8.JNS24915
17. Kirmani AR, Sarmast AH, Bhat AR. Role of external ventricular drainage in the management of intraventricular hemorrhage; its complications and management. Surg Neurol Int. 2015 Dec 23;6:188. doi: 10.4103/2152-7806.172533
18. Nawabi NLA, Stopa BM, Lassarén P, Bain PA, Mekary RA, Gormley WB. External ventricular drains and risk of freehand placement: A systematic review and meta-analysis. Clin Neurol Neurosurg. 2023 Aug;231:107852. doi: 10.1016/j.clineuro.2023.107852
19. Brenke C, Fürst J, Katsigiannis S, Carolus AE. High accuracy of external ventricular drainage placement using anatomical landmarks. Neurochirurgie. 2020 Dec;66(6):435-441. doi: 10.1016/j.neuchi.2020.09.009
20. Li Y, Zhang H, Wang X, She L, Yan Z, Zhang N, Du R, Yan K, Xu E, Pang L. Neuroendoscopic surgery versus external ventricular drainage alone or with intraventricular fibrinolysis for intraventricular hemorrhage secondary to spontaneous supratentorial hemorrhage: a systematic review and meta-analysis. PLoS One. 2013 Nov 13;8(11):e80599. doi: 10.1371/journal.pone.0080599
21. Mezzacappa FM, Weisbrod LJ, Schmidt CM, Surdell D. Neuroendoscopic Evacuation Improves Outcomes Compared with External Ventricular Drainage in Patients with Spontaneous Intraventricular Hemorrhage: A Systematic Review with Meta-Analyses. World Neurosurg. 2023 Jul;175:e247-e253. doi: 10.1016/j.wneu.2023.03.061
22. Haldrup M, Miscov R, Mohamad N, Rasmussen M, Dyrskog S, Simonsen CZ, Grønhøj M, Poulsen FR, Bjarkam CR, Debrabant B, Korshøj AR. Treatment of Intraventricular Hemorrhage with External Ventricular Drainage and Fibrinolysis: A Comprehensive Systematic Review and Meta-Analysis of Complications and Outcome. World Neurosurg. 2023 Jun;174:183-196.e6. doi: 10.1016/j.wneu.2023.01.021
23. Xia D, Jiang X, Li Z, Jin Y, Dai Y. External ventricular drainage combined with continuous lumbar drainage in the treatment of ventricular hemorrhage. Ther Clin Risk Manag. 2019 May 30;15:677-682. doi: 10.2147/TCRM.S207750

Original article

Ukrainian Neurosurgical Journal. 2025;31(4):61-67
doi: 10.25305/unj.333185

Status and prognostic impact of IDH1 in adult grade 4 diffuse gliomas

Mouna Zghal [1], Slim Charfi [1], Wicem Siala [2], Soumaya Graja [1], Fatma Kolsi [3], Wafa Ghribi [1], Lobna Ayedi [1], Mohamed Zaher Boudawara [3], Jamel Daoud [2], Tahya Sellami Boudawara [1]

[1] Pathology Department and Research Laboratory LR18SP10, Habib Bourguiba University Hospital, Sfax, Tunisia
[2] Medical Radiotherapy Department, Habib Bourguiba University Hospital Sfax, Tunisia
[3] Neurosurgery Department, Habib Bourguiba University Hospital Sfax, Tunisia

Received: 20 June 2025
Accepted: 20 August 2025

Address for correspondence: *Mouna Zghal, Department of Pathology, Habib Bourguiba University Hospital, El Ain Road Km 0.5, Sfax, 3029, Tunisia, e-mail: mona0zghal@gmail.com*

Background and objectives: The fifth edition of the WHO Classification of Tumors of the Central Nervous System divides grade 4 diffuse glioma based on *IDH1* mutation in grade 4 astrocytoma, IDH-mutant and glioblastoma, IDH-wild type tumors. This study aimed to evaluate the *IDH1* status in grade 4 diffuse glioma as well as its correlation with clinicopathological features and patient survival. To our knowledge, no Tunisian studies on the molecular profile of diffuse glioma have yet been published.

Methods: This is a retrospective study including all cases of adult, grade 4 diffuse glioma collected in the pathology department of Habib Bourguiba hospital.

Results: A total of 67 patients were included in the final analysis. The expression of *IDH1* was positive in 22 cases (32%). *IDH1*-positive tumors were classified as grade 4 astrocytoma, *IDH1*-mutant while, 45 *IDH1*-negative tumors were classified as glioblastoma, *IDH1*-wild type tumors (68%). *IDH1* expression was correlated with younger age (≤ 40 years old), frontal location, complete surgical resection and well-defined borders. *IDH1*-positive tumors were associated significantly with better prognosis. The 1-year overall survival (OS) for grade 4 astrocytoma, *IDH1*-mutant was 86% compared with 8% in glioblastoma, IDH1-wild type (p=0.008).

Conclusion: Our study investigated *IDH1* expression in grade 4 diffuse glioma and proved that grade 4 astrocytoma, IDH1 positive tumors displayed different characteristics with a more favorable outcome compared to glioblastoma, IDH1 negative. Thus, evaluation of *IDH1* mutation should be standardized routinely not only as diagnostic marker but also to refine the prognostic classification of these tumors.

Key words: *grade 4 diffuse glioma; IDH1; astrocytoma grade 4; glioblastoma; pathology; prognosis*

Introduction

Diffuse gliomas (DGs) are the most common primary tumors of the central nervous system (CNS) [1]. Traditionally, CNS tumor has been classified exclusively based on histological features. During recent years, large-scale researches have made rapid advances in understanding glioma genetics. The identification of genetic impairments involved in gliogenesis led to 2021 World Health Organization (WHO) classification based on an integrated histo-molecular diagnosis [2] including radiation, chemotherapy (temozolomide and PCV [procarbazine, lomustine, vincristine]. The isocitrate dehydrogenase 1 (IDH1) mutation and its prognostic impact remain the most studied. Despite their histological similarity, this classification divides the grade 4 DGs based on IDH1 mutation into two different prognostic entities: *grade 4 astrocytoma, IDH-mutant* and *glioblastoma, IDH-wild type* tumors. The most frequent IDH mutation is IDH1-R132H, which is detectable by immunohistochemistry using a specific antibody; other IDH mutations are rare (about 10%) and require DNA sequencing [3]. IDH 1 mutation is a landmark in the history of gliomas as a favorable prognostic biomarker, which is associated with a good clinical outcome [4]. In addition, several other genetic alterations have been identified in the pathogenesis of IDH-wild type glioblastoma such as *TERT* promoter mutation, *EGFR* amplification and +7/−10 copy number changes [5].

Therefore, the aim of our study was to evaluate the IDH1 status in grade 4 DGs and to assess its correlation with clinicopathological and survival features.

Methods

Study design and population

This is a retrospective study including all consecutive cases of grade 4 DG collected in the pathology and radiotherapy departments at the Habib Bourguiba University Hospital over a period of 9 years from 2016 through 2024.

Patients were enrolled in this study according to the following criteria: histological diagnosis of grade 4 DG (according to 2021 CNS WHO classification) [2], age over 18 years-old and available clinical and survival data. This report follows the Strengthening the Reporting

of Observational Studies in Epidemiology (STROBE) guidelines. All procedures performed in studies involving human participants were in accordance with the ethical standards of the institutional and the national research committee of Habib Bourguiba University Hospital and with the 1964 Helsinki declaration and its later amendments or comparable ethical standards.

Immunohistochemical study

Immunohistochemistry was performed on 5-µm –thick formalin fixed paraffin embedded tissues sections using antibodies against IDH1-R132H mutant protein (mouse monoclonal, clone IHC132-100, 1:400; Genome-Me). The expression of IDH1-R132H was determined by semi-quantitatively assessing the proportion of positively stained tumor cells. Cytoplasmic staining involving more than 10% of tumor cells was considered positive. Cases with less than 10% of tumor cells or staining of macrophages were considered as negative [6, 7].

Statistical analysis

Statistical analysis was performed using SPSS software version 22.0. Categorical variables were described as frequencies and percentages. For quantitative variables, means and standard deviations were used when their distributions were normal. Otherwise, medians and extreme values were reported. To examine the association of IDH1 expression with the different clinicopathological features the Pearson's chi-square test or Fisher's exact test was applied for categorical variables. Survival analysis was performed using the Kaplan-Meier estimator and log-rank test to assess the significant association of IDH1 expression with overall survival (OS) and progression free survival (PFS) times in diffuse gliomas patients. A $p \leq 0.05$ was considered statistically significant.

Results

Clinicopathological characteristics of study patients

The study population consisted of 67 patients representing 58.2 % of all DGs. The mean age at diagnosis was 56,7 years ± 12,9. The cohort included 36 males and 31 females (sex ratio: 1,16). The mean tumor size was 47.6 mm ± 14,8 mm. The tumors were localized at the cerebral hemispheres in 56 cases (83.5%) followed by diencephalon in 8 cases (12%) and ventricles in 2 cases (3%). Only one case was in the cerebellum. For hemispheres location, the frontal lobe was involved in 23 cases (34.3%) followed by the temporal lobe in 17 cases (25.4%) and the parietal lobe in 12 cases (17.9%) (***Table 1***).

Table1. Comparison of grade 4 diffuse glioma characteristics according to IDH1 expression

Variables			IDH1		p
			Negative (%)	Positive (%)	
Age (years)	≤ 40		5 (21.8)	18 (78.2)	< 0.001
	> 40		40 (90)	4 (10)	
sex	Male		26 (7.7)	10 (27.7)	0.14
	Female		19 (72.3)	12 (38.7)	
Location	hemispheres	Frontal	8 (34.8)	15 (65.2)	0.02
		Temporal	14(82.4)	3 (17.6)	
		Parietal	10 (83.3)	2 (16.7)	
		Occipital	4	0	
	Diencephalon		7	1	
	Ventricles		2	0	
	Cerebellum		0	1	
size (cm)	< 5		12 (63.2)	7 (36.8)	0.4
	≥ 5		19 (73)	7 (27)	
Surgical margins	Complete		8 (38.1)	13 (61.9)	0.006
	Partial		21 (77.8)	6 (22.2)	
	Biopsy		10 (83.3)	2 (16.7)	
Borders	Well-defined		2 (12.5)	14 (87.5)	<0.001
	Ill-defined		28 (90.3)	3 (9.7)	
p53	Negative		6 (57)	8 (43)	0.5
	Positive		16 (30,2)	37 (69,8)	

Notes. Data reported in bold refers to $p \leq 0.05$
Pearson's chi-square test was used to compare categorical variables
*Fisher test was used instead of chi-square test if one or more variables had an expected frequency of less than five.

Immunohistochemical analysis of IDH1

The expression of IDH1 was positive in 22 cases (32%). IDH1 positive tumors were classified as grade 4 astrocytoma, IDH1-mutant (***Fig. 1***) while IDH1 negative tumors were classified as glioblastoma, IDH1-wild type tumors (N= 45; 68%) (***Fig. 2***).

Comparison of tumor characteristics according to IDH1 expression

The clinical and pathological data of grade 4 astrocytoma, IDH1-mutant and glioblastoma, IDH1 wild type tumors are described and compared in (***Table 1)***. The two tumors displayed significant differences in various characteristics. Grade 4 astrocytoma, IDH1-mutant was associated with a younger patient age (<40 years) (p<0,001), a frontal location of the tumor (p=0,02), complete surgical resection (p=0.006) and well-defined borders (p<0.001). No correlation was observed with other the factors including sex, tumor size and p53 expression.

Survival analysis

IDH1 positive tumors were associated with a more favorable outcome. The OS of patients with grade 4 astrocytoma, IDH1 mutant were significantly longer than glioblastoma, IDH1 wild-type tumors (1- year OS: 82% versus 8%; p=0.008) (***Fig. 3***). In addition, grade 4 astrocytoma, IDH1 mutant showed a prolonged 1-year PFS compared to glioblastoma (48% versus 29%; p= 0.01) (***Fig. 4***).

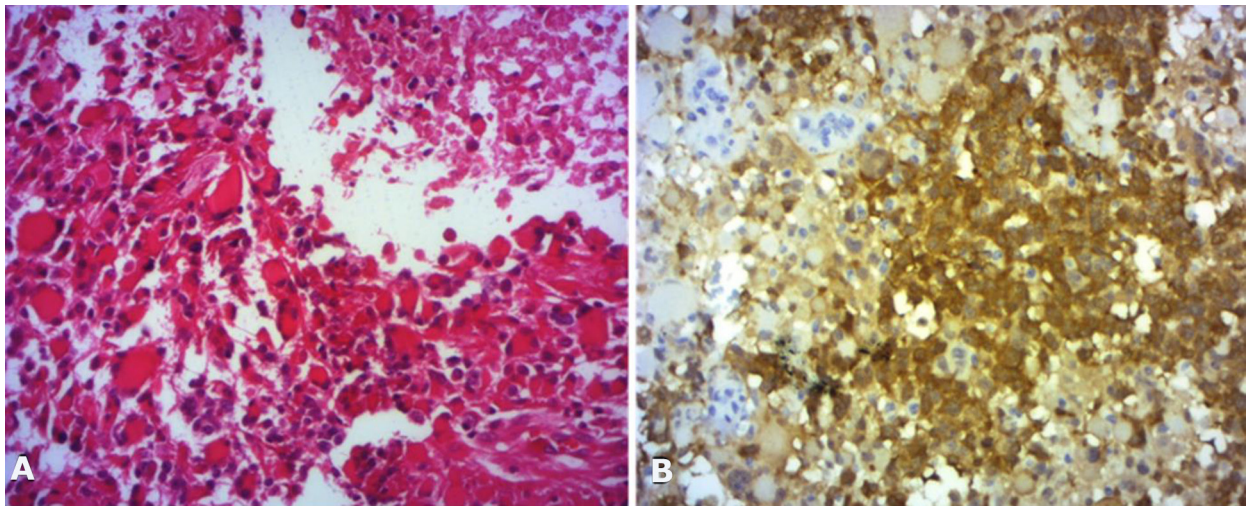

Fig. 1. Grade 4 astrocytoma, IDH1 positive (A) Gemistocytic astrocytoma grade 4 (H&E x 200) (B) Positive stain for IDH1 (X200)

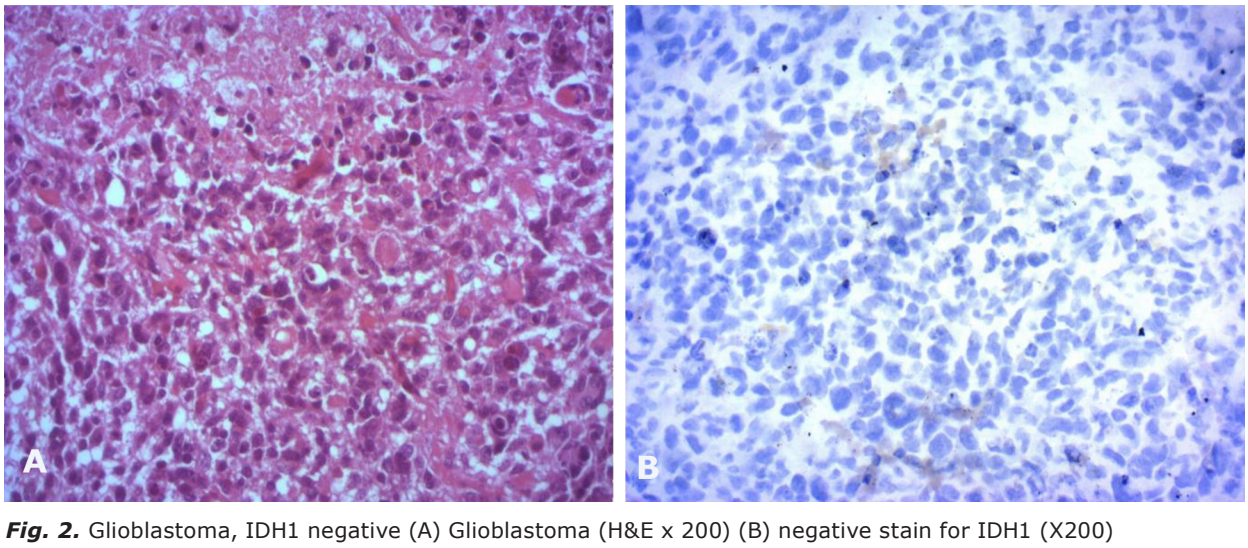

Fig. 2. Glioblastoma, IDH1 negative (A) Glioblastoma (H&E x 200) (B) negative stain for IDH1 (X200)

This article contains some figures that are displayed in color online but in black and white in the print edition.

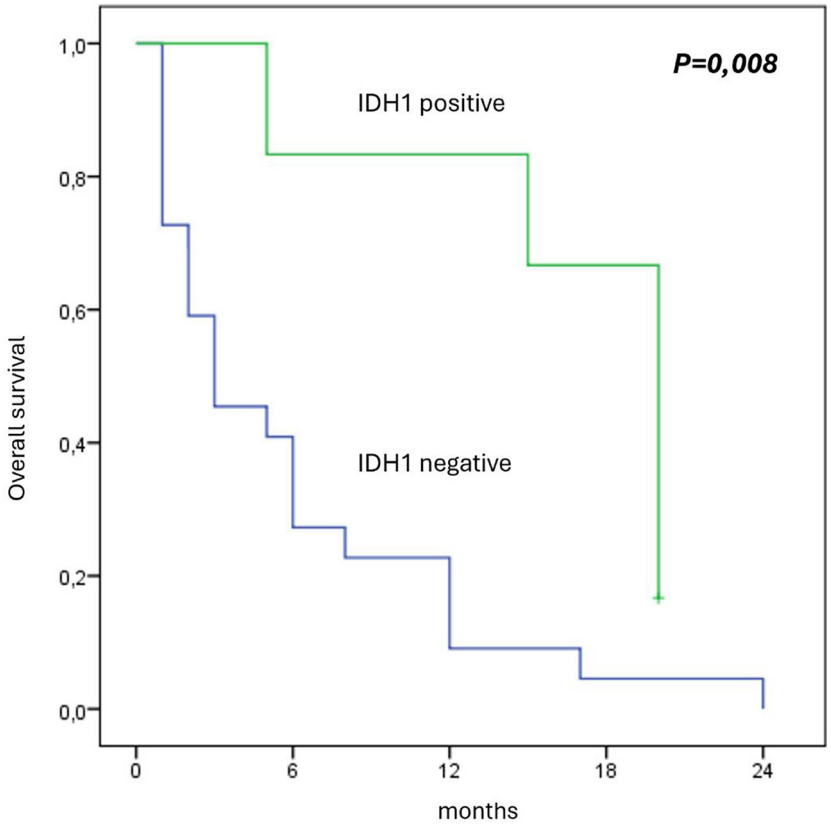

Fig. 3. Overall survival of grade 4 DG according to IDH1 expression

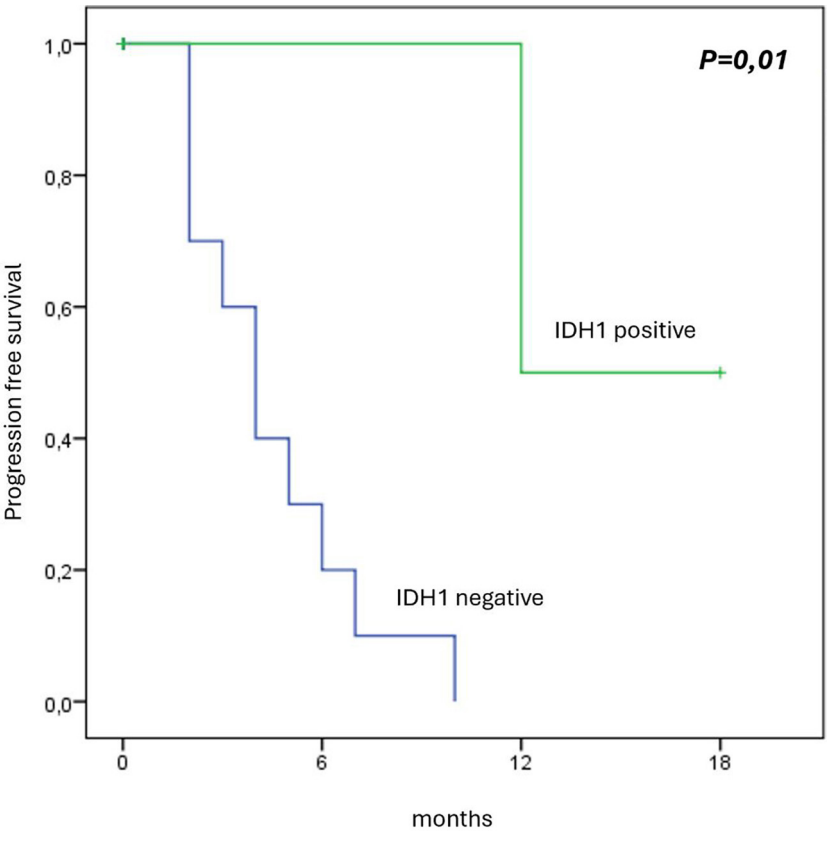

Fig. 4. Progression free survival of grade 4 DG according to IDH1 expression

Discussion

In the present study, we detected the IDH1-R132H expression using immunohistochemistry in grade 4 DG, and assessed its favorable prognostic impact among grade 4 astrocytoma compared with IDH1-negative glioblastoma. To our knowledge, this is the first study reporting the impact of IDH1 expression in grade 4 DG in Tunisia.

Nowadays, IDH1 mutation is commonly established as a hallmark molecular feature of diffuse gliomas [3]. IDH1–R132H is the most common mutation (90%), followed at a distance by IDH1- R132L, IDH1- R132S, IDH1- R132C and IDH1-R132G mutations [8]. Currently, immunohistochemistry is considered a reproducible and available method for assessing IDH1 mutation. IDH1-R132H antibody is highly specific for detecting the most common mutation in the gene and has a sensitivity of 94% because of the lack of detection of other types of IDH1 mutations [9, 10]. Immunohistochemical expression rates of IDH1 in grade 4 DG have varied across studies. A meta-analysis conducted by Chen et al. demonstrated a wide range in the reported frequency of IDH1 mutation with rates ranging from 18% to 81.8% [11].

The fifth edition of the WHO classification of tumors of the CNS incorporates numerous refinements and advances since the publication of the 2016 revised fourth edition. Notably, the nomenclature of diffuse gliomas has been significantly revised [2]. In the 2016 classification, IDH-mutant diffuse astrocytic tumors were divided into three distinct entities—diffuse astrocytoma, anaplastic astrocytoma, and glioblastoma based on histological criteria. In the updated classification, however, all IDH-mutant diffuse astrocytic tumors are grouped under a single category (IDH-mutant astrocytoma) and are assigned a CNS WHO grade of 2, 3, or 4. Furthermore, grading is no longer based solely on histology, as the presence of a homozygous deletion of *CDKN2A* and/or *CDKN2B* now qualifies the tumor for a WHO grade 4 designation, even in the absence of microvascular proliferation or necrosis [5]. Moreover, the 2021 fifth edition of WHO CNS classification emphasizes the role of molecular diagnosis building on the sixth update of the Consortium to Inform Molecular and Practical Approaches to CNS Tumor Taxonomy (cIMPACT- NOW) recommendations and 2016 WHO classification [12]. For IDH-wildtype diffuse astrocytic tumors, the presence of one or more of three genetic parameters: TERT promoter mutation, EGFR gene amplification, combined gain of chromosome 7 and loss of chromosome 10 are sufficient to assign the diagnosis of *glioblastoma, IDH-wild type* even in the absence of necrosis or microvascular proliferation [12, 13].

IDH1-mutant gliomas occur commonly in younger age compared to wild type tumors. According to a recent study, the median age at diagnosis of IDH1-mutant astrocytomas was 36 and versus 52 years in Glioblastoma, IDH1-negative [14]. Consistent with this, we found a positive association between IDH1 and age (< 40 years). In addition, tumor location also appears to correlate with IDH1 status. IDH1-wild type tumors are more deeply situated with more infiltrative pattern, although mutant gliomas are located frequently in the frontal lobe [16]. To date, correlation of IDH1 mutation with tumor size is unclear; some studies found that IDH1-wild type tumors are larger [17] while other authors didn't found such association [18] IDH status was determined on 114 and 27 patients, respectively. On univariable analysis, improved five-year survival was independently associated with concurrent TMZ (46.2 vs. 29.3 %, p = 0.02. Several studies have demonstrated an association between IDH1 status and the extent of tumor resection. Astrocytomas harboring IDH1 mutations are more likely to undergo complete tumor resection compared to IDH1-wildtype glioblastomas [19].

The association of IDH1 mutation with TP53 mutation has been widely studied in the literature and has led to contradictory results. IDH1 mutation was found associated with TP53 mutation in several studies [10, 21], whereas other authors did not found such an association, consistent to our results [22, 23]. Immunohistochemistry is a practicable surrogate for a molecular assay. Strong p53 staining of 10% of tumor cells is highly predictive of TP53 mutation with a sensitivity and specificity of 78.8% and 96.7% respectively [24]. TP53 mutation is common in grade 4 astrocytoma, IDH mutant, observed in about 70% of cases. However, this mutation is less common in glioblastoma, IDH-wild type (less than 30%) [25].

Based on previous research, IDH1 mutant gliomas present an improved outcome [20, 25–27]. The aim of our study was to establish a correlation between the survival outcome of grade4 DGs and IDH1 immunohistochemical expression.

Survival analysis based on IHC results showed a statistically significant better survival in both OS and PFS in IDH1 positive tumors than their counterparts. These results were consistent with several other reports. Sanson et al, have shown that the 5-year-OS of patients with grade 4 astrocytoma, IDH1-positive was 27.4 months versus 14 months in their counterparts [28]. Similarly in the study of Wang et al, glioblastoma presented a poor outcome with an OS of 14.2 months compared to grade 4 astrocytoma of which the OS was 26.6 months [20].

However, other authors haven't found such a correlation. Cai et al. reported that OS and PFS in IDH1-mutant grade 4 astrocytoma were not significantly better than those in glioblastoma [18]. These results were in line with those obtained by July et al; who concluded that IDH1 mutation was not a prognostic factor in grade 4 DGs [4].

Ultimately, our study provides a brand-new update of the value of IDH1 expression among grade 4 DGs; a subject not well elucidated in our population. Our study presented some limitations. The sample study may be limited; thus further larger investigations are recommended to better understand grade 4 diffuse gliomas. In addition, molecular profile supporting the diagnosis of glioblastoma IDH-wild type—such as TERT promoter mutation, EGFR amplification and +7/–10 copy number changes—were not available in our department.

Conclusion

The immunohistochemical profile of IDH1 is of significant importance for the diagnosis and prognosis in patients with grade 4 diffuse gliomas. In this study, we revealed that immunohistochemical staining of IDH1 in grade 4 astrocytoma was associated with distinct clinicopathological factors as well a good outcomes with

significant increased survival rates, compared to their counterparts of IDH1-negative glioblastomas. Thus, the evaluation of IDH1 mutation with other genomic markers, should be standardized and integrated into daily clinical practice — not only as diagnostic markers but also to refine the prognostic classification of these tumors.

Disclosure

Data availability

The datasets generated and/or analyzed during the current study are available from the corresponding author on reasonable request.

Ethical approval

All procedures performed in studies involving human participants were in accordance with the ethical standards of the institutional and the national research committee of Habib Bourguiba Hospital and the 1964 Helsinki declaration and its later amendments or comparable ethical standards.

Informed consent

General informed consent was obtained from all individual participants included in the study, upon admission to the hospital.

Funding declaration

This research did not receive any specific grant from funding agencies in the public, commercial, or not-for-profit sectors.

Conflict of interest

The authors have no conflicts of interest to disclose.

References

1. Louis DN, Ohgaki H, Wiestler OD, Cavenee WK (Eds): WHO Classification of Tumors of the Central Nervous System (4th edition). IARC; Lyon. 2016.
2. Louis DN, Ohgaki H, Wiestler OD, Cavenee WK. (Eds): WHO Classification of Tumors of the central Nervous System (5th edition). IARC; Lyon. 2021.
3. Rousseau A. [Molecular diagnostics of diffuse gliomas]. Revue Francophone des Laboratoires. 2018;(506):61-7. French. doi: 10.1016/S1773-035X(18)30324-1
4. July J, Patricia D, Gunawan PY, Setiajaya H, Ginting TE, Putra TP, Wuisan Z, Budhiarko D, Masykura N, Prayogi G, Utomo AR, Tandean S, Loe ML. Clinicopathological associations and prognostic values of IDH1 gene mutation, MGMT gene promoter methylation, and PD-L1 expressions in high-grade glioma treated with standard treatment. Pan Afr Med J. 2020 Aug 20;36:309. doi: 10.11604/pamj.2020.36.309.24831
5. Thomas DL. 2021 updates to the World Health Organization classification of adult-type and pediatric-type diffuse gliomas: a clinical practice review. Chin Clin Oncol. 2023 Feb;12(1):7. doi: 10.21037/cco-22-120
6. Takano S, Kato Y, Yamamoto T, Kaneko MK, Ishikawa E, Tsujimoto Y, Matsuda M, Nakai K, Yanagiya R, Morita S, Tsuboi K, Matsumura A. Immunohistochemical detection of IDH1 mutation, p53, and internexin as prognostic factors of glial tumors. J Neurooncol. 2012 Jul;108(3):361-73. doi: 10.1007/s11060-012-0837-0
7. Lewandowska MA, Furtak J, Szylberg T, Roszkowski K, Windorbska W, Rytlewska J, Jóźwicki W. An analysis of the prognostic value of IDH1 (isocitrate dehydrogenase 1) mutation in Polish glioma patients. Mol Diagn Ther. 2014 Feb;18(1):45-53. doi: 10.1007/s40291-013-0050-7
8. Gondim DD, Gener MA, Curless KL, Cohen-Gadol AA, Hattab EM, Cheng L. Determining IDH-Mutational Status in Gliomas Using IDH1-R132H Antibody and Polymerase Chain Reaction. Appl Immunohistochem Mol Morphol. 2019 Nov/Dec;27(10):722-725. doi: 10.1097/PAI.0000000000000702
9. Gülten G, Yalçın N, Baltalarlı B, Doğu G, Acar F, Doğruel Y. The importance of IDH1, ATRX and WT-1 mutations in glioblastoma. Pol J Pathol. 2020;71(2):127-137. doi: 10.5114/pjp.2020.97020
10. Capper D, Weissert S, Balss J, Habel A, Meyer J, Jäger D, Ackermann U, Tessmer C, Korshunov A, Zentgraf H, Hartmann C, von Deimling A. Characterization of R132H mutation-specific IDH1 antibody binding in brain tumors. Brain Pathol. 2010 Jan;20(1):245-54. doi: 10.1111/j.1750-3639.2009.00352.x
11. Chen JR, Yao Y, Xu HZ, Qin ZY. Isocitrate Dehydrogenase (IDH)1/2 Mutations as Prognostic Markers in Patients With Glioblastomas. Medicine (Baltimore). 2016 Mar;95(9):e2583. doi: 10.1097/MD.0000000000002583
12. Miller JJ, Shih HA, Andronesi OC, Cahill DP. Isocitrate dehydrogenase-mutant glioma: Evolving clinical and therapeutic implications. Cancer. 2017 Dec 1;123(23):4535-4546. doi: 10.1002/cncr.31039
13. Larsen C. Anomalies génétiques et moléculaires des glioblastomes (GBM) [Genetic and molecular abnormalities of glioblastomas (GBM)]. Bull Cancer. 2010 Nov;97(11):1389-407. French. doi: 10.1684/bdc.2010.1215
14. Molinaro AM, Taylor JW, Wiencke JK, Wrensch MR. Genetic and molecular epidemiology of adult diffuse glioma. Nat Rev Neurol. 2019 Jul;15(7):405-417. doi: 10.1038/s41582-019-0220-2
15. Suh CH, Kim HS, Jung SC, Choi CG, Kim SJ. Imaging prediction of isocitrate dehydrogenase (IDH) mutation in patients with glioma: a systemic review and meta-analysis. Eur Radiol. 2019 Feb;29(2):745-758. doi: 10.1007/s00330-018-5608-7
16. Olar A, Raghunathan A, Albarracin CT, Aldape KD, Cahill DP 3rd, Powell SZ, Goodman JC, Fuller GN. Absence of IDH1-R132H mutation predicts rapid progression of nonenhancing diffuse glioma in older adults. Ann Diagn Pathol. 2012 Jun;16(3):161-70. doi: 10.1016/j.anndiagpath.2011.08.010
17. Kizilbash SH, Giannini C, Voss JS, Decker PA, Jenkins RB, Hardie J, Laack NN, Parney IF, Uhm JH, Buckner JC. The impact of concurrent temozolomide with adjuvant radiation and IDH mutation status among patients with anaplastic astrocytoma. J Neurooncol. 2014 Oct;120(1):85-93. doi: 10.1007/s11060-014-1520-4
18. Cai J, Zhu P, Zhang C, Li Q, Wang Z, Li G, Wang G, Yang P, Li J, Han B, Jiang C, Sun Y, Jiang T. Detection of ATRX and IDH1-R132H immunohistochemistry in the progression of 211 paired gliomas. Oncotarget. 2016 Mar 29;7(13):16384-95. doi: 10.18632/oncotarget.7650
19. De Leeuw BI, Van Baarsen KM, Snijders TJ, Robe PAJT. Interrelationships between molecular subtype, anatomical location, and extent of resection in diffuse glioma: a systematic review and meta-analysis. Neurooncol Adv. 2019 Oct 1;1(1):vdz032. doi: 10.1093/noajnl/vdz032
20. Wang XW, Ciccarino P, Rossetto M, Boisselier B, Marie Y, Desestret V, Gleize V, Mokhtari K, Sanson M, Labussière M. IDH mutations: genotype-phenotype correlation and prognostic impact. Biomed Res Int. 2014;2014:540236. doi: 10.1155/2014/540236
21. Jakovlevs A, Vanags A, Gardovskis J, Strumfa I. Molecular classification of diffuse gliomas. Pol J Pathol. 2019;70(4):246-258. doi: 10.5114/pjp.2019.93126
22. Stancheva G, Goranova T, Laleva M, Kamenova M, Mitkova A, Velinov N, Poptodorov G, Mitev V, Kaneva R, Gabrovsky N. IDH1/IDH2 but not TP53 mutations predict prognosis in Bulgarian glioblastoma patients. Biomed Res Int. 2014;2014:654727. doi: 10.1155/2014/654727
23. Balss J, Meyer J, Mueller W, Korshunov A, Hartmann C, von Deimling A. Analysis of the IDH1 codon 132 mutation in brain tumors. Acta Neuropathol. 2008 Dec;116(6):597-602. doi: 10.1007/s00401-008-0455-2
24. Takami H, Yoshida A, Fukushima S, Arita H, Matsushita Y, Nakamura T, Ohno M, Miyakita Y, Shibui S, Narita Y, Ichimura K. Revisiting TP53 Mutations and Immunohistochemistry--A Comparative Study in 157 Diffuse Gliomas. Brain Pathol. 2015 May;25(3):256-65. doi: 10.1111/bpa.12173
25. Chaurasia A, Park SH, Seo JW, Park CK. Immunohistochemical Analysis of ATRX, IDH1 and p53 in Glioblastoma and Their Correlations with Patient Survival. J Korean Med Sci. 2016 Aug;31(8):1208-14. doi: 10.3346/jkms.2016.31.8.1208
26. Barresi V, Eccher A, Simbolo M, Cappellini R, Ricciardi GK, Calabria F, Cancedda M, Mazzarotto R, Bonetti B, Pinna G, Sala F, Ghimenton C, Scarpa A. Diffuse gliomas

in patients aged 55 years or over: A suggestion for IDH mutation testing. Neuropathology. 2020 Feb;40(1):68-74. doi: 10.1111/neup.12608
27. Rajmohan KS, Sugur HS, Shwetha SD, Ramesh A, Thennarasu K, Pandey P, Arivazhagan A, Santosh V. Prognostic significance of histomolecular subgroups of adult anaplastic (WHO Grade III) gliomas: applying the 'integrated' diagnosis approach. J Clin Pathol. 2016 Aug;69(8):686-94. doi: 10.1136/jclinpath-2015-203456
28. Sanson M, Marie Y, Paris S, Idbaih A, Laffaire J, Ducray F, El Hallani S, Boisselier B, Mokhtari K, Hoang-Xuan K, Delattre JY. Isocitrate dehydrogenase 1 codon 132 mutation is an important prognostic biomarker in gliomas. J Clin Oncol. 2009 Sep 1;27(25):4150-4. doi: 10.1200/JCO.2009.21.9832

Original article

Ukrainian Neurosurgical Journal. 2025;31(4):68-73
doi: 10.25305/unj.338929

Phalen's test. Classic or modern?

Irakli B. Goginava [1], Sergey A. Goloborod'ko [1], Mariia V. Riezunenko [2], Giorgi L. Giorgidze [3]

[1] Department of Pelvic Fractures Surgery, West Georgia Medical Center, Kutaisi, Georgia
[2] Department of Traumatology and Orthopedics, West Georgia Medical Center, Kutaisi, Georgia
[3] Department of Neurology, West GeorgiaMedical Center, Kutaisi, Georgia

Received: 10 September 2025
Accepted: 25 September 2025

Address for correspondence*:*
Irakli Borisovich Goginava, Department of Pelvic Fractures Surgery, West Georgia Medical Center, Javakhishvili str., 83a, Kutaisi, 4600, Georgia, e-mail: igoginava@evex.ge

Objective: to compare the sensitivity and specificity of the classic and modified Phalen test and to give recommendations on the expediency of using the tests in the diagnosis of carpal tunnel syndrome (CTS).

Materials and methods. The experimental group included 21 women (15 right and 14 left hands) with signs of idiopathic carpal tunnel syndrome. The control group also included 21 women (15 right and 14 left hands) without characteristic clinical manifestations of carpal tunnel syndrome. The mean age of the participants in both groups averaged 52 years.

Twenty-one women in the experimental and, respectively, in the control groups were randomized to perform both the classical and modified Phalen tests on 29 hands. In the classic Phalen test, the subject places her flexed elbows on the table so that the forearms are in a vertical position. The hands under the action of gravity are flexed as far as possible, the fingers remain in extension. When performing the modified Phalen test, the subject is asked to connect the dorsal surfaces of both hands, relax the upper limbs and, while maintaining this relaxed state, lower the elbows below the horizontal line.

Results. The sensitivity of the classic Phalen test was 93%, and that of the modified test was 96%. The specificity of the classical Phalen test was 96%, modified - 93%. The positive predictive value (PPV) of the classic Phalen test was 96%, the negative predictive value (NPV) was 93%. The PPV and NPV of the modified test were 93% and 96%, respectively.

Conclusion. The sensitivity of the classic Phalen test (93%) was slightly lower than the sensitivity of the modified test (96%), and the specificity of the classic test (96%) was higher than that of the modified test (93%). Due to high specificity and sensitivity, both tests have significant diagnostic value and can be successfully used in the diagnosis of carpal tunnel syndrome.

Keywords: *carpal tunnel syndrome; classic Phalen test; modified Phalen test; sensitivity; specificity*

Introduction

Carpal tunnel syndrome (CTS, G56.0) is a fairly common condition, affecting between 5-16% of the general population [1]. It is a mononeuropathy of the median nerve caused by compression of the nerve in the carpal tunnel. The primary pathophysiological mechanism of this condition is an increase of carpal tunnel pressure, leading to a disruption in the function and structure of the median nerve. The diagnosis of CTS is based on medical history and clinical examination. Electrodiagnostic and ultrasound examination are not absolutely necessary in routine cases of CTS. Instead of these instrumental examinations, only the clinical manifestations and clinical assessment tools, such as the CTS-6 diagnostic scale [2], can be used to diagnose the disease with a high degree of reliability. Electrodiagnostic studies (EDS), ultrasound, or MRI should only be performed in unclear cases and for differential diagnosis. Various provocation tests are widely used in clinical research [3]. The most well-known and popular provocation test due to its high sensitivity and specificity is the Phalen test [4, 5]. In the CTS-6 diagnostic scale, which is quite authoritative among specialists, the Phalen test has the highest diagnostic score among the six clinical diagnostic signs of CTS [6].

Scientific literature describes the use of both the classic Phalen test and its modifications [4]. The most recognized, clear, and memorable modification of the classic Phalen test involves the subject joining the back surfaces of both hands and applying pressure to create maximum flexion at the wrist joints [3, 4, 7]. The modified Phalen test differs from the classic version in its mechanism of execution. Therefore, the diagnostic value of the modified test may differ from that of the classic one. This raises the question of the appropriateness of using the modified test for the diagnosis of CTS. A review of the available literature revealed no studies directly comparing the diagnostic value of the classic and modified Phalen tests.

Objective: to compare the sensitivity and specificity of the classic and modified Phalen tests and to provide recommendations on the advisability of using these tests in the diagnosis of carpal tunnel syndrome.

Materials and methods

Experimental group

The experimental group consisted of 21 women aged between 39 to 73 years (mean age 52.5 years) (***Table 1***).

All of these women had clear clinical signs of idiopathic carpal tunnel syndrome in 29 hands (15 right and 14 left) including numbness or paresthesia in the median nerve innervation area, pain, especially at night, positive tests of Phalen (reverse), Tanzer's, the "tourniquet test", Hoffmann-Tinel, Goloborod'ko, Jungo, etc. Sixteen women underwent surgical treatment on 18 hands: 13 median nerve transpositions [8] and 5 retinaculotomies [9]. After surgery, all patients either completely lost their signs of CTS or their condition improved over time, thereby confirming the presence of CTS in this group of patients. In five women (patients 10-14 in Table 1), the clinical diagnosis was confirmed by EDS data.

Patients presenting with signs of polyneuropathy, diabetes mellitus, hypothyroidism, cervical radiculopathy, other numerous neurological diseases, wrist contractures, or acute hand injuries were excluded from the experimental group.

Control group

The control group comprised 21 women aged 37 to 73 (average age 52.2). As in the experimental group, the study was conducted on 29 hands (15 right and 14 left) (***Table 2***).

Table 1. Phalen tests results in the experimental group

№	Gender/ Age (yr)	Hand	Classic Phalen test/ Time of response (in seconds)	Modified Phalen test / Time of response (in seconds)	Operation
1	F/51	Right	+/4	+/5	retinaculotomy
2	F/59	Left	+/21	-	retinaculotomy
3	F/51	Left	+/50	+/33	median nerve transposition
4	F/51	Left	+/7	+/13	median nerve transposition
5	F/61	Right	+/9	+/21	median nerve transposition
6	F/55	Left	+/10	+/12	median nerve transposition
7	F/65	Right	+/10	+/9	median nerve transposition
8	F/41	Right	+/8	+/11	median nerve transposition
9	F/53	Left	+/11	+/26	median nerve transposition
10	F/40	Right	-	+/56	—
11	F/39	Left	+/34	+/19	—
12	F/44	Right	+/11	+/22	—
13	F/52	Right	+/37	+/32	—
14	F/73	Right Left	- +/39	+/28 +/28	— —
15	F/50	Right Left	+/25 +/25	+/32 +/17	median nerve transposition —
16	F/41	Right Left	+/12 +/14	+/10 +/11	median nerve transposition median nerve transposition
17	F/54	Right Left	+/12 +/16	+/21 +/17	median nerve transposition —
18	F/64	Right Left	+/20 +/20	+/21 +/21	retinaculotomy retinaculotomy
19	F/47	Right Left	+/11 +/11	+/7 +/12	median nerve transposition —
20	F/60	Right Left	+/20 +/20	+/21 +/21	retinaculotomy —
21	F/51	Right Left	+/11 +/18	+/10 +/19	median nerve transposition —

Notes. F = female; + = positive provocative test; - = negative provocative test.

This article contains some figures that are displayed in color online but in black and white in the print edition.

Table 2. Phalen tests results in the control group

№	Gender/Age (yr)	Hand	Classic Phalen test/ Time of response (in seconds)	Modified Phalen test / Time of response (in seconds)
1	F/51	Right	+/30	—
2	F/59	Left	—	—
3	F/51	Left	—	—
4	F/51	Left	—	—
5	F/61	Right	—	—
6	F/57	Left	—	—
7	F/63	Right	—	—
8	F/41	Right	—	—
9	F/53	Left	—	—
10	F/40	Right	—	—
11	F/39	Left	—	—
12	F/43	Right	—	—
13	F/52	Right	—	—
14	F/73	Right Left	— —	— —
15	F/50	Right Left	— —	— —
16	F/37	Right Left	— —	+/47 —
17	F/54	Right Left	— —	— —
18	F/64	Right Left	— —	— —
19	F/47	Right Left	— —	— —
20	F/59	Right Left	— —	+/49 —
21	F/51	Right Left	— —	— —

Notes. F = female; + = positive provocative test; - = negative provocative test.

The participants in the control group were recruited from among visitors to outpatient trauma and neurology clinics. None of them had a history of clinical manifestations of CTS. This group also excluded individuals with signs of polyneuropathy, diabetes mellitus, hypothyroidism, cervical radiculopathy, other numerous neurological diseases with a clinical picture similar to CTS, as well as those with wrist joint contractures, or acute hand injuries.

All participants in both the experimental and control groups signed a voluntary informed consent form for clinical and EDS examination and, in indicated cases, for surgery. The participants were not familiar with the purpose of the study, the presumptive diagnosis, or the test techniques.

Twenty-one women in the experimental and control groups, respectively, underwent both classic and modified Phalen tests on 29 hands (15 right and 14 left) in a randomized order. A time interval of 2-3 minutes was observed between tests. The procedures were performed and evaluated by certified orthopedic traumatologists and a neurologist.

The technique for performing the classic Phalen test was as follows. The subject was asked to place their flexed elbow joints on the table so that their forearms were in a vertical position. Under the influence of gravity, the hands were flexed maximally, with the fingers remaining extended (***Fig. 1***). This position was maintained for 1 minute. If signs of median nerve compression (numbness, paresthesia, pain in all 3.5 radial fingers or in some of them) appear during this time, the test was considered positive. In the absence of any clinical manifestations of CTS, the test was considered negative [10].

The modified test is performed as follows. The subject is asked to join the back surfaces of both hands, relax the upper limbs, and, in this relaxed state, lower the elbow joints below the horizontal line [7]. This technique of lowering the elbow joints actively increases the angle of flexion in the wrist joints. The fingers should be extended during the test (***Fig. 2***). If the characteristic signs of CTS are reproduced within one minute, the test is considered positive. If these symptoms are not present, the result is considered negative.

In patients in the experimental group with positive classic and modified Phalen tests, the time during which CTS symptoms appeared while performing these tests was recorded.

Results

The results of the tests in the experimental and control groups are presented in Tables 1 and 2. In the experimental group, a negative classic Phalen provocation test was observed in two patients on both right hands. Moreover, in one patient, the test was negative on the right hand and positive on the left hand. It should also be noted that a negative response was observed in patients who did not undergo surgery. In all other 19 patients on 27 hands, the classic Phalen test was positive. In the same experimental group, the modified Phalen test was negative in one patient on the left hand. In all other 20 subjects (28 hands), the test was positive. In the control group, one participant exhibited

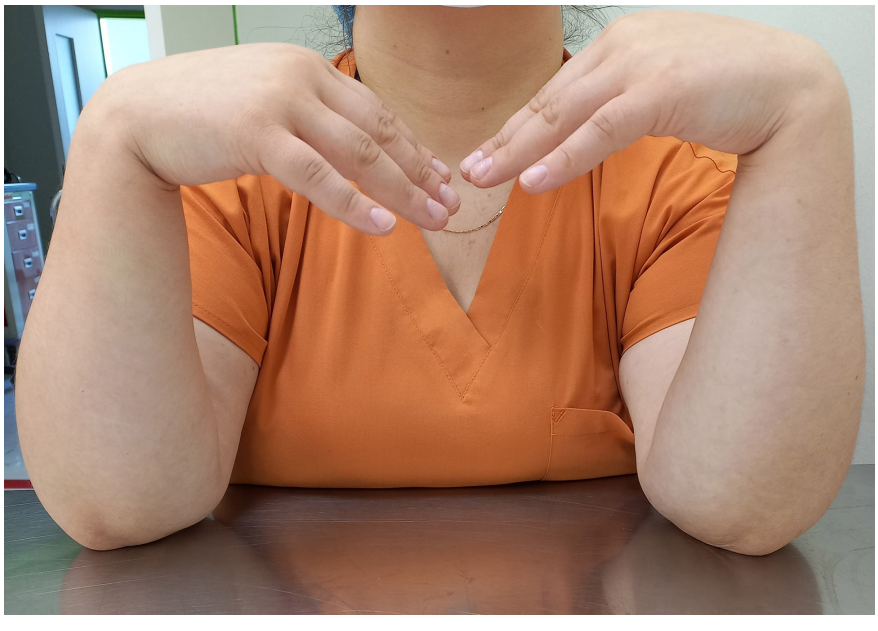

Fig. 1. Classic Phalen test

Fig. 2. Modified Phalen test

a positive classic Phalen test on the right hand. On all other 28 hands, it was negative. The modified Phalen test was positive on two right hands in two participants, while in the remaining 27 hands, the test was negative. The sensitivity, specificity, and positive and negative predictive value results were determined using the generally accepted method [11].

The sensitivity of the classic Phalen test was 93%, and that of the modified test was 96%. The specificity of the classic Phalen test was 96%, and that of the modified test was 93%. The PPV of the classic Phalen test was 96%, and the negative predictive value was 93%. The PPV of the modified Phalen test was 93%, and the negative predictive value was 96%.

The time to a positive response to the classic Phalen test on 27 hands in 19 patients ranged from 4 to 50 seconds (average 18 seconds). The time to a positive response to the modified Phalen test on 28 hands in 20 patients ranged from 5 to 56 seconds (average 20 seconds).

Discussion

CTS is a compression-ischemic neuropathy of the median nerve. The median nerve is compressed due to increased carpal tunnel pressure. The diagnosis of CTS is based on medical history and clinical signs of pathology. Instrumental examination methods (EDS, ultrasound, MRI) serve as supplementary tools, used mainly for differential diagnosis. In clinical examination, great importance is attached to the use of various provocation tests. One of the most well-known and popular tests is the Phalen test [5].

According to a recent meta-analysis, the sensitivity of the Phalen test is 70% and its specificity is 80% [12]. Therefore, in the modern CTS-6 diagnostic scoring scale, the Phalen test is assigned the highest diagnostic value score of 5 points.

In the 1950s, American hand surgeon Phalen GS published scientific papers on the diagnosis and treatment of carpal tunnel syndrome [13]. These scientific papers described a new diagnostic provocative test, known as the wrist flexion test. The essence of the test was that when the wrist was flexed for 60 seconds, patients with CTS experienced numbness, paresthesia, or pain in all or some of the 3.5 radial fingers, i.e., the clinical picture of carpal tunnel syndrome was reproduced. Phalen explained the mechanism of the test by the fact that when the wrist was flexed, the median nerve was bent over the flexor retinaculum and subjected to compression from the proximal edge of the flexor retinaculum on the palmar surface and from the flexor tendons of the fingers on the dorsal surface. There is another reason for the compression of the median nerve. Although the carpal tunnel is anatomically an open system, it behaves like a closed space in which a certain carpal tunnel pressure is created [14]. In healthy people in a neutral hand position, the carpal tunnel pressure ranges from 2.5 to 13 mm Hg [14], whereas in patients with signs of CTS, it averages 32 mm Hg [15]. During active flexion of the wrist in patients with CTS, the carpal tunnel pressure increases to 94 mm Hg [15]. If the carpal tunnel pressure exceeds 30 mm Hg, axoplasmic transport is disrupted, causing mild paresthesia in healthy subjects. In individuals with carpal tunnel syndrome this level is 32 mm Hg. If the carpal tunnel pressure exceeds the above level, a mechanism of pathological changes in the function and even structure of the median nerve is triggered (impaired epineural blood circulation, epineural edema, blockage of axoplasmic transport, etc.), which clinically manifests itself in symptoms characteristic of CTS [14]. Therefore, if during the Phalen test in a patient with CTS the carpal tunnel pressure exceeds the critical level by more than 3 times, it becomes clear why the clinical picture of CTS is reproduced within such a short period of time (within the first 60 seconds). It should also be emphasized that during the Phalen test, the already pathologically altered structures of the median nerve are compressed. Notably, even healthy people may experience numbness, paresthesia, and pain when carpal tunnel pressure increases during forced flexion of the wrist in the Phalen test. However, the symptoms will only appear after 10 minutes or more, rather than within the first 60 seconds, as in patients with CTS [10].

Since the description of the classic Phalen test, several modifications of this test have appeared. Technically, these modifications differ from the classic test in certain aspects. It is not entirely clear how much the modified tests differ in a positive or negative way in terms of diagnosing CTS. Therefore, we decided to compare the classic Phalen test and one of the most common and memorable modified version. The classic Phalen test differs from the modified one in certain aspects. For example, when performing the classic test, the forearms are in a vertical position, and the hands are much higher than the heart. In other words, in this case, the flexion test is combined to some extent with the elevation component, which can have a positive effect on the sensitivity and specificity of the test. When performing the modified test, the forearms are almost horizontal, and the hands are at heart level. Thus, there is virtually no combination with the elevation test. Another important distinction relates to the manner of wrist flexion. More than 40 years after first describing his test, Phalen confirmed that when performing the test, the hands should be only flexed under the action of gravity, without touching each other, and most importantly, neither the patient nor the doctor should actively bend the hands: only passive flexing due to gravity [10]. If either the patient or the physician actively bends the wrist, the difference between flexion of the wrist under the influence of gravity and flexion with external force can be as much as 20 degrees. The significance of this difference in bending angles on the test result is still unknown [16]. Therefore, considering the above differences between the classic and modified tests, we decided to compare the effectiveness of the two diagnostic tests in the same group of patients with CTS and determine the legitimacy of using either the classic or modified test.

The results of this study showed that the sensitivity of the classic Phalen test (93%) was lower than that of the modified version (96%). The specificity of the classic Phalen test (96%) was higher than that of the modified one (93%). The PPV of the classic Phalen test (96%) was higher than that of a PPV of the modified test (93%). The negative predictive value of the classic test (93%) was lower than that of a negative predictive value of the modified Phalen version (96%).

According to MacDermid JC and Wessel J [4], if the sensitivity or specificity of clinical provocation tests

is greater than 50%, such tests can be classified as "potentially useful for the diagnosis of CTS." In our study, the classic and modified Phalen tests significantly exceeded the 50% threshold for both sensitivity and specificity. Therefore, based on the data we have presented, we can confidently conclude that both the classic and modified Phalen tests can be successfully and legitimately used to diagnose CTS.

Conclusion

The sensitivity of the classic Phalen test (93%) was slightly lower than that of the modified version (96%), while its specificity (96%) was higher than that of the modified test (93%). Due to their high specificity and sensitivity, both tests have significant diagnostic value and can be successfully used in clinical practice for diagnosing CTS.

Disclosure

Conflict of interest statement

The authors declare no conflict of interest.

Funding

The research had no sponsor support.

References

1. Genova A, Dix O, Saefan A, Thakur M, Hassan A. Carpal tunnel syndrome: a review of literature. Cureus. 2020 Mar;12(3):e7333. doi: 10.7759/cureus.7333
2. American Academy of Orthopaedic Surgeons. Management of carpal tunnel syndrome Evidence-Based Clinical Practice Guideline. 2024;1-72. https://www.aaos.org/globalassets/quality-and-practice-resources/carpal-tunnel/carpal-tunnel-2024/cts-cpg.pdf
3. Georgiew F. Provocative tests used in the diagnosis of carpal tunnel syndrome. Med Rehab. 2007;11(4):7-17. https://rehmed.pl/article/93217/en
4. MacDermid JC, Wessel J. Clinical diagnosis of carpal tunnel syndrome: a systematic review. J Hand Ther. 2004 Apr-June;17(2):309–319. doi: 10.1197/j.jht.2004.02.015
5. Valdes K, LaStayo P. The value of provocative tests for the wrist and elbow: a literature review. J Hand Ther.2013 Jan-Mar;26(1):32-43. doi: 10.1016/j.jht.2012.08.005
6. Graham B. The value added by electrodiagnostic testing in the diagnosis of carpal tunnel syndrome. J Bone Joint Surg Am. 2008 Dec;90(12):2587-93. doi: 10.2106/JBJS.G.01362
7. Middleton SD, Anakwe RE. Carpal tunnel syndrome. BMJ. 2014 Nov 6;349:g6437. doi: 10.1136/bmj.g6437
8. Goloborod'ko SA. A surgical method for treatment of the carpal tunnel syndrome. Indian J Orthop. 2000;34(1):35-8.
9. Vasilinets MM, Goloborod'ko SA.A method of surgical treatment of carpal tunnel syndrome. Orthop Traum Prosth. 2010 Oct;(1):37-40. Ukrainian. doi: 10.15674/0030-59872010137-40
10. Vargas Busquets MA. Historical commentary: the wrist flexion test (Phalen sign). J Hand Surg Am. 1994 May;19(3):521. doi: 10.1016/0363-5023(94)90075-2
11. Trevethan R. Sensitivity, specificity, and predictive values: foundations, pliabilities, and pitfalls in research and practice. Front Public Health. 2017 Nov;5(307):1-7. doi: 10.3389/fpubh.2017.00307
12. Ozdag Y, Hu Y, Hayes DS, Manzar S, Akoon A, Klena JC, Grandizio LC. Sensitivity and specificity of examination maneuvers for carpal tunnel syndrome: a meta-analysis. Cureus. 2023 Jul;15(7):e42383. doi: 10.7759/cureus.42383
13. Phalen GS. Spontaneous compression of the median nerve at the wrist. J Am Med Assoc. 1951 Apr;145(15):1128-1133. doi: 10.1001/jama.1951.02920330018006
14. Wright AR, Atkinson RE. Carpal tunnel syndrome: an update for the primary care physician. Hawaii J Health Soc Welf. 2019 Nov;78(11 Suppl 2):6-10.
15. Aboonq MS. Pathophysiology of carpal tunnel syndrome. Neurosciences (Riyadh). 2015 Jan;20(1):4-9.
16. Urbano FL. Tinel's sign and Phalen's maneuver: physical signs of carpal tunnel syndrome. Hosp Physician. 2000 Jul;36(7):39-44.

Case report

Ukrainian Neurosurgical Journal. 2025;31(4):74-76
doi: 10.25305/unj.334674

Unexpected detection of a meningioma on ^{18}F-Fluorocholine PET/CT in a prostate cancer patient

Yassir Benameur [1,2], Ikram Zahfir [1,2], Meryem Aboussabr [1,2], Salah Nabih Oueriagli [1,2], Jaafar El Bakkali [1,2], Omar Ait Sahel [1,2], Abderrahim Doudouh [1,2]

[1]Department of Nuclear Medicine, Mohammed V Military Teaching Hospital, Rabat, Morocco.
[2]Faculty of Medicine and Pharmacy, Mohammed V University of Rabat, Morocco.

Received: 06 July 2025
Accepted: 21 July 2025

Address for correspondence: *Yassir Benameur, Department of Nuclear Medicine, Mohammed V Military Teaching Hospital, Av. Abderrahim Bouabid, Rabat, Morocco. email: benameur.yassir@gmail.com*

A 77-year-old man with a prior diagnosis of prostate adenocarcinoma, previously treated with radiotherapy and hormone therapy, presented with rising PSA levels suggestive of biochemical recurrence. While no evidence of metastatic prostate disease was detected, the PET/CT (positron emission tomography–computed tomography) scan incidentally revealed an area of abnormal radiotracer uptake in the left temporal lobe of the brain, unrelated to the patient's known malignancy. The imaging characteristics raised the suspicion of a meningioma. A subsequent brain MRI confirmed the presence of an extra-axial lesion consistent with a meningioma. This unexpected finding highlights the additional diagnostic value of ^{18}F-fluorocholine PET/CT beyond its primary role in prostate cancer imaging, particularly in detecting clinically significant incidental intracranial lesions. This case underscores the importance of careful and systematic interpretation of imaging studies during oncologic evaluations, even in regions outside the primary area of concern.

Keywords: *prostate cancer; meningioma; ^{18}F-Fluorocholine; PET-CT*

Introduction

Meningiomas are the most common primary intracranial tumors, often discovered incidentally during imaging studies conducted for unrelated conditions. Although they are typically benign and asymptomatic, their detection can have significant clinical implications, particularly in oncologic patients undergoing advanced imaging for cancer surveillance. ^{18}F-fluorocholine PET/CT (^{18}F-FCH) is widely used to detect biochemical recurrence in prostate cancer due to its high sensitivity in identifying areas of increased choline metabolism. However, ^{18}F-FCH can also uncover unexpected findings, such as meningiomas, due to their elevated phospholipid metabolism. This clinical case describes the incidental discovery of a meningioma on ^{18}F-FCH PET/CT in a patient with prostate cancer and explores the clinical relevance of such findings.

Case report

A 77-year-old male with a history of prostate adenocarcinoma, initially treated with radiotherapy and hormone therapy, presented with biochemical recurrence, evidenced by a rising prostate-specific antigen (PSA) level of 2.54 ng/ml. To localize the site of recurrence, an ^{18}F-FCH PET/CT scan was performed. The scan revealed an isolated focus of moderate radiotracer uptake in the left temporal lobe of the brain, with a maximum standardized uptake value (SUVmax = 5.4). No other abnormal foci of ^{18}F-FCH uptake were identified from the vertex to the mid-thigh, ruling out metastatic disease or local recurrence in the prostate bed or pelvic region. The temporal lobe uptake was considered unusual, as metastases from prostate cancer to the brain are rare, and meningiomas are typically not associated with significant ^{18}F-FCH avidity. Given the unexpected PET/CT findings, a contrast-enhanced brain MRI was performed for further characterization of the lesion. The MRI revealed a well-defined, extra-axial lesion in the left temporal lobe, measuring 16mm x 6mm. The lesion exhibited homogeneous contrast enhancement and was associated with a dural tail sign, both classic imaging features of a meningioma. No significant perilesional edema or mass effect was observed (***Fig. 1***). The imaging findings were consistent with a World Health Organization (WHO) Grade I meningioma, a benign and slow-growing tumor. The patient remained asymptomatic with respect to the meningioma, with no neurological deficits or symptoms suggestive of intracranial hypertension. Given the incidental nature of the finding and the absence of complications, no immediate surgical intervention was deemed necessary. The patient was referred to the neurosurgery department for long-term monitoring and management, with a plan for periodic imaging follow-up to assess any changes in the size or characteristics of the lesion.

Discussion

^{18}F-FCH PET/CT is widely used for restaging prostate cancer in patients with biochemical recurrence, as it has high sensitivity and specificity for detecting local and distant metastases [1]. The radiotracer ^{18}F-FCH is taken up by prostate cancer cells due to increased choline kinase activity, which is involved in phospholipid metabolism and cell membrane synthesis [2]. However,

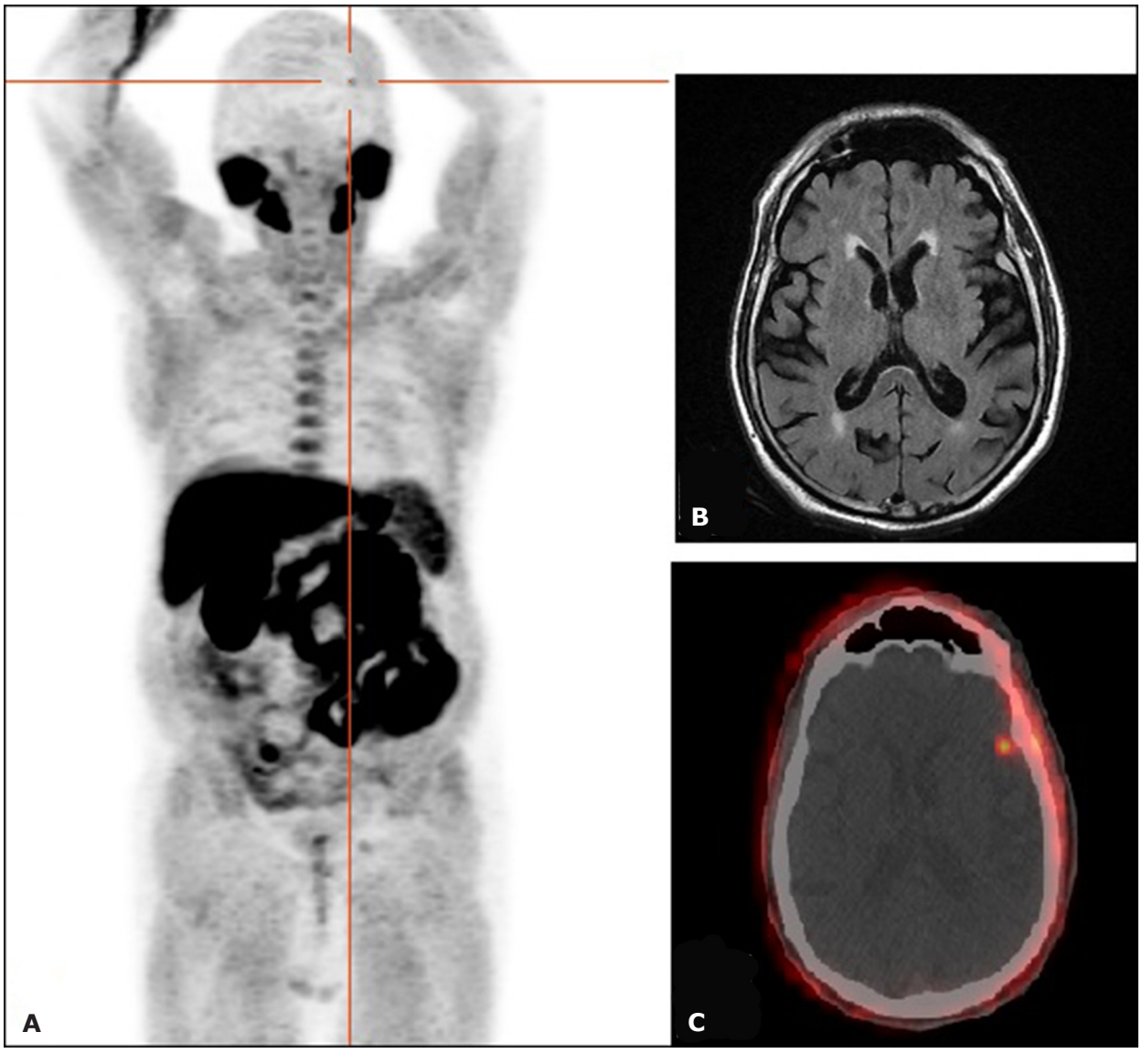

Fig. 1. A: ^{18}F-fluorocholine PET/CT MIP; B: axial Brain MRI T2 Flair; C: ^{18}F-fluorocholine PET/CT axial fusion image of the brain: an isolated uptake focus is noted in the left temporal lobe. Brain MRI confirmed the meningioma diagnosis

^{18}F-FCH uptake is not entirely specific to prostate cancer, as benign conditions and other malignancies can also exhibit radiotracer avidity [3]. In this case, the isolated focus of ^{18}F-FCH uptake in the left temporal lobe was initially suspicious for a metastatic lesion, given the patient's history of prostate adenocarcinoma. However, the absence of other abnormal foci and the subsequent MRI findings confirmed that the lesion was a meningioma.

Meningiomas are typically benign, slow-growing tumors that arise from the meninges. While they are usually detected on MRI, incidental uptake on PET/CT has been reported with various radiotracers, including ^{18}F-FCH [4]. The mechanism of ^{18}F-FCH uptake in meningiomas is not fully understood but may be related to increased cell membrane turnover or overexpression of choline transporters [2]. A study by Beheshti et al. demonstrated that meningiomas can exhibit moderate to intense ^{18}F-FCH uptake, which can lead to diagnostic challenges in differentiating them from metastatic lesions [5]. In our case, the SUVmax of the lesion was moderate, which is consistent with previous reports of ^{18}F-FCH-avid meningiomas.

Brain MRI remains the gold standard for diagnosing meningiomas due to its superior soft tissue resolution. Typical MRI features include a well-defined, extra-axial lesion with homogeneous contrast enhancement, a dural tail sign, and occasional calcifications [6]. In this case, the MRI findings were classic for a meningioma, with no evidence of perilesional edema or mass effect. These features helped confirm the diagnosis and ruled out other possibilities, such as brain metastases or primary gliomas. Additionally, ^{68}Ga-DOTATOC PET/CT imaging has proven valuable in detecting meningiomas, as it

This article contains some figures that are displayed in color online but in black and white in the print edition.

highlights areas with increased somatostatin receptor expression, a hallmark of these tumors [7].

The incidental detection of meningiomas during imaging procedures is becoming increasingly common, largely due to the widespread use of advanced imaging modalities. Most incidental meningiomas are asymptomatic and do not require immediate intervention. According to the European Association of Neuro-Oncology (EANO) guidelines, asymptomatic meningiomas can be managed with observation and periodic imaging, while symptomatic or growing lesions may require surgical resection or radiotherapy [8]. In this case, the patient was asymptomatic, and the decision was made to monitor the lesion with regular follow-up imaging.

Conclusion

This case underscores the importance of considering non-malignant etiologies for unexpected ^{18}F-FCH uptake, particularly in the context of prostate cancer imaging. It also highlights the complementary roles of PET/CT and MRI in characterizing intracranial lesions. While ^{18}F-FCH PET/CT is highly valuable for restaging prostate cancer, clinicians should be aware of its limitations and the potential for incidental findings that may require further investigation. Future studies are needed to better understand the mechanisms of ^{18}F-FCH uptake in meningiomas and to establish guidelines for managing such incidentalomas in є oncologic patients.

Disclosure

Conflict of Interests

The authors declare no conflict of interest in this study.

Acknowledgments

None.

References

1. Vali R, Loidl W, Pirich C, Langesteger W, Beheshti M. Imaging of prostate cancer with PET/CT using (18)F-Fluorocholine. Am J Nucl Med Mol Imaging. 2015 Jan 15;5(2):96-108
2. Henriksen G, Herz M, Hauser A, Schwaiger M, Wester HJ. Synthesis and preclinical evaluation of the choline transport tracer deshydroxy-[18F]fluorocholine ([18F] dOC). Nucl Med Biol. 2004 Oct;31(7):851-8. doi: 10.1016/j.nucmedbio.2004.05.004
3. Evangelista L, Zattoni F, Guttilla A, Saladini G, Zattoni F, Colletti PM, Rubello D. Choline PET or PET/CT and biochemical relapse of prostate cancer: a systematic review and meta-analysis. Clin Nucl Med. 2013 May;38(5):305-14. doi: 10.1097/RLU.0b013e3182867f3c
4. Galldiks N, Albert NL, Sommerauer M, Grosu AL, Ganswindt U, Law I, Preusser M, Le Rhun E, Vogelbaum MA, Zadeh G, Dhermain F, Weller M, Langen KJ, Tonn JC. PET imaging in patients with meningioma-report of the RANO/PET Group. Neuro Oncol. 2017 Nov 29;19(12):1576-1587. doi: 10.1093/neuonc/nox112
5. Beheshti M, Imamovic L, Broinger G, Vali R, Waldenberger P, Stoiber F, Nader M, Gruy B, Janetschek G, Langsteger W. ^{18}F choline PET/CT in the preoperative staging of prostate cancer in patients with intermediate or high risk of extracapsular disease: a prospective study of 130 patients. Radiology. 2010 Mar;254(3):925-33. doi: 10.1148/radiol.09090413
6. Buetow MP, Buetow PC, Smirniotopoulos JG. Typical, atypical, and misleading features in meningioma. Radiographics. 1991 Nov;11(6):1087-106. doi: 10.1148/radiographics.11.6.1749851
7. Einhellig HC, Siebert E, Bauknecht HC, Tietze A, Graef J, Furth C, Schulze D, Miszczuk M, Bohner G, Schatka I, Makowski MR. Comparison of diagnostic value of 68Ga-DOTATOC PET/MRI and standalone MRI for the detection of intracranial meningiomas. Sci Rep. 2021 Apr 27;11(1):9064. doi: 10.1038/s41598-021-87866-9
8. Goldbrunner R, Stavrinou P, Jenkinson MD, Sahm F, Mawrin C, Weber DC, Preusser M, Minniti G, Lund-Johansen M, Lefranc F, Houdart E, Sallabanda K, Le Rhun E, Nieuwenhuizen D, Tabatabai G, Soffietti R, Weller M. EANO guideline on the diagnosis and management of meningiomas. Neuro Oncol. 2021 Nov 2;23(11):1821-1834. doi: 10.1093/neuonc/noab150